THE ASTRONOMICAL JOURNAL

FOUNDED BY B. A. GOULD

PUBLISHED BY THE AMERICAN ASTRONOMICAL SOCIETY

VOLUME 61 1956 April ~ No. 1237 *NUMBER 3*

REDSHIFTS AND MAGNITUDES OF EXTRAGALACTIC NEBULAE *

BY M. L. HUMASON, N. U. MAYALL, AND A. R. SANDAGE

Abstract. There are three main sections to the present discussion. Part I contains redshifts of 620 extragalactic nebulae observed at Mount Wilson and Palomar. Included in these data are redshifts for 26 clusters of nebulae. Part II contains redshifts for 300 nebulae observed at Lick, together with a comparison of results for 114 nebulae in common with the Mount Wilson-Palomar lists. Part III is a discussion of these new redshift data in combination with photometric data. The redshift-apparent magnitude relation is investigated for (1) field nebulae with and without regard to nebular type, (2) isolated groups, and (3) clusters of nebulae. The principal corrections applied to the apparent magnitudes are discussed in two of the three appendices. Appendix A gives the procedure for correcting the published magnitudes for the effect of different photometer apertures. Appendix B describes the theory and computation of the correction for the selective effect of redshifts. In the final Appendix C, a provisional evaluation of the Hubble redshift parameter H is made by two independent methods.

The principal results of this study may be stated as follows. (1) For those nebulae observed in common there is a negligible mean systematic difference between the redshifts from the two sources. (2) Spectrographic coverage is 63 per cent complete to $m_{pg} = 12.9$ in the Shapley-Ames catalogue for nebulae north of $\delta = -30°$. (3) The log redshift-magnitude relation for field nebulae with and without regard to type is linear to within the accuracy of the data. (4) The log redshift-magnitude relation for the cluster data confirms the linearity for small $\Delta\lambda/\lambda_0$ and shows an apparently significant departure from linearity for shifts of the order of $\Delta\lambda/\lambda_0 = 0.2$. This non-linearity indicates deceleration of the expansion if interpretation is made by theoretical equations due to Robertson. Because of the cosmological significance of this last result, the accuracies of the various quantities that lead to it are examined. It is concluded that a deceleration should be regarded as tentative until Whitford's results are available for the spectral energy distribution of the distant nebulae, and until an adequate theory of stellar evolution is advanced to explain the Stebbins-Whitford effect. (5) The Hubble redshift parameter H is provisionally estimated from (a) the magnitudes of resolved stars in NGC 4321 that have been isolated from the emission H II regions, and (b) from the assumption that the brightest field and cluster nebulae are giants of luminosity comparable to the Andromeda nebula, with the result that $H = 180$ km/sec per 10^6 pc.

GENERAL INTRODUCTION

More than 25 years ago Hubble (1929) announced a relationship between velocities and distances of extragalactic nebulae. Since he realized that this first formulation referred to only a relatively small distance, he initiated an exploratory program to follow the relationship to the greatest distances attainable with the largest telescope. The successful outcome of that program has become widely known, especially through publication of his book, *The Realm of the Nebulae* (Hubble 1936a), and his professional lectures. The last of these (Hubble 1953) summarizes the observational basis for the early restricted velocity-distance relation, and the later far-reaching law of redshifts.

Despite the comprehensiveness of Hubble's extragalactic researches that used the 100-inch to the limits of its power for observations of faint nebulae, he regarded them in sum as a "preliminary reconnaissance." This appraisal, although a characteristic understatement, emphasized the need for many more nebular redshifts and magnitudes. These spectrographic and photometric data are now available in considerable numbers, on a systematic basis, and with improved precision, chiefly as the result of Hubble's inspiring influence on his colleagues.

This paper contains as its principal new material redshifts for over 800 nebulae observed during the 20-year interval from 1935 to 1955. While these redshifts doubtless could be discussed alone, one of the main reasons for obtaining them was their use as the higher-precision, independent variable in correlations with nebular magnitudes. This unified treatment of spectrographic and

* Mount Wilson and Palomar Observatories, Reprint No. 181. Lick Observatory Bulletin, No. 542.

photometric data follows previous practice by Hubble, who, had he lived, would have participated as the senior author in the analysis and discussion.

Since photography of nebular spectra 20 years ago required much more telescope time than now, a cooperative program of nebular spectroscopy was started in 1935 at the Mount Wilson and Lick Observatories. The field was divided according to the instrumental facilities. At Mount Wilson, the fainter catalogued nebulae and the faintest and smallest cluster nebulae were natural selections for the superior light-gathering power and scale of the 100-inch; at Lick, the brighter catalogued nebulae and the larger spirals of low surface brightness were appropriate objects for the moderate capabilities of the 36-inch Crossley. At both observatories the Shapley-Ames *Catalogue of Bright External Galaxies* (1932) was used as the principal finding list and source of magnitudes. Originally, the two programs separated the nebulae north of $\delta = -30°$ at the catalogue magnitude of 11.6, except that the Crossley was used for most objects north of the 100-inch limit at $\delta = +64°$. As the work progressed, considerable overlap resulted over a fairly wide range in magnitude because of interest in individual objects for special purposes, and more than 100 nebulae were observed in common.

The remainder of this paper is divided into three parts, which were written by the authors in the order shown by the line following the title. These parts may be described as follows:

Part I. *The Mount Wilson-Palomar Lists of Redshifts*. These are subdivided into three tables that include non-cluster objects, bright nebulae in clusters, and faint nebulae in clusters. This arrangement reflects the basic programs and facilitates the treatment of the material for the numerous brighter nebulae in the nearer clusters, such as those in Virgo and Coma, and the fewer fainter nebulae in the more distant clusters. Because of the considerable mass of the material, which was obtained with several different telescopes and with a variety of spectrographs and dispersions, it was impracticable to include in the tables all the detailed data for individual plates. Instead, the number of plates and the dispersions are indicated in a summary column, and a mean redshift is given for each nebula.

Part II. *The Lick List of Redshifts*. These are given in a single table, because the observing program placed no special emphasis on cluster nebulae. Since all the plates were obtained with the same telescope, spectrograph and two-prism dispersion (except for one nebula observed with three prisms), it was feasible to list for each plate such details as slit-width, emulsion, exposure, and an index of accuracy based on the agreement between redshifts for different spectral features. Such information reveals something of the technique, observing time, and order of precision involved in low-dispersion spectroscopy of nebulae.

Following the last list of spectrographic data, Table V and notes, the redshifts are discussed for (1) systematic differences for nebulae observed in common at Mount Wilson-Palomar and at Lick, and (2) degree of completeness in terms of the Shapley-Ames catalogue magnitudes.

Part III. *Discussion of the Spectrographic and Photometric Data*. This section contains quantitative evaluations of the relationships between redshifts and magnitudes for (1) field nebulae with and without regard to nebular type, (2) isolated groups, and (3) the cluster nebulae. The magnitudes for field nebulae were obtained principally from Pettit's (1954) large catalogue, supplemented with measures by Stebbins and Whitford (1952). The magnitudes for the faintest cluster nebulae were obtained photographically with the 200-inch and a jiggle-camera. Before the magnitudes were used, all were corrected for the effects of different photometer apertures by the procedure given in Appendix A. The appendix gives, moreover, the list of corrected magnitudes for field nebulae, together with an analysis of the overlap between the Pettit and the Stebbins and Whitford photoelectric data, on the one hand, and between the Pettit data and Holmberg's unpublished precision photographic material, on the other. Additional corrections to all magnitudes were made for the effects of redshift. These so-called K corrections were computed by the procedure given in Appendix B. The redshift-magnitude correlations are discussed with theoretical relations given by Robertson (1955), in simplified form for the nearer field nebulae, and with a second-order term for the cluster nebulae. Finally, in Appendix C a provisional evaluation of the Hubble redshift parameter H is made from distance indicators calibrated in the nearby resolved systems.

PART I. MOUNT WILSON-PALOMAR LISTS OF REDSHIFTS

The systematic spectroscopic observation of extragalactic nebulae at the Mount Wilson Observatory was begun in 1928 at the request of

Edwin Hubble, in order to test further the relation he had found (Hubble 1929) between redshifts in nebular spectra and the apparent brightness of the nebulae.

First results from the spectroscopic program became available (Humason 1931, 1936) when the redshifts for 146 nebulae observed at Mount Wilson had been measured. The present Mount Wilson-Palomar lists contained in Tables I, II, and III give the redshifts for 620 individual objects, of which 474 are new. The remainder are revised values for the 146 objects previously published.

Up to 1950 all the observations were made with the Mount Wilson instruments, as described in the two earlier publications cited above. Since June 1950 the work has been carried on at Palomar with a prime-focus nebular spectrograph. The Palomar spectrograph has a beam diameter of 3 inches and, as originally designed, contained two 62° LBF2 glass prisms. Two cameras have been used, both of the thick-mirror Schmidt type. Their focal lengths and F ratios are 1.4 inches and 0.47 for one, and 2.8 inches and 0.95 for the second. Dispersions are 430 A/mm and 215 A/mm at λ4340.

In February 1952 an important revision to the spectrograph was made when the two prisms were replaced by a newly ruled first-order grating having 600 lines per millimeter. The dispersions then became 370 A/mm for the 1.4-inch camera and 190 A/mm for the 2.8-inch camera. Allowing for the difference in dispersion, the grating spectra compare exceedingly well with the prism spectra, both in speed and definition. This, and the added advantage of linear dispersion, led to the ruling of several more gratings, until there are now five Babcock-Swanson gratings which are interchangeable for different wave-length regions and dispersions. The various combinations of gratings and cameras provide dispersions from 80 to 750 A/mm. The type of emulsion most often used is Eastman IIa-O and 103a-O. The IIa-O plates are baked for 24 hours at a temperature of 65°C, which increases their speed some three times for exposures of five hours or more.

Many combinations of spectrographs and cameras have been used in the twenty-five years of the current program with the Mount Wilson 60-inch and 100-inch telescopes and the Palomar 200-inch. At Mount Wilson, the dispersion for about 90 per cent of the plates is of the order of 450 A/mm at $H\gamma$. Almost all the observations were made at the Cassegrain focus with a spectrograph which could not be rotated, using the long way of the slit in an east-west position. At Palomar the spectrograph can be rotated to any position angle. Most of the Palomar observations have been made with the slit in a north-south position. The slit length was usually 2.5 mm, which corresponds to 12″ at the Cassegrain focus of the 100-inch, and to 30″ at the prime focus of the 200-inch. Observations are of the nuclear regions unless otherwise indicated in the notes.

Redshifts of objects previously published have been included for the following reasons. (1) As data were accumulated it became possible to improve upon the initial wave-length system used in the reductions. (2) Additional spectrograms have been obtained of objects which at the beginning had been poorly observed. (3) Redshifts corrected for the solar motion with respect to the local group are included for the first time. (4) Investigators in this field may appreciate having all known redshifts available in one paper.

Wave lengths used for the reduction of features most often observed and measured on small-scale spectrograms of extragalactic nebulae are 3727.3, the blended emission lines of [*O* II], absorption at 3933.7 (K), 3968.5 (H), 4101.7 $H\delta$, 4226.7 blend, 4304.4 G-band blend, 4340.5 $H\gamma$, 4385.0 blend. Other emission and absorption features are measured when they appear.

Some of the first Mount Wilson spectrograms of extragalactic nebulae were of poor quality as compared with those obtained now. This was necessarily so, as no high-speed short-focus cameras were then available and plate speeds were far below those of today. Many of the objects observed between 1928 and 1935 have therefore been re-observed to reduce the plate errors in the final redshifts. In cases where the redshift had been measured from under-exposed plates or on plates of very poor quality, the old measures were discarded as being uncertain enough to do actual harm to the values measured from later and better plates.

Most of the revisions to the old values are small; the total revision of many being due only to the fact that the older values were given to the nearest 50 or 100 km/sec. None of the earlier measures were reduced to the sun. All of the tabulated redshifts have now been reduced to the sun and corrected for curvature of the spectrograph slit. Results are given to the nearest whole kilometer.

Re-observation has shown that the formerly

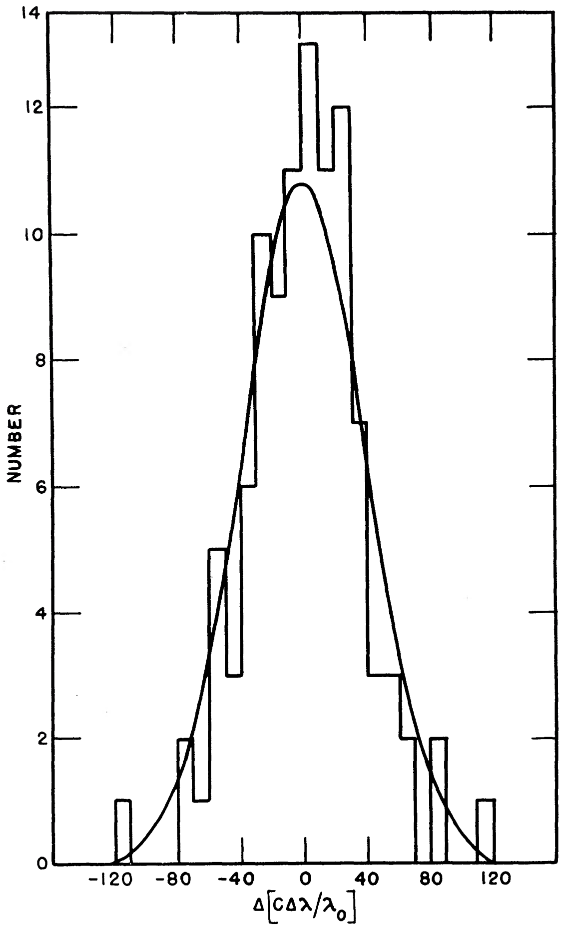

Figure 1. The distribution of residuals in the measured redshifts for the Mount Wilson-Palomar material when two or more plates are available for a given nebula. The normal error curve is drawn with $\overline{\Delta[c\,\Delta\lambda/\lambda_0]} = 0$ and with dispersion $\sigma = 39.4$ km/sec. This corresponds to a probable error of ± 27 km/sec.

published redshifts for five nebulae are in error. They are NGC 1700, 6207, and 6702 in Table I and 4192 and 4569 in Table II. The redshift for NGC 1700 was formerly given as +800 km/sec (Pease 1918; Stromberg 1925); from two very good plates of this object the redshift is now known to be +3,976 km/sec; the reason for the discrepancy in the two values is not known. The redshift for NGC 4192 is −124 km/sec; the former value was +1150 km/sec (Humason 1931); the plate from which this value was measured was obtained by Pease and measured by the writer; it is an extremely weak plate and the single absorption feature measured was either incorrectly identified or not real. The negative shifts, −200 km/sec for NGC 4569 and −250 km/sec for NGC 6207 (Humason 1936), were found in each case to be that of a star projected on the nebula. The redshifts are +960 km/sec for NGC 4569 and +869 km/sec for NGC 6207. The redshift of NGC 6702 is +4749 km/sec; it was formerly given as +2250 km/sec (Humason 1931); the early observation was by Pease, who probably observed the nearby nebula NGC 6703, whose redshift is +2,316 km/sec, for 6702.

The random errors in the tabulated redshifts of Tables I, II, and III arise from two principal causes. These are (1) the personal error of measurement and (2) the error caused by various photographic effects, such as emulsion creepage and graininess. These two effects may be separately evaluated by analysis of the residuals in the measured redshifts from (1) plates measured more than once and (2) several plates taken on the same object. A formal analysis of all available Mount Wilson spectra with dispersions of approximately 450 A/mm at $H\gamma$ yields distributions of the residuals which give the probable error of personal measurement, on good to very good quality plates, of the order of p.e. $= \pm 11$ km/sec with a total spread of about 5 times this value. The probable error for the plate error is about ± 24 km/sec, again with a spread of 5 times this value.

Figure 1 shows the distribution of redshift residuals where two or more good quality plates are available on a given nebula. Since the true redshifts were not known, the mean redshift from the various plates on a given object was adopted

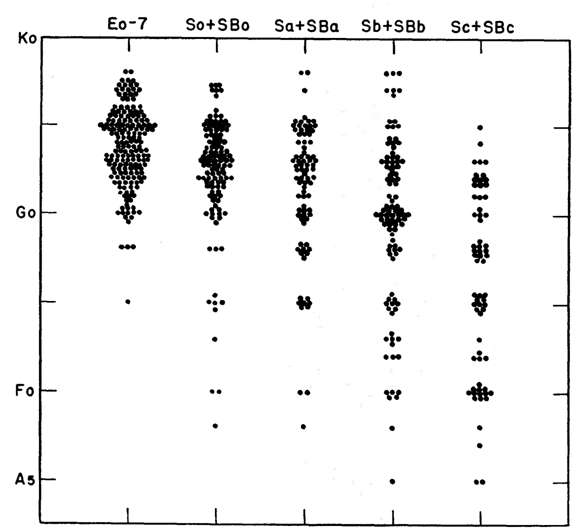

Figure 2. The distribution of spectral type as a function of nebular type for 546 nebulae from Tables I and II.

and residuals from the mean computed. This procedure tends to symmetrize the distribution, but the effect should not be serious. The normal error function was drawn with the mean equal to zero and with $\sigma = 39.4$ km/sec. This gives a formal probable error of ± 26.6 km/sec for the tabulated redshifts, for good to very good quality plates. It is the combined plate and measuring error. For poor quality plates the probable error of the tabulated values is about ± 35 km/sec. The conclusion from this formal analysis is that all tabulated redshifts of Table I, II, and III are expected to be within $5 \times 35 = 175$ km/sec of their true value with more than half within 35 km/sec of their true value. The errors are smaller for higher dispersion plates.

Since this formal analysis is somewhat unrealistic due to the small number of objects involved, estimated errors based upon experience with the plates have been tabulated instead. The size of the estimated errors for small-scale plates is usually an indication of plate quality although other factors can also affect these estimates. One of these factors is the character of the absorption features. The Mount Wilson-Palomar spectra indicate that absorption lines in the spectra of elliptical and So nebulae are narrower and deeper than they are for the Sa, Sb, and for some of the Sc nebulae. Noticeable line widening begins to appear in the Sa objects. In many of the Sb's the absorption features are wider and more poorly defined than in other types. Both wide or narrow lines are, however, observed in the nuclear regions of the Sc's. Exceptions to these observations occur in all types but the wide, shallow features observed in most Sb nebulae make their measurement on small-scale spectra more difficult and tend to increase the size of the estimated error.

A typical example of the type of line widening observed in many of the Sb objects can be seen in Plate III, if the spectrum of the Sb nebula NGC 224 is compared with that of the elliptical NGC 221. Spectra of both objects were obtained at Mount Wilson under exactly the same conditions and differences in the widths of the absorption features are obvious. Absorption lines in the spectrum of the Sb nebula are estimated to be four times wider and noticeably shallower than those observed in a non-rotating stellar source of comparable spectral type. Lines in the spectrum of the elliptical nebula are approximately two times wider than normal stellar lines. In some Sb nebulae the lines are again as wide as those observed in NGC 224. It is probable that widening of the absorption features in many of the extragalactic nebulae is caused by a mixture of velocities and spectral types, and that this characteristic is less pronounced in the elliptical and Sc nebulae than for many of the Sb's, and some Sa's.

Spectral types of nebulae in Tables I and II have been estimated in the same way as in the past (Humason 1936). Although absorption features in small-scale spectra are few, those that do appear are good indicators of type. Nevertheless the accuracy of the estimates is not high, especially for some of the Sb objects having wide lines. For these, the error is probably larger than one-half of a spectral division; for the other groups, not greater than one-half a division.

In Figure 2 the spectral types of 546 nebulae from Table I and Table II have been plotted against Hubble's determinations of nebular type. The picture is not greatly changed from that of the 1936 plot when only 136 objects were shown (Humason 1936). With the exception of four, all elliptical nebulae have been classified as G. For the spirals the number of blue objects gradually increases toward earlier nebular type until the distribution of the Sc's is almost uniform between types F0 and G3. The mean spectral type for each group is shown in Table IVA.

The frequency of the occurrence of $\lambda 3727$ [*O* II] in the spectra of extragalactic nebulae has been estimated by Mayall (1939) and by Humason (1947). The new data have not greatly increased the number of spectra available for inspection, nor changed the percentage values. From 278 spectra well enough exposed in the ultraviolet to show $\lambda 3727$, if present, the percentage frequencies shown in Table IVB were estimated.

The Mount Wilson and Palomar redshifts have been subdivided into three groups in order to separate the non-cluster and the cluster nebulae. Table I contains the redshifts for non-cluster nebulae and groups. In general they are the brighter nebulae, most of them being NGC or IC objects. Among the nebulae designated "anonymous" are several originally observed as possible members of clusters, but later found to be field nebulae with redshifts not in agreement with those obtained from cluster members.

Table II contains the redshifts from clusters of bright nebulae. Most of them are catalogued objects. All tabulated redshifts in Table II are smaller than +12,000 km/sec.

In Table III are the uncatalogued faint cluster nebulae with redshifts larger than +12,000 km/sec.

TABLE I. REDSHIFTS OF EXTRAGALACTIC NEBULAE. NON-CLUSTER OBJECTS

NGC *IC (1)	1950 RA (2)	1950 Dec (3)	Gal Long (4)	Gal Lat (5)	Type Neb (6)	Type Spec (7)	Redshift $c\Delta\lambda/\lambda_0$ (8)	Corr Redshift (9)	Plts Disp (10)	Est Error (11)	
							km/sec	km/sec		km/sec	
7814	0^h $0^m.7$	+15°51'	76°	−45°	Sa	G3	+ 1,047	+ 1,245	2a	50	
16	6.5	+27 27	80	−34	SB0	G5	+ 3,110	+ 3,335	1a	50	
23	7.3	+25 39	80	−36	Sb	F5*	+ 4,568	+ 4,790	1a	100	Absorption lines are broad and indistinct.
45	11.4	−23 27	30	−82	Sc	Em	+ 450	+ 488	1a	30	Bright em patch 0'.8 nf nucleus.
55	12.5	−39 30	296	−77	Sc	Em	+ 210	+ 177	1a	50	Em patch 2'.7 p nucleus. p of two. Observed by Hubble.
68	15.8	+29 48	83	−32	S0	G3	+ 5,787	+ 6,012	1a	65	This and next four are members of a group.
69	15.8	+29 46	83	−32	SB0	G2	+ 6,637	+ 6,862	1a	150	
71	15.8	+29 47	83	−32	E2	G3	+ 6,591	+ 6,816	1a	150	
72	15.9	+29 46	83	−32	SBa	G7	+ 6,976	+ 7,201	1a	150	
Anon	16.0	+29 46	83	−32	E4	G3	+ 6,807	+ 7,032	1a	130	Brighter and p of 3 faint neb. 1'.3 sf NGC 72.
* 10	17.5	+59 2	87	− 3	Sc	Em	− 343	− 88	1b	12	Br em patch in sf part. Possible member local group.
80	18.6	+22 5	83	−40	S0	G5	+ 5,586	+ 5,790	1a	100	This and next one are members of a group.
83	18.8	+22 9	83	−40	E0	G3	+ 6,541	+ 6,745	1a	150	
Anon	25.2	+22 25	85	−40	Sb	G0*	+37,052	+37,251	1a	60	See note 1 at end of table.
Anon	26.1	+ 2 40	82	−60	Sa	G0*	+ 4,460	+ 4,594	1a	50	Neb 5'.6 n, 9'.5 p NGC 128.
125	26.3	+ 2 34	82	−60	S0	G5*	+ 5,289	+ 5,423	1a	50	
127	26.6	+ 2 36	82	−60	Sa	G0	+ 4,094	+ 4,228	2a	40	
128	26.7	+ 2 35	82	−60	S0	G7*	+ 4,250	+ 4,384	2a	50	
157	32.2	− 8 40	82	−71	Sc	G4	+ 1,826	+ 1,913	1a	100	
160	33.4	+23 41	87	−37	Sa	G8	+ 5,255	+ 5,456	1a	50	See note 2 at end of table.
182	35.6	+ 2 28	87	−60	Sa	G4	+ 5,234	+ 5,360	1a	50	
185	36.1	+48 4	89	−14	Ep	G0	− 266	− 24	1a	75	Member local group.
185	36.2	+48 4	89	−14		F8	− 344	− 102	1a	150	Globular cluster in NGC 185. 1'.1 sf nucleus.
194	36.7	+ 2 46	87	−59	E1	G5	+ 5,105	+ 5,237	1a	50	
205	37.6	+41 25	89	−21	SB0	A8	− 239	− 8	3b	12	Member local group.
214	38.8	+25 14	89	−37	Sc	G3*	+ 4,535	+ 4,731	1a	50	
221	40.0	+40 36	89	−22	E2	G3	− 214	+ 17	1c,3d	10	Member local group.
224	40.0	+41 0	89	−21	Sb	G5	− 266	− 35	1c,3d	15	Member local group.
227	40.1	− 1 48	89	−64	E4	G3	+ 5,315	+ 5,423	1a	65	
247	44.5	−21 2	94	−83	Sc	Fm	− 28	+ 1	1a	35	Bright em patch 5'.0 sf nucleus.
253	45.1	−25 34	105	−88	Sc	Em	− 81	− 72	1a	35	Em patch 2'.7 n of nucleus.
Anon	47.1	+42 19	91	−20	E2	G5	+60,980	+61,208	1a	250	For this and next one see note 3 at end of table.
Anon	47.1	+42 20	91	−20	Sb	F3*	+23,908	+24,136	1a	30	
278	49.2	+47 17	91	−15	Sb	F0*	+ 622	+ 854	1a,1b	30	One plate by Hubble.
300	0 52.7	−37 58	259	−80	Sc	Em	+ 248	+ 200	1a	40	Brighter of two em patches 2'.8 sp nucleus.
357	1 0.8	− 6 37	103	−69	SBa	G4	+ 2,541	+ 2,613	1a	50	
*1613	2.5	+ 1 52	99	−60	Irr	Em	− 238	− 130	1b	10	Em patch 0'.9s, 10'.8f BD +1°200. Member local group.
375	4.3	+32 5	95	−30	E5	G5	+ 6,011	+ 6,209	2a	40	This and next eight are members of a group.
379	4.5	+32 15	95	−30	S0	G6	+ 5,374	+ 5,572	1a	65	
380	4.5	+32 13	95	−30	E2	G5	+ 4,341	+ 4,539	1a	150	
382	4.6	+32 8	95	−30	E0	G5	+ 5,156	+ 5,354	1a	50	
383	4.6	+32 9	95	−30	S0	G0	+ 4,888	+ 5,086	1a	50	Absorption lines are somewhat broad and shallow.
384	4.6	+32 2	95	−30	S0	G1	+ 4,401	+ 4,599	2a	100	Absorption lines are somewhat broad and indistinct.
385	4.7	+32 3	95	−30	E3	G5	+ 4,845	+ 5,043	2a	150	
386	4.7	+32 6	95	−30	E3	G2	+ 5,555	+ 5,753	1a	150	Absorption lines are indistinct.
388	5.0	+32 3	95	−30	E3	G5	+ 5,114	+ 5,312	1a	100	
404	6.6	+35 27	95	−26	S0	F8*	− 55	+ 152	1b	30	
474	17.4	+ 3 9	107	−58	E0	G5	+ 2,306	+ 2,402	2a	40	
488	19.2	+ 5 0	107	−56	Sb	G7	+ 2,180	+ 2,282	1a	150	
495	20.1	+33 13	99	−28	S0	G5	+ 4,114	+ 4,306	1a	50	This and next two are members of a group.
499	20.4	+33 12	99	−28	S0	G3	+ 4,375	+ 4,567	1a	50	
507	20.8	+33 0	99	−28	E3	G7	+ 4,929	+ 5,121	1a	50	
514	21.4	+12 39	104	−49	Sc	G0	+ 2,487	+ 2,616	1a	60	
524	22.3	+ 9 17	106	−52	S0	G3	+ 2,470	+ 2,587	1a	65	
560	24.9	− 2 11	113	−63	S0	G1	+ 5,503	+ 5,578	1a	150	
564	25.2	− 2 9	114	−62	E3	G4	+ 5,851	+ 5,923	1a	150	
584	28.8	− 7 7	120	−67	E3	G5	+ 1,827	+ 1,878	1a	75	
596	30.3	− 7 17	121	−67	E0	G3	+ 2,049	+ 2,097	1a	65	
598	31.0	+30 24	102	−31	Sc	A7	− 189	− 12	1b,1c	15	Member of local group.
604	1 31.7	+30 32	102	−31	Sc	Em	− 226	− 49	2b	12	Em patch in NGC 598.

TABLE I. REDSHIFTS OF EXTRAGALACTIC NEBULAE. NON-CLUSTER OBJECTS

NGC *IC (1)	1950 RA (2)	1950 Dec (3)	Gal Long (4)	Gal Lat (5)	Type Neb (6)	Type Spec (7)	Redshift $c\Delta\lambda/\lambda_0$ (8)	Corr Redshift (9)	Plts Disp (10)	Est Error (11)	
							km/sec	km/sec		km/sec	
628	$1^h\ 34^m.0$	+15°32'	108	−45°	Sc	F5*	+ 561	+ 687	2a	50	
636	36.6	− 7 46	125	−66	E1	G5	+ 1,941	+ 1,983	1a	50	
*1727	44.7	+27 5	107	−33	Sc	Em	+ 362	+ 518	1a	50	Em patch in sf end of IC 1727.
681	46.7	−10 40	135	−67	Sa	G5*	+ 1,750	+ 1,768	1a	60	
720	50.6	−13 59	143	−69	E5	G4	+ 1,808	+ 1,814	1a	100	
736	53.8	+32 48	107	−27	E1	G2	+ 4,366	+ 4,528	2a	40	
741	53.8	+ 5 23	122	−53	E0	G5	+ 5,559	+ 5,637	1a	50	
750	54.6	+32 58	107	−26	E0	G7	+ 5,130	+ 5,295	1b	40	p neb. This and 751 appear to be physically connected.
751	54.6	+32 58	107	−26	E0	G2	+ 5,126	+ 5,291	1a	60	f neb. Forms close pair with 750.
772	56.6	+18 46	113	−40	Sb	G4	+ 2,431	+ 2,553	1a	150	
788	1 58.6	− 7 3	135	−63	Sa	G0"	+ 4,137	+ 4,161	1a	65	Abs. lines are weak and shallow.
821	2 5.7	+10 45	120	−47	E6	G5	+ 1,778	+ 1,865	1a	100	
890	19.3	+33 2	112	−25	S0	G4	+ 4,043	+ 4,193	1a	65	
891	19.3	+42 7	108	−17	Sb	G1	+ 72	+ 246	1a	100	Abs. lines are somewhat broad and shallow.
925	24.3	+33 21	113	−24	Sc	F0*	+ 420	+ 564	1a	200	Abs. lines are broad and indistinct.
936	25.1	− 1 22	137	−54	SBa	G3*	+ 1,343	+ 1,367	1a	50	
972	31.3	+29 6	117	−27	Sb	F3*	+ 1,538	+ 1,664	2a	60	Abs. lines are narrow and weak.
Anon	34.6	+34 12	115	−23	SBa	F8	+ 4,800	+ 4,938	1b	150	Observed and measured by Minkowski.
1003	36.1	+40 39	112	−17	Sc	F0*	+ 585	+ 741	3a	60	
1023	37.2	+38 51	113	−18	SB0	G5	+ 557	+ 709	1a, 1b	60	One plate by Hubble.
1049	37.7	−34 29	202	−64	Ep	F0	+ 40	− 71	1a, 2b	30	Bright cl in For syst. Member of local group.
For	38.1	−34 41	202	−64	Ep	F7	+ 35	− 76	1a	60	Faint cl in For syst.
1052	38.6	− 8 28	150	−56	E3	G5*	+ 1,439	+ 1,424	3a	40	
1068	40.3	− 0 13	141	−51	Sb	Fo"	+ 1,020	+ 1,032	1b	40	Both abs. and em lines are broad and indistinct.
1079	41.6	−29 13	189	−63	SBa	G3	+ 2,252	+ 2,156	1a	250	
1084	43.6	− 7 47	151	−55	Sc	F5	+ 1,558	+ 1,540	1a	100	
1087	43.9	− 0 42	142	−50	Sc	F0	+ 1,824	+ 1,835	1a	200	Abs. lines are weak.
1097	44.2	−30 29	193	−63	SBb	F8	+ 1,326	+ 1,224	1a	100	
1140	52.1	−10 14	156	−55	Irr	F2"	+ 1,544	+ 1,511	1a	40	
1156	2 56.7	+25 2	125	−28	Irr	Em	+ 405	+ 495	1a	40	Two em patches p center of neb.
1199	3 1.3	−15 48	167	−56	E3	G2	+ 2,581	+ 2,518	1a	50	
1201	2.0	−26 15	185	−60	S0	G5	+ 1,722	+ 1,626	1a	50	
1209	3.7	−15 47	167	−55	E6	G4*	+ 2,568	+ 2,502	1a	150	Observed by Hubble.
1302	17.7	−26 14	187	−56	Sa	G3	+ 1,730	+ 1,616	1a	75	
1316	20.8	−37 24	206	−56	Irr	G2	+ 1,878	+ 1,728	1a	75	Observed by Hubble.
1317	20.8	−37 17	206	−56	Sa	G4	+ 2,060	+ 1,913	1a	100	Observed by Hubble.
1332	24.1	−21 31	179	−53	S0	G2	+ 1,609	+ 1,507	1a	50	
1380	34.6	−35 9	202	−53	Sa	G5	+ 1,856	+ 1,706	1a	75	
1395	36.3	−23 11	183	−50	E2	G7	+ 1,690	+ 1,573	2a	40	
1399	36.6	−35 37	203	−52	E2	G4	+ 1,458	+ 1,302	1a	200	Observed by Hubble.
1404	36.9	−35 45	204	−52	E1	G4	+ 2,044	+ 1,885	1a	200	Observed by Hubble.
1400	37.3	−18 51	177	−49	E1	G4	+ 483	+ 379	2a	40	
1407	37.9	−18 44	177	−49	E0	G3	+ 1,811	+ 1,706	1a	50	
1415	38.8	−22 42	183	−50	Sa	F8*	+ 1,508	+ 1,388	1a	50	
1417	39.5	− 4 52	160	−42	Sb	G0	+ 4,101	+ 4,044	1a	50	
1426	40.6	−22 16	182	−50	E4	G4	+ 1,358	+ 1,241	1a	50	
* 342	41.9	+67 57	106	+11	Sc	F0"	− 10	+ 176	2b	20	Possible member of local group.
1439	42.6	−22 4	182	−49	E0	G2	+ 1,997	+ 1,878	1a	100	Lines are somewhat broad.
1441	43.2	− 4 15	160	−41	Sa	G5	+ 4,262	+ 4,202	1a	150	
1449	43.6	− 4 17	160	−41	S0	G3	+ 4,176	+ 4,116	1a	100	
1451	43.7	− 4 13	160	−41	E3	G5	+ 3,927	+ 3,867	1a	75	
1453	3 44.0	− 4 7	160	−41	E1	G0*	+ 3,919	+ 3,859	3a	40	
1521	4 6.1	−21 11	184	−43	E3	G5	+ 4,222	+ 4,060	1a	50	
1569	26.0	+64 45	111	+12	Irr	Em	− 34	+ 131	1b	30	Em patches. p. a. slit 112°. Observed by Mayall.
1587	28.1	+ 0 33	162	−29	E1	G2	+ 3,890	+ 3,812	1a	75	
1600	29.2	− 5 12	168	−32	E5	G7	+ 4,830	+ 4,728	1a	100	
1601	29.2	− 5 10	168	−32	S0	G5	+ 4,997	+ 4,895	1a	100	
Anon	38.1	+ 4 9	160	−25	Sa	G2	+ 4,600	+ 4,531	1a	50	Brightest neb in vicinity.
1637	38.9	− 2 57	167	−29	Sc	F8*	+ 695	+ 596	2a	50	Abs. lines are broad and shallow.
1700	4 54.5	− 4 56	171	−26	E3	G4	+ 3,976	+ 3,859	2a	40	Pease vel +800. Pease, F. G. 1918, Pub. A. S. P., 30, 255.

TABLE I. REDSHIFTS OF EXTRAGALACTIC NEBULAE. NON-CLUSTER OBJECTS

NGC *IC (1)	1950 R A (2)	Dec (3)	Gal Long (4)	Lat (5)	Type Neb (6)	Spec (7)	Redshift $c\Delta\lambda/\lambda_o$ (8)	Corr Redshift (9)	Plts Disp (10)	Est Error (11)	
							km/sec	km/sec		km/sec	
1832	5^h $9^m.9$	−15°46′	184°	−27°	Sb	G4	+ 2,037	+ 1,869	1a	200	Observed by Hubble.
1889	5 20.3	−11 32	181	−23	E0	G2	+ 2,472	+ 2,310	2a	40	
2146	6 10.7	+78 23	103	+26	Sap	F0"	+ 785	+ 965	1a	50	
2207	14.2	−21 21	196	−16	Sc	G1*	+ 2,680	+ 2,455	1a, 1b	60	p neb of close double. Abs. lines are weak.
2217	6 19.7	−27 13	202	−17	SBa	G2	+ 1,585	+ 1,345	1a	150	Observed by Hubble.
2314	7 3.8	+75 19	107	+28	E3	G5	+ 3,843	+ 4,005	3a	30	
2339	5.4	+18 52	165	+14	Sb	G0*	+ 2,361	+ 2,262	2a	40	Abs. lines somewhat broadened.
2300	16.5	+85 49	95	+28	E1	G5	+ 1,946	+ 2,150	3a	30	One plate by Minkowski.
2379	24.2	+33 55	153	+23	E0	G1	+ 4,030	+ 3,994	1a	65	
2403	32.0	+65 43	118	+30	Sc	F2*	+ 70	+ 187	5a	40	
2460	7 52.7	+60 31	124	+32	Sb	G2*	+ 1,442	+ 1,533	2a	50	
2532	8 7.0	+34 6	155	+32	Sc	F8*	+ 5,153	+ 5,111	1a	50	Abs. lines are weak and poorly defined.
2535	8.2	+25 22	165	+30	Sb	F5*	+ 4,243	+ 4,153	1a	75	Abs. lines are very weak.
2537	9.7	+46 9	141	+35	Sc	Em	+ 397	+ 415	2a, 1b	20	Brightest em patch np center.
2549	15.0	+57 58	127	+35	S0	G4	+ 1,082	+ 1,157	1a	75	Observed by Hubble.
2562	17.5	+21 18	170	+30	Sa	G5	+ 4,963	+ 4,852	1a	50	This and next one are members of a group.
2563	17.7	+21 14	170	+30	S0	G2	+ 4,775	+ 4,664	2a	50	
2613	31.2	−22 48	213	+12	Sb	G1	+ 1,710	+ 1,438	2a	40	
2608	32.2	+28 38	163	+36	Sa	F5	+ 2,119	+ 2,041	1a	100	
2623	35.4	+25 56	167	+35	SBc	A5*	+ 5,435	+ 5,342	2a	40	Observed by Minkowski as possible radio source.
2639	40.1	+50 23	136	+40	Sa	G5	+ 3,314	+ 3,350	1a	75	
2654	44.3	+60 28	123	+39	Sa	G5	+ 1,360	+ 1,450	1a	65	
2672	46.5	+19 16	175	+36	E1	G4	+ 4,223	+ 4,100	1a	100	
2673	46.6	+19 16	175	+36	E0	G3	+ 3,792	+ 3,669	1a	65	
2655	49.2	+78 25	102	+33	S0p	G1*	+ 1,299	+ 1,473	1a	65	
2683	49.6	+33 37	158	+40	Sb	G0*	+ 336	+ 285	1a	65	
2681	50.0	+51 30	134	+41	Sa	F8	+ 703	+ 748	1b	30	Observed by Hubble.
2685	52.2	+58 59	125	+40	S0p	G5*	+ 884	+ 961	1a, 1b	40	
2693	53.5	+51 33	134	+41	E2	G2	+ 4,956	+ 4,998	1a	50	
2694	53.5	+51 32	134	+41	E0	G4	+ 5,123	+ 5,165	1a	75	
2716	55.0	+ 3 17	194	+31	Sa	G1	+ 3,537	+ 3,342	1a	50	
Anon	55.3	+ 3 23	194	+31	Sb	F5*	+30,403	+30,208	1a	50	For this and next one see note 4 at end of table.
Anon	55.4	+ 3 21	194	+31	Sa	F8*	+20,575	+20,380	1a	50	
2712	56.2	+45 6	143	+42	SBb	G1	+ 1,840	+ 1,849	1a	200	Abs. lines shallow and not well defined.
2723	8 57.7	+ 3 23	194	+31	S0	G2	+ 3,725	+ 3,530	1a	65	
2744	9 1.8	+18 40	178	+39	Sb	F8"	+ 3,450	+ 3,325	1a	50	Abs. lines are very weak.
2749	2.5	+18 31	178	+39	E2	G0*	+ 4,203	+ 4,076	2a	40	Abs. lines are wide and rather shallow.
2775	7.7	+ 7 15	191	+35	Sa	G3	+ 1,135	+ 958	1a	75	
2768	7.8	+60 15	122	+42	S0	G5	+ 1,408	+ 1,497	1a	175	
2782	11.0	+40 19	149	+45	Sa	F0"	+ 2,517	+ 2,502	1a, 1b	20	λ3727 strong. Lines show rotational inclination.
2811	13.9	−16 6	214	+23	Sa	G3	+ 2,514	+ 2,256	1a	75	Observed by Hubble.
2798	14.4	+42 10	147	+46	SBa	F5"	+ 1,708	+ 1,699	1a	75	
2787	14.9	+69 25	111	+39	SBa	G5	+ 639	+ 768	2a	40	
Anon	15.7	−11 53	211	+26	S0	F5*	+16,160	+15,914	1a	60	Observed by Minkowski as possible radio source.
2831	16.8	+33 59	159	+46	E1	G5	+ 5,155	+ 5,104	1a	65	This and next one are members of a group.
2832	16.8	+33 59	159	+46	E2	G0	+ 6,946	+ 6,895	2a	50	
2841	18.6	+51 12	134	+45	Sb	G0*	+ 584	+ 625	2a, 1b	40	
2855	19.1	−11 41	212	+27	S0	G3*	+ 1,908	+ 1,652	2a	50	One plate by Hubble, one by Minkowski.
2865	21.2	−22 58	221	+20	E4	G2	+ 2,714	+ 2,441	1a	75	Observed by Hubble.
2859	21.3	+34 44	158	+47	SB0	G3	+ 1,694	+ 1,649	1a	100	
2880	25.7	+62 44	118	+43	SB0	G4	+ 1,514	+ 1,616	1a	50	
2903	29.3	+21 44	177	+46	Sc	F0*	+ 642	+ 531	1a	65	
2911	31.0	+10 22	191	+42	S0p	F8*	+ 3,140	+ 2,978	1a	75	Abs. lines broad and not well defined.
2914	31.4	+10 20	191	+42	Sa	F8	+ 3,370	+ 3,208	1a	100	
.2950	39.0	+59 5	122	+46	SB0	G2	+ 1,430	+ 1,512	1a	50	
2964	40.0	+32 5	162	+51	Sc	F5"	+ 1,340	+ 1,286	1a	50	Abs. lines are weak.
2974	40.0	− 3 29	208	+36	E4	G5*	+ 2,013	+ 1,797	1a	50	
2983	41.3	−20 14	223	+25	SBa	G5	+ 2,015	+ 1,748	1a	100	
2986	41.8	−21 3	223	+25	E2	G7	+ 2,397	+ 2,130	1a	100	
3003	9 45.6	+33 39	160	+52	Sb	F0*	+ 1,476	+ 1,428	2a	60	Abs. lines are weak.

TABLE I. REDSHIFTS OF EXTRAGALACTIC NEBULAE. NON-CLUSTER OBJECTS

NGC *IC (1)	1950 R A (2)	Dec (3)	Gal Long (4)	Gal Lat (5)	Type Neb (6)	Type Spec (7)	Redshift $c\Delta\lambda/\lambda_o$ (8) km/sec	Corr Redshift (9) km/sec	Plts Disp (10)	Est Error (11) km/sec	
2985	9^h $46^m.0$	+72°31'	106°	+39°	Sb	G3	+ 1,277	+ 1,424	1a	50	
3032	49.2	+29 28	168	+52	S0	G2	+ 1,568	+ 1,496	1a	150	Observed by Hubble.
3031	51.5	+69 18	109	+42	Sb	G3*	− 55	+ 77	2b	20	One plate by Hubble, one by Minkowski.
3034	51.9	+69 56	108	+41	Irr	A5	+ 263	+ 400	1b	75	Observed by Minkowski.
Anon	52.8	+ 8 37	197	+46	Pec	Em	+ 1,283	+ 1,118	1a	100	Observed by Minkowski as possible radio source.
3067	55.4	+32 37	162	+54	Sb	F2*	+ 1,506	+ 1,452	2a	50	Abs. very shallow, spectrum almost continuous.
3078	9 56.2	−26 41	230	+22	E2	G0	+ 2,481	+ 2,203	1a	50	
3115	10 2.8	− 7 28	216	+38	E7	G5	+ 648	+ 423	1b, 1c	12	
Sex	8.7	− 4 28	215	+41	Irr	Em	+ 369	+ 156	1a	30	Em patch 1'.8 sf brightest star within limits of syst.
Sex	8.7	− 4 28	215	+41	Irr	Em	+ 371	+ 158	1a	30	Em very close to and nf above. Possible mem local gr.
3162	10.8	+22 59	179	+56	Sc	F5	+ 1,456	+ 1,363	1a	65	Abs. lines are weak. Observed by Minkowski.
3158	10.9	+39 1	150	+57	E3	G3	+ 7,024	+ 7,008	1a	50	Member of a group.
3166	11.2	+ 3 40	207	+47	Sa	G1*	+ 1,381	+ 1,201	1a	50	
3169	11.7	+ 3 43	207	+47	Sa	G5*	+ 1,281	+ 1,101	2a	60	Observed by Hubble.
3147	12.8	+73 39	103	+40	Sb	G7	+ 2,721	+ 2,874	1a	80	
3177	13.8	+21 23	182	+56	Sb	F8	+ 1,220	+ 1,118	1a	65	Abs. lines are not well defined.
3185	14.9	+21 56	181	+56	SBa	F5*	+ 1,241	+ 1,142	2a	65	Abs. lines weak, spectrum almost continuous.
3184	15.2	+41 40	145	+57	Sc	F3*	+ 443	+ 443	1a	100	Abs. lines weak, spectrum almost continuous.
3190	15.4	+22 5	181	+56	Sa	G3*	+ 1,319	+ 1,220	1b	60	Observed by Hubble.
3193	15.7	+22 9	181	+57	E2	G1	+ 1,371	+ 1,272	1a	50	
3222	19.8	+20 8	185	+57	SB0	G0	+ 5,577	+ 5,472	1a, 1b	40	One plate by Hubble.
3226	20.7	+20 9	185	+57	E1	G2*	+ 1,338	+ 1,233	4a	15	
3227	20.7	+20 7	185	+57	Sb	F3"	+ 1,111	+ 1,006	2b	20	Abs. lines are very weak. One plate by Hubble.
3245	24.5	+28 46	170	+60	S0	G2	+ 1,261	+ 1,198	1a, 1b	30	One plate by Hubble.
3254	26.5	+29 45	168	+60	Sb	G4*	+ 1,228	+ 1,168	1a	60	
3277	30.3	+28 47	170	+61	Sa	F5*	+ 1,460	+ 1,399	1a	75	Abs. lines are weak.
3301	34.2	+22 9	184	+61	Sa	G2*	+ 1,333	+ 1,241	1a	75	
3310	35.7	+53 46	123	+55	Sb	A8"	+ 1,039	+ 1,104	1a	30	Abs. lines are weak and shallow.
3344	40.8	+25 11	178	+63	Sc	F5*	+ 579	+ 504	1a	150	Abs. lines are broad and weak.
3351	41.3	+11 58	203	+58	SBb	F5	+ 688	+ 553	1a	200	
3348	43.4	+73 6	101	+42	E0	G5	+ 2,855	+ 3,011	1a	75	
3367	44.0	+14 1	200	+59	SBc	F5*	+ 2,879	+ 2,753	1a	100	Observed by Minkowski.
3368	44.1	+12 5	203	+58	Sa	G0	+ 927	+ 792	1b	40	Observed by Hubble.
3377	45.1	+14 15	200	+60	E6	G2	+ 718	+ 595	2a	40	
3379	45.2	+12 51	203	+59	E0	G7	+ 862	+ 730	1b	30	Observed by Hubble.
3384	45.7	+12 54	203	+59	SB0	G5	+ 781	+ 649	1a, 1b	30	
3412	48.3	+13 41	202	+60	SB0	G0	+ 861	+ 735	1a	75	
3414	48.6	+28 14	172	+65	SB0	G5	+ 1,449	+ 1,392	1a	100	
Anon	55.4	+57 3	115	+55	E1	G3	+19,150	+19,237	1a	100	See note 5 at end of table.
3486	57.7	+29 15	170	+67	Sc	G3	+ 1,116	+ 1,065	1a	100	
3489	10 57.7	+14 10	204	+62	S0p	G0*	+ 692	+ 572	1a	65	
3504	11 0.5	+28 15	173	+68	SBb	F3"	+ 1,513	+ 1,459	1a	50	Abs. lines are broad and shallow.
Anon	1.0	+41 5	141	+65	Pec	Em	+10,346	+10,355	1a	60	Observed by Minkowski as possible radio source.
3521	3.3	+ 0 14	225	+54	Sb	G3	+ 789	+ 615	1b	30	
3516	3.4	+72 50	99	+43	SB0	F0	+ 2,614	+ 2,770	1b	50	Observed and measured by Seyfert.
3556	8.6	+55 57	114	+57	Sc	F0"	+ 636	+ 720	1a	75	Abs. lines are broad and shallow.
3585	10.9	−26 29	246	+31	E6	G3	+ 1,491	+ 1,233	1a	75	Observed by Hubble.
3593	12.0	+13 5	210	+64	S0p	F5*	+ 547	+ 427	1a	75	Abs. lines are weak and not well defined.
3605	14.2	+18 17	200	+68	E4	G3	+ 693	+ 600	1a	65	
3607	14.3	+18 19	200	+68	S0	G3	+ 951	+ 858	2a	40	
3608	14.4	+18 26	200	+68	E1	G0	+ 1,210	+ 1,117	1a	50	
3611	14.9	+ 4 50	223	+59	Sa	F5*	+ 1,754	+ 1,602	1a	75	Abs. lines are weak.
3610	15.6	+59 4	109	+55	SB0	G2	+ 1,765	+ 1,867	1a	50	This and next one are members of UMa cld.
3613	15.7	+58 17	110	+56	E5	G3	+ 2,054	+ 2,150	1a	75	
3623	16.3	+13 22	211	+65	Sa	G0*	+ 705	+ 588	1a	50	
3619	16.5	+58 2	110	+56	S0	G3*	+ 1,649	+ 1,745	1a	75	Member of UMa cld. Observed by Minkowski.
3626	17.5	+18 38	200	+69	Sa	G0	+ 1,452	+ 1,362	1a	100	
3627	17.6	+13 16	212	+66	Sb	G2	+ 744	+ 633	1b	50	Observed by Hubble.
3640	18.5	+ 3 31	226	+58	E2	G4	+ 1,354	+ 1,198	2a	40	
3642	11 19.5	+59 21	108	+55	Sb	G0*	+ 1,623	+ 1,727	1a	50	Member of UMa cld.

TABLE I. REDSHIFTS OF EXTRAGALACTIC NEBULAE. NON-CLUSTER OBJECTS

NGC *IC (1)	1950 R A (2)	1950 Dec (3)	Gal Long (4)	Gal Lat (5)	Type Neb (6)	Type Spec (7)	Redshift $c\Delta\lambda/\lambda_0$ (8)	Corr Redshift (9)	Plts Disp (10)	Est Error (11)	
							km/sec	km/sec		km/sec	
3665	11h 22.0	+39° 2'	140°	+70°	S0	G1	+ 2,002	+ 2,011	1a	50	This and next one are members of UMa cld.
3675	23.4	+43 52	129	+67	Sb	G2	+ 688	+ 721	2a	40	
3681	23.9	+17 9	206	+69	Sb	G3	+ 1,314	+ 1,221	1a	65	
3684	24.6	+17 18	206	+69	Sc	F0	+ 1,422	+ 1,329	1a	75	Abs lines are rather broad.
3686	25.1	+17 30	206	+69	Sb	F3"	+ 1,022	+ 929	1a	60	Both em and abs are weak.
3718	29.8	+53 21	113	+61	S0p	G0*	+ 1,050	+ 1,128	1a	100	Abs lines broad. This and next one members UMa cld.
3726	30.7	+47 19	121	+66	Sc	A8*	+ 948	+ 999	1a	75	
3810	38.4	+11 45	224	+68	Sc	G0	+ 972	+ 862	1a	65	
3818	39.4	− 5 53	243	+53	E5	G5	+ 1,498	+ 1,318	1a	65	Observed by Hubble.
3872	43.2	+14 3	222	+70	E3	G1	+ 3,109	+ 3,009	1a	75	
Anon	44.5	− 3 34	224	+55	SBb	F2"	+ 5,108	+ 4,940	1a	50	sp of 3. Wild connecting triple system.
Anon	44.7	− 3 34	224	+55	Sb	?"	+ 5,008	+ 4,840	1a	50	Brightest and middle of 3.
Anon	44.8	− 3 35	224	+55	Sc	F0"	+ 5,396	+ 5,228	1a	75	nf of 3.
3893	46.1	+49 0	113	+66	Sc	F2"	+ 1,042	+ 1,108	2a	40	This and next one are members of UMa cld.
3898	46.6	+56 22	105	+60	Sa	G5*	+ 1,038	+ 1,134	1a	75	
3900	46.6	+27 17	179	+78	Sa	G1	+ 1,702	+ 1,666	1a	50	
3904	46.7	−29 2	256	+32	E2	G3	+ 1,613	+ 1,376	1a	75	
3923	48.5	−28 33	256	+32	E4	G5	+ 1,788	+ 1,551	1a	65	
3941	50.3	+37 16	136	+76	SB0	G7	+ 972	+ 984	1a	50	This and next three are members of UMa cld.
3945	50.7	+60 57	101	+56	SB0	G3	+ 1,220	+ 1,337	1a	75	
3949	51.1	+48 8	113	+67	Sc	G0	+ 681	+ 744	1a	150	
3953	51.2	+52 37	107	+63	SBb	G3	+ 938	+ 1,022	2a	50	
3962	52.1	−13 42	252	+47	E1	G2*	+ 1,794	+ 1,599	1a	65	
3992	55.0	+53 39	105	+63	SBb	G4	+ 1,059	+ 1,146	1a	100	This and next three are members of UMa cld.
3998	55.4	+55 44	104	+61	S0	G1*	+ 1,109	+ 1,205	1a	50	λ3727 very strong.
4026	56.9	+51 14	107	+65	S0	G5	+ 878	+ 956	1a	75	
4036	58.9	+62 10	99	+55	S0	G2*	+ 1,382	+ 1,506	2a	50	
4038	59.5	−18 36	256	+43	Sc	F0*	+ 1,673	+ 1,469	1a	75	Observed by Minkowski as possible radio source.
4039	11 59.5	−18 37	256	+43	Sc	F5*	+ 1,660	+ 1,456	2a	50	Forms pair with above. One plate by Minkowski.
4051	12 0.6	+44 48	113	+71	Sb	A5"	+ 627	+ 679	2b	20	This and next one are members of UMa cld.
4102	3.8	+52 59	103	+64	Sa	F8*	+ 908	+ 996	1a	50	
4105	4.1	−29 30	260	+32	E2	G5*	+ 1,895	+ 1,664	1a	50	
4106	4.2	−29 31	260	+32	SB0	G7*	+ 2,178	+ 1,947	1a	50	
4111	4.5	+43 21	114	+72	S0	G3*	+ 784	+ 832	1b, 1c	15	This and next one are members of UMa cld.
4125	5.6	+65 27	96	+52	E6	G5	+ 1,305	+ 1,445	2a	50	
4136	6.7	+30 12	160	+82	Sc	F8*	+ 445	+ 433	1a	50	
4138	7.0	+43 57	111	+72	Sa	G2	+ 1,039	+ 1,092	1a	100	This and next one are members of UMa cld.
4143	7.1	+42 49	113	+73	SB0	G5	+ 784	+ 830	1a	100	
4150	8.0	+30 41	157	+82	S0	G2*	+ 244	+ 235	1a	50	
4151	8.0	+39 41	119	+76	Sa	A8"	+ 960	+ 990	3	8	Member of UMa cld. See note 6 at end of table.
4203	12.6	+33 29	136	+81	SB0	G3	+ 1,001	+ 1,009	1a	150	
4214	13.1	+36 36	123	+79	Irr	Em	+ 295	+ 317	1a	30	Bright em patch at center.
4220	13.7	+48 10	103	+69	Sa	G2	+ 979	+ 1,051	1a	50	Abs lines weak. Member of UMa cld.
4245	15.1	+29 53	157	+84	SBa	G0	+ 890	+ 882	1a	65	Abs lines weak.
4251	15.6	+28 27	171	+84	S0	G3	+ 1,014	+ 998	1a	75	
4258	16.5	+47 35	102	+69	Sb	G0"	+ 420	+ 494	1b	40	Observed by Hubble. Member of UMa cld.
4274	17.3	+29 54	160	+84	Sa	G3	+ 767	+ 758	1a	150	
4278	17.6	+29 34	160	+84	E1	G5*	+ 624	+ 615	2a	40	
4283	17.8	+29 35	159	+84	E0	G8	+ 1,071	+ 1,062	1b	65	Observed by Hubble.
4291	18.1	+75 40	92	+42	E2	G3	+ 1,785	+ 1,963	1a	50	
4314	20.0	+30 10	152	+85	SBa	G2	+ 883	+ 880	1a	85	
4414	24.0	+31 30	136	+85	Sc	G2	+ 715	+ 718	1a	100	
4448	25.8	+28 54	162	+86	Sb	G2*	+ 693	+ 687	1a	65	
4449	25.8	+44 22	100	+73	Irr	F0"	+ 206	+ 268	1a	50	Spectrum of bright central part.
4490	28.2	+41 55	101	+76	Sc	A5*	+ 625	+ 675	1a, 1b	50	Abs lines somewhat broadened.
4494	28.9	+26 3	207	+87	E1	G7	+ 1,333	+ 1,318	1a	65	
*3481	30.3	+11 40	259	+74	E3	G0	+ 7,086	+ 7,011	1a	80	np of 3. Zwicky connected system.
Anon	30.5	+11 40	260	+74	S0	F5*	+ 7,304	+ 7,229	1a	65	sf IC 3481, connected with. See note 7, end of table.
4565	33.9	+26 16	216	+87	Sb	G0	+ 1,223	+ 1,213	1a	100	
4589	12 35.5	+74 28	91	+42	E1	G5	+ 1,825	+ 2,003	1a	75	

TABLE I. REDSHIFTS OF EXTRAGALACTIC NEBULAE. NON-CLUSTER OBJECTS

NGC *IC (1)	1950 R A (2)	Dec (3)	Gal Long (4)	Gal Lat (5)	Type Neb (6)	Type Spec (7)	Redshift $c\Delta\lambda/\lambda_o$ (8)	Corr Redshift (9)	Plts Disp (10)	Est Error (11)	
							km/sec	km/sec		km/sec	
4631	$12^h\ 39^m.8$	+32°49'	97°	+85°	Sc	Em	+ 591	+ 611	1a	65	Brightest em patch 1!3 f center.
4725	48.0	+25 46	302	+88	Sb	G4	+ 1,114	+ 1,108	1a	65	
4736	48.5	+41 24	85	+76	Sb	G0*	+ 282	+ 345	1a	50	
4800	52.4	+46 48	85	+71	Sb	F8*	+ 746	+ 830	1a	50	Abs lines are shallow.
4814	53.3	+58 37	88	+59	Sb	G3	+ 2,531	+ 2,660	1a	65	
4826	54.3	+21 57	295	+83	Sb	G7*	+ 382	+ 364	1b	30	Observed by Hubble.
Anon	54.5	+32 42	63	+84	Pec	F8*	+13,418	+13,448	2a	50	Zwicky neb. Cont very weak. λ3727 strong.
4915	12 58.8	− 4 16	278	+58	E0	G5	+ 3,152	+ 3,036	2a	40	One plate by Minkowski.
5005	13 8.6	+37 20	62	+79	Sb	G0	+ 1,013	+ 1,069	1a	65	
5018	10.3	−19 15	279	+43	E4	G7	+ 2,897	+ 2,739	1a	75	
5033	11.2	+36 51	58	+78	Sc	Gi	+ 924	+ 987	1b	40	Observed by Hubble.
5049	13.3	−16 8	281	+46	S0	G2	+ 2,744	+ 2,600	1a	65	
5055	13.6	+42 18	69	+75	Sb	F8*	+ 500	+ 575	1b	30	
5077	16.9	−12 24	283	+49	E3	G2*	+ 2,647	+ 2,515	1a	100	
5087	17.8	−20 21	281	+41	S0	G2	+ 1,832	+ 1,675	1a	150	Observed by Hubble.
5128	22.4	−42 46	278	+19	Ep	F8*	+ 468	+ 261	2a	40	
5173	26.3	+46 50	69	+69	E0	G4*	+ 2,404	+ 2,506	1a	50	
5194	27.8	+47 27	69	+68	Sc	F8"	+ 438	+ 546	1a, 1b	35	One plate by Hubble.
5195	27.9	+47 31	69	+68	Ep	F5*	+ 542	+ 650	2a, 1b	35	One plate by Hubble.
5198	28.1	+46 56	69	+68	E1	G2	+ 2,482	+ 2,590	1a	50	
5236	34.2	−29 37	283	+31	Sc	F0"	+ 491	+ 319	1b	30	Observed by Hubble.
5248	35.0	+ 9 8	306	+68	Sc	F8	+ 1,176	+ 1,140	1a	50	
5253	37.1	−31 23	283	+29	Irr	Em	+ 432	+ 258	1a, 1b	30	One plate by Hubble.
5273	39.9	+35 54	38	+75	S0	F0"	+ 1,022	+ 1,095	1b	20	Abs lines very weak and narrow.
5308	45.4	+61 14	77	+55	S0	G5	+ 2,046	+ 2,206	1a	75	Observed by Hubble.
5322	47.6	+60 26	76	+55	E4	G8	+ 1,902	+ 2,063	1a	75	
5353	51.4	+40 32	47	+71	S0	G3	+ 2,188	+ 2,284	1a	65	
5363	53.6	+ 5 30	310	+62	Irr	G0*	+ 1,138	+ 1,102	1a	50	
5371	53.6	+40 44	46	+70	Sb	G3*	+ 2,551	+ 2,652	2a	40	
5364	53.7	+ 5 15	310	+62	Sc	G2	+ 1,393	+ 1,357	1a	150	
5377	54.3	+47 28	59	+66	Sa	F8*	+ 1,830	+ 1,951	1a	100	Abs lines broad and shallow.
5394	13 56.4	+37 41	38	+72	Sb	F0*	+ 3,558	+ 3,651	1a	100	Abs lines are very weak and shallow.
5448	14 1.0	+49 25	60	+64	Sa	G2*	+ 1,970	+ 2,102	1a	50	
5457	1.4	+54 35	67	+60	Sc	F8*	+ 247	+ 394	1a, 1b	30	One plate by Miller.
5461	1.9	+54 33	67	+60	Sc	Em	+ 298	+ 495	1a, 1b	30	Em patch in NGC 5457. One plate by Seyfert.
5473	3.0	+55 8	68	+59	SB0	G3	+ 1,976	+ 2,127	1a	50	
5485	5.5	+55 14	67	+59	S0	G5	+ 1,985	+ 2,136	1a	50	
5493	8.9	− 4 48	306	+51	Sa	G5	+ 2,627	+ 2,565	1a	75	Observed by Hubble.
Anon	9.8	+52 35	63	+60		F8*	+ 8,733	+ 8,880	1a	75	Observed by Minkowski as possible radio source.
5533	14.0	+35 35	28	+69	Sb	G0*	+ 3,781	+ 3,877	1a	60	
5548	15.7	+25 22	359	+69	Sa	F5"	+ 4,930	+ 4,990	1a, 1b	50	Em lines are broad, no abs. One plate by Hubble.
5557	16.4	+36 43	30	+68	E1	G3	+ 3,195	+ 3,297	1a	60	
5566	17.8	+ 4 11	318	+57	SBa	G5	+ 1,455	+ 1,436	1a	150	
5574	18.4	+ 3 28	318	+57	SB0	G0	+ 1,716	+ 1,694	1a	50	
5576	18.5	+ 3 30	318	+57	E4	G1	+ 1,528	+ 1,509	1a	100	Observed by Hubble.
5614	22.0	+35 5	25	+68	Sa	G4	+ 3,872	+ 3,969	1a	75	
5631	25.0	+56 48	65	+56	S0	G3*	+ 1,979	+ 2,144	1a	60	Observed by Seyfert.
5633	25.6	+46 22	49	+62	Sb	F5*	+ 2,316	+ 2,457	1a	50	Abs lines are narrow and weak.
5638	27.1	+ 3 27	320	+55	E1	G3	+ 1,677	+ 1,662	1a	50	
5672	30.5	+31 53	17	+66	Sb	F5*	+ 3,701	+ 3,797	1a	65	
5668	30.9	+ 4 40	323	+55	Sc	F0*	+ 1,780	+ 1,771	1a	50	Abs lines are weak.
5687	33.3	+54 42	62	+56	E3	G3	+ 2,119	+ 2,286	1a	75	Observed by Hubble.
5689	33.7	+48 58	52	+60	S0	G2	+ 2,205	+ 2,354	1a	50	
5713	37.7	− 0 5	320	+51	Sb	F2"	+ 1,870	+ 1,853	1a	100	Abs lines are not well defined.
5746	42.4	+ 2 10	324	+52	Sb	G2*	+ 1,789	+ 1,783	2a	40	
Anon	48.0	+26 23	4	+62	E0	G5	+35,084	+35,174	1a	60	s p one of faint pair.
Anon	48.0	+26 23	4	+62	E3	G5	+35,506	+35,596	1a	60	8" n of above neb.
5820	57.2	+54 5	56	+54	S0	G4	+ 3,269	+ 3,444	1a	60	Observed by Hubble.
5806	57.5	+ 2 5	327	+49	Sb	G0	+ 1,301	+ 1,307	1a	65	
5812	14 58.3	− 7 16	318	+42	E1	G7	+ 2,066	+ 2,039	1a	50	

TABLE I. REDSHIFTS OF EXTRAGALACTIC NEBULAE. NON-CLUSTER OBJECTS

NGC *IC (1)	1950 R A (2)	1950 Dec (3)	Gal Long (4)	Gal Lat (5)	Type Neb (6)	Type Spec (7)	Redshift $c\Delta\lambda/\lambda_0$ (8)	Corr Redshift (9)	Plts Disp (10)	Est Error (11)	
							km/sec	km/sec		km/sec	
5813	$14^h\ 58^m.7$	+ 1°54′	327°	+48°	E1	G5	+ 1,882	+ 1,890	1a	65	Observed by Hubble.
5831	15 1.6	+ 1 24	328	+48	E3	G5	+ 1,684	+ 1,696	1a	50	
5838	2.9	+ 2 18	329	+48	S0	G2	+ 1,427	+ 1,441	1a	50	
5846	4.0	+ 1 48	329	+47	E0	G0*	+ 1,768	+ 1,782	1a	50	Abs lines broad and shallow.
Anon	4.0	+ 1 47	329	+47	E2	G2	+ 2,278	+ 2,292	1a, 1b	40	40″ s of NGC 5846.
5850	4.6	+ 1 44	329	+47	SBb	G4*	+ 2,319	+ 2,333	1a	50	
5866	5.1	+55 57	58	+52	S0	G2*	+ 740	+ 924	2a	40	λ3727 very weak.
5857	5.2	+19 47	354	+57	Sb	G2	+ 4,616	+ 4,695	1a	150	
5854	5.3	+ 2 45	330	+48	SBa	G1	+ 1,626	+ 1,644	1a	65	
5859	5.3	+19 46	354	+57	Sb	G0	+ 4,664	+ 4,743	1a	150	
5879	8.5	+57 11	59	+51	Sb	F8*	+ 876	+ 1,064	1a	65	
5878	11.0	−14 5	315	+35	Sb	G8	+ 2,111	+ 2,068	1a	65	
5899	13.3	+42 14	35	+56	Sb	F5″	+ 2,549	+ 2,706	1a	50	
5907	14.6	+56 31	58	+51	Sb	G3	+ 553	+ 741	1a	75	This and next three observed by Hubble.
5898	15.3	−23 55	309	+27	E0	G2	+ 2,304	+ 2,231	1a	200	
5903	15.7	−23 51	309	+27	E2	G3	+ 2,612	+ 2,539	1a	150	
5921	19.5	+ 5 15	336	+46	SBb	G0	+ 1,389	+ 1,430	1a	150	
5962	34.2	+16 46	354	+49	Sc	G0	+ 1,993	+ 2,089	1a	75	
5970	36.1	+12 20	348	+47	SBb	F8	+ 2,034	+ 2,115	2a	50	
5982	37.6	+59 31	59	+46	E4	G7	+ 2,864	+ 3,071	10a	10	
5985	38.6	+59 30	59	+47	Sb	G0*	+ 2,467	+ 2,674	2a	40	
6015	50.7	+62 28	62	+44	Sc	F8*	+ 646	+ 860	1a	50	
6027(a)	57.0	+20 54	2	+45	Sa	G2	+ 4,031	+ 4,159	1a	50	This and 6027(d) members of Seyfert group.
6027(d)	15 57.0	+20 54	2	+45	Sc	G2	+ 4,415	+ 4,543	1a	50	
6070	16 7.4	+ 0 50	340	+34	Sc	F8	+ 2,091	+ 2,157	1a	125	
6181	30.1	+19 56	4	+38	Sc	G2	+ 2,158	+ 2,307	1	250	Dispersion used 1000 A/mm.
6217	34.8	+78 18	78	+33	Sc	F8″	+ 1,386	+ 1,617	1b	30	Observed and measured by Seyfert.
6207	41.3	+36 55	26	+40	Sc	F8″	+ 869	+ 1,073	1a	40	λ3727 is very strong.
Anon	16 48.2	+45 33	38	+38	S0	G3*	+ 9,386	+ 9,608	1a	50	Zwicky connecting triple system. Brighter of 3.
6340	17 11.1	+72 22	70	+33	Sa	G3	+ 2,109	+ 2,351	1	300	Dispersion used 1000 A/mm.
6359	17.4	+61 50	58	+34	E1	G5	+ 2,948	+ 3,197	1b	75	
6384	30.0	+ 7 6	358	+19	Sb	G5	+ 1,784	+ 1,940	1a	50	
6478	47.5	+51 11	45	+30	Sc	G2	+ 6,857	+ 7,113	1a	50	
6482	17 49.8	+23 5	16	+22	E3	G0	+ 3,922	+ 4,138	2a	60	
6574	18 9.6	+14 58	10	+14	Sb	F8*	+ 2,355	+ 2,559	2a	50	
6627	20.4	+15 39	11	+12	SBb	G0*	+ 5,206	+ 5,416	1a	100	
6643	21.2	+74 33	72	+28	Sb	G0*	+ 1,494	+ 1,748	1a	50	
6658	31.9	+22 50	19	+13	S0	G0*	+ 4,270	+ 4,507	1a	50	
6661	32.5	+22 52	19	+12	S0	G7	+ 4,370	+ 4,607	1a	50	
6674	36.5	+25 20	22	+13	SBb	G5	+ 3,502	+ 3,747	1a	50	
6702	45.5	+45 39	42	+19	E2	G3	+ 4,749	+ 5,025	1a	65	
6703	45.9	+45 30	42	+19	S0	G3	+ 2,316	+ 2,592	2a	40	
6710	18 48.6	+26 46	25	+11	Sa	G5	+ 4,556	+ 4,811	2a	50	
*1302	19 29.0	+35 39	36	+ 7	Sb	F8*	+ 4,575	+ 4,857	1a	50	Member of a group.
6814	40.0	−10 26	357	−17	Sb	F0″	+ 1,437	+ 1,590	1a	40	Abs lines are weak.
6822	42.1	−14 53	353	−20	Irr	Em	− 34	+ 98	2b	20	Em V, Plate II, Hubble, E., 1925, Ap. J., 62, 409.
*1308	42.3	−14 51	353	−20	Irr	Em	− 30	+ 102	1b	30	In 6822 a member of local group.
6824	42.6	+55 59	56	+15	Sb	G0*	+ 3,386	+ 3,676	1a, 1b	30	
Anon	19 57.7	+40 35	44	+ 5	?	Em″	+16,804	+17,098	5a	30	Obs, measured by Minkowski as radio source.
6921	20 26.4	+25 33	35	− 9	Sa	G0*	+ 4,317	+ 4,596	2a	40	
Anon	30.2	+ 9 42	22	−18	E7	G5	+ 4,419	+ 4,659	1	250	Dispersion 1000 A/mm. This and next 3 in group.
6927	30.2	+ 9 43	22	−18	S0	G3	+ 4,277	+ 4,517	1a	50	Anon above is 2′.0 sp 6927.
6928	30.4	+ 9 45	22	−18	Sa	G0	+ 4,754	+ 4,994	1a	75	
6930	30.6	+ 9 41	22	−19	Sb	G3*	+ 4,182	+ 4,419	1a	75	
6946	33.9	+59 58	63	+11	Sc	F5*	+ 38	+ 330	2a	50	Possible member local group.
6946	34.1	+59 59	63	+11	Sc	Em	− 70	+ 222	1b	25	Em patch 4′.1 nf nucleus of 6946.
6944	35.9	+ 6 49	20	−21	E1	G3	+ 4,375	+ 4,604	3a	40	
6954	41.6	+ 3 1	18	−24	Sb	F5	+ 4,011	+ 4,231	1a	100	Abs lines somewhat broad and shallow.
6962	44.7	+ 0 8	15	−27	Sb	G0*	+ 4,183	+ 4,387	1a	75	
6963	20 44.8	+ 0 20	16	−27	E0	G0	+ 4,351	+ 4,555	1a	50	

TABLE I. REDSHIFTS OF EXTRAGALACTIC NEBULAE. NON-CLUSTER OBJECTS

NGC *IC (1)	1950 R A (2)	1950 Dec (3)	Gal Long (4)	Gal Lat (5)	Type Neb (6)	Type Spec (7)	Redshift $c\Delta\lambda/\lambda_0$ (8)	Corr Redshift (9)	Plts Disp (10)	Est Error (11)	
							km/sec	km/sec		km/sec	
6964	20^h $44^m.8$	+ 0° 7'	15°	−27°	E4	G2	+ 3,832	+ 4,036	1a	100	
Anon	58.5	+16 7	32	−20	E1	G5	+ 9,148	+ 9,408	1	250	Dispersion 1000 A/mm. 11'.6 np NGC 7006.
Anon	58.8	+15 56	32	−20	Sa	G5	+11,255	+11,515	1a	50	6'.8 sp NGC 7006.
Anon	20 59.6	+15 56	32	−20	S0	G3	+11,965	+12,225	1a	50	7'.9 sf NGC 7006.
7171	21 58.3	−13 31	12	−49	Sb	G0	+ 2,632	+ 2,776	1a	50	
7177	58.3	+17 29	44	−30	Sb	G0*	+ 1,105	+ 1,360	1a	75	
7217	22 5.6	+31 7	55	−20	Sb	G7*	+ 911	+ 1,192	2a, 1b	30	
Anon	13.2	+37 2	60	−16	S0	G0	+ 5,984	+ 6,272	1a	75	3'.6 sp NGC 7242. May be 7240.
7242	13.5	+37 3	60	−16	E3	F8	+ 5,684	+ 5,972	1a	100	Brightest of small group, v small neb. 0'.5 nf.
7252	18.0	−24 56	356	−58	S0	F3*	+ 4,733	+ 4,815	1a	65	
7302	29.7	−14 23	16	−56	S0	G7	+ 2,586	+ 2,716	1a	65	
7314	33.0	−26 18	355	−61	Sc	F8"	+ 1,766	+ 1,838	1a	50	
7317	33.6	+33 41	61	−21	E4	G5	+ 6,736	+ 7,014	1a	65	This and next three members of a group.
7318(a)	33.7	+33 42	61	−21	E2	G5	+ 6,638	+ 6,916	2a	50	p one of double neb.
7318(b)	33.7	+33 42	61	−21	SBb	G5	+ 5,638	+ 5,916	3a	40	f of pair.
7319	33.8	+33 43	61	−21	SBb	G0"	+ 6,657	+ 6,935	1a	50	
7331	34.8	+34 9	62	−21	Sb	G8*	+ 780	+ 1,058	3a, 1b	20	
7332	35.0	+23 32	56	−30	S0	G3	+ 1,204	+ 1,464	1a	50	
7335	35.0	+34 11	62	−20	Sa	G5	+ 6,298	+ 6,576	1a	60	Probably member of group near NGC 7318(above).
7343	36.4	+33 48	62	−22	E3	G2	+ 1,216	+ 1,492	1a	200	Very poor value, redshift uncertain.
7377	45.1	−22 35	4	−63	S0p	G2	+ 3,416	+ 3,501	1a	65	
7385	47.4	+11 21	50	−41	E0	G1	+ 7,829	+ 8,054	1a	65	
7386	47.6	+11 26	50	−41	S0	G2	+ 7,198	+ 7,423	1a	65	
*1460	54.5	+ 4 25	47	−49	S0	F5*	+ 7,262	+ 7,457	1a	75	
7448	57.6	+15 43	56	−40	Sc	G2	+ 2,419	+ 2,649	1	250	Dispersion used 1000 A/mm.
7457	22 58.6	+29 53	65	−27	S0	G2	+ 525	+ 788	1	250	Dispersion used 1000 A/mm.
7469	23 0.7	+ 8 36	52	−46	Sa	F5"	+ 4,780	+ 4,988	1b	40	Observed and measured by Seyfert. Broad em.
7479	2.4	+12 3	55	−43	SBb	G3*	+ 2,492	+ 2,711	1a	65	
7507	9.4	−28 49	351	−70	E0	G5	+ 1,637	+ 1,684	1a	75	
7541	12.2	+ 4 16	52	−51	Sc	F2	+ 2,672	+ 2,860	1a	100	Abs lines are poor.
7576	14.8	− 5 0	43	−59	Sa	G2	+ 3,616	+ 3,766	2a	50	One plate by Hubble.
7585	15.4	− 4 55	44	−59	S0p	G0	+ 3,333	+ 3,485	1a	65	
7600	16.3	− 7 51	40	−62	E5	G3	+ 3,391	+ 3,527	1a	60	
7606	16.5	− 8 46	39	−62	Sc	G2	+ 2,341	+ 2,477	1a	75	
7611	17.1	+ 7 47	57	−49	S0	G7	+ 3,383	+ 3,579	1a	65	This and next four members of a group.
7617	17.6	+ 7 53	57	−49	S0	G3	+ 4,072	+ 4,268	1a	150	
7619	17.8	+ 7 56	57	−49	E3	G5	+ 3,757	+ 3,953	1a	50	
7623	18.0	+ 8 7	57	−49	E4	G3	+ 3,463	+ 3,659	1a	65	
7626	18.2	+ 7 56	57	−49	E1	G3	+ 3,357	+ 3,553	1a	50	
7625	18.0	+16 57	63	−41	S0	G1*	+ 1,706	+ 1,930	1a	100	
7678	26.1	+22 9	68	−37	Sc	F5"	+ 3,446	+ 3,676	1a	65	
7679	26.2	+ 3 14	56	−54	S0	F5*	+ 5,202	+ 5,378	2a	40	
7716	33.9	+ 0 1	56	−58	Sb	G8	+ 2,546	+ 2,705	1a	150	
7727	37.3	−12 34	41	−69	Sa	G8*	+ 1,839	+ 1,943	3a	30	
Anon	39.3	− 3 54	55	−62	Sc	G3	+ 6,777	+ 6,918	1a	60	Zwicky connecting pair. 6'.8 sf IC 1505.
Anon	39.5	− 3 50	55	−62	Sb	F5"	+ 7,016	+ 7,157	1a	60	nf of pair. 5'.8 sf IC 1505.
7741	41.4	+25 48	73	−34	SBc	F2	+ 729	+ 965	1a	50	Abs lines weak.
7742	41.8	+10 29	67	−49	Sb	G0*	+ 1,629	+ 1,821	2a	40	
7743	41.8	+ 9 39	66	−50	SBa	G0*	+ 1,802	+ 1,991	2a	65	
7785	52.8	+ 5 38	68	−55	E5	G5	+ 3,846	+ 4,014	1a	65	
7793	55.9	−32 51	330	−79	Sc	F5	+ 286	+ 292	2a	200	Observed and measured by Hubble.
WLM	23 59.2	−15 43	48	−74	Irr	F5	− 78	+ 3	3a, 1b	20	Possible member local group. See note 8.

NOTES TO TABLE I

1. A very faint field nebula. Not a member of Cl 0025 +2223. Object No. 9 on identification chart No. 1.
2. The previously published velocity of +2600 km/sec in Mt. W. Contr. 531 is an error.
3. Two very faint field nebulae. First one is No. 1, second one is No. 2 on chart No. 2.
4. Two very faint field nebulae. Not members of Cl 0855 +0321. First one is No. 10, second one No. 11 on chart No. 7.
5. A faint field nebula. Not a member of Cl 1055 + 5702. Object No. 1 on chart No. 9.
6. Emission bands in NGC 4151 measured to determine constancy of $\Delta\lambda/\lambda$ for nebular redshifts. Wilson, O. C. 1949, Pub. A. S. P., 61, 132.
7. Zwicky believes IC3483 also connected with this pair. The discrepancy in the velocities, however, indicates that 3483 is a member of the Virgo Cl and not physically connected with this pair. See Table 2 for redshift of 3483.
8. Wolf-Lundmark-Melotte system. Redshift is the mean from 2 em patches n of center and cluster p center.

TABLE II. REDSHIFTS FROM BRIGHT NEBULAE IN CLUSTERS

NGC *IC (1)	1950 RA (2)	1950 Dec (3)	Gal Long (4)	Gal Lat (5)	Type Neb (6)	Type Spec (7)	Redshift $c\Delta\lambda/\lambda_0$ (8)	Corr Redshift (9)	Plts Disp (10)	Est Error (11)	
	PERSEUS CLUSTER						km/sec	km/sec		km/sec	
1270	$3^h\ 15^m.6$	+41°18'	118°	−12°	E3	G4	+ 4,905	+ 5,038	2a	65	
1273	16.1	+41 22	118	−12	E1	G2	+ 5,354	+ 5,487	1a	50	
1275	16.5	+41 20	118	−12	Irr	?"	+ 5,160	+ 5,293	2b	40	Neb. type Sc + Sb? Wide em bands. Radio source.
1277	16.6	+41 24	119	−12	E4	G3	+ 4,974	+ 5,104	1a	50	
1278	3 16.6	+41 23	119	−12	E1	G3	+ 6,115	+ 6,245	2a	50	
	VIRGO CLUSTER										
4179	12 10.3	+ 1 35	252	+63	E7	F8	+ 1,279	+ 1,149	1a	50	
4192	11.3	+15 11	238	+75	Sb	G0*	− 124	− 202	2a	40	Pease vel (+1150) in Mt. W. Contr. 426 is an error.
4216	13.4	+13 25	242	+74	Sb	G3	+ 32	− 49	1a, 1b	40	
4254	16.3	+14 42	244	+75	Sc	G2	+ 2,485	+ 2,408	1a	50	
4261	16.8	+ 6 6	253	+68	E3	G7	+ 2,202	+ 2,094	1a	75	
4267	17.2	+13 3	247	+74	SB0	G3	+ 1,260	+ 1,179	1a	75	
4270	17.3	+ 5 45	254	+67	E7	G5	+ 2,347	+ 2,236	1a	50	
4273	17.4	+ 5 37	254	+67	Sc	F5"	+ 2,302	+ 2,191	2a	40	Abs lines are weak.
4281	17.8	+ 5 40	254	+67	S0	G3	+ 2,602	+ 2,492	1a	50	
4303	19.4	+ 4 45	255	+66	Sc	G1	+ 1,671	+ 1,557	1a	150	
4321	20.4	+16 6	245	+77	Sc	F5	+ 1,617	+ 1,551	1a	75	
4324	20.6	+ 5 31	256	+67	Sa	G5	+ 1,714	+ 1,605	1a	50	
4339	21.0	+ 6 22	256	+68	E0	G3	+ 1,278	+ 1,173	1a	100	
4343	21.1	+ 7 16	255	+69	S0	G3	+ 714	+ 614	1a	50	20.'0 s p NGC 4365.
4350	21.4	+16 58	245	+78	S0	G5	+ 1,184	+ 1,122	1a	60	
4365	21.9	+ 7 36	255	+69	E2	G5	+ 1,171	+ 1,069	4a	30	
4374	22.5	+13 10	251	+75	S0	G5*	+ 954	+ 880	1a	50	
4382	22.9	+18 28	243	+80	S0	G5	+ 773	+ 721	1b	30	
4387	23.2	+13 5	252	+75	E4	G3	+ 511	+ 439	1a	65	
4394	23.4	+18 29	243	+80	SBb	G3	+ 772	+ 720	1a	150	
4406	23.7	+13 13	252	+74	E3	G7	− 374	− 452	1a	50	
4421	24.5	+15 44	250	+77	SBa	G3	+ 1,692	+ 1,628	1	250	Disp 1000 A/mm. Observed and measured by Sinclair Smith.
4425	24.7	+13 1	253	+75	Sa	G2	+ 1,883	+ 1,809	1a	50	
4429	24.9	+11 23	255	+72	S0	G3	+ 1,114	+ 1,027	1a	65	
4435	25.1	+13 21	253	+75	SB0	G5	+ 869	+ 796	1a	100	
4438	25.2	+13 17	253	+75	Sap	G3	− 32	− 105	1a	75	
4442	25.5	+10 5	256	+72	SB0	G5	+ 580	+ 493	1a	100	
4450	25.9	+17 21	249	+79	Sb	G3	+ 2,048	+ 1,995	1a	150	
4458	26.4	+13 31	254	+75	E0	G7	+ 383	+ 309	1	250	Disp 1000 A/mm. Observed and measured by Sinclair Smith.
4459	26.5	+14 15	254	+76	S0	G3	+ 1,111	+ 1,042	1a	75	
4461	26.5	+13 28	254	+75	S0	G5	+ 1,887	+ 1,813	2a	40	
4464	26.8	+ 8 26	258	+70	E3	G3	+ 1,199	+ 1,104	1a	50	
4467	27.0	+ 8 16	258	+70	E2	G5	+ 1,474	+ 1,379	1	300	Disp 1000 A/mm. Observed and measured by Sinclair Smith.
4472	27.2	+ 8 16	258	+70	E1	G7	+ 1,013	+ 918	1b	50	Observed by Hubble.
4473	27.3	+13 42	255	+76	E5	G7	+ 2,241	+ 2,173	1b	75	
4474	27.4	+14 21	255	+76	S0	G3	+ 1,526	+ 1,458	1a	50	
4477	27.5	+13 55	255	+76	SB0	G3	+ 1,263	+ 1,195	1a	75	
4478	27.8	+12 36	256	+75	E2	G5	+ 1,482	+ 1,410	1a	75	
4479	27.8	+13 51	255	+76	S0	F8	+ 822	+ 753	1a	100	Observed by Minkowski. Abs lines very weak.
Anon	27.9	+12 47	256	+75	E0	G5	+ 1,486	+ 1,414	1a	50	7.'3 n p NGC 4486.
4486	28.3	+12 40	256	+75	E0	G5*	+ 1,290	+ 1,218	4a, 2b	20	Two plates by Minkowski.
4492	28.4	+ 8 21	260	+70	Sa	G3	+ 1,735	+ 1,642	1a	200	
4501	29.5	+14 42	255	+78	Sc	G5	+ 2,120	+ 2,060	1a	100	
Anon	30.1	+ 9 27	260	+72	E0	G2	+ 1,317	+ 1,233	1	300	Disp 1000 A/mm. Obs, meas by S. Smith. 4.'8n, 3.'0p BD+9°2637.
*3483	30.6	+11 37	260	+74	Scp	G0*	+ 108	+ 33	2a	40	See note 7 at end of Table 1.
4526	31.5	+ 7 58	263	+70	S0	G4	+ 447	+ 357	1a	50	Abs lines somewhat wide and shallow.
4527	31.6	+ 2 56	263	+65	Sb	G2	+ 1,727	+ 1,615	1a, 1b	75	
4535	31.8	+ 8 28	262	+71	Sc	F0"	+ 1,930	+ 1,843	1c	20	Observed by Minkowski.
4546	32.9	− 3 31	265	+59	SB0	G3*	+ 1,014	+ 882	2a	40	Southern extension of Virgo Cluster.
4548	32.9	+14 46	260	+77	SBb	G5*	+ 433	+ 372	1a	50	
4550	33.0	+12 30	261	+75	E7	G3*	+ 350	+ 280	1a	50	
4551	33.1	+12 31	261	+75	E4	G5	+ 978	+ 908	1	300	Disp 1000 A/mm. Observed, measured by Sinclair Smith.
4552	33.1	+12 50	261	+76	E0	G7	+ 276	+ 210	1a	65	
4569	34.3	+13 26	262	+76	Sb	G0*	+ 960	+ 896	1a	50	Vel in Mt. W. Contr. 531 is that of a star projected on nucl.
4570	12 34.4	+ 7 31	264	+70	E7	G7	+ 1,730	+ 1,640	1a	75	

TABLE II. REDSHIFTS FROM BRIGHT NEBULAE IN CLUSTERS

NGC *IC (1)	1950 R A (2)	Dec (3)	Gal Long (4)	Lat (5)	Type Neb (6)	Spec (7)	Redshift $c\Delta\lambda/\lambda_0$ (8)	Corr Redshift (9)	Plts Disp (10)	Est Error (11)	
VIRGO CLUSTER (Cont'd)							km/sec	km/sec		km/sec	
4578	12^h $35^m.0$	+ 9°50'	264°	+72°	E2	G0	+ 2,282	+ 2,201	1a	50	
4579	35.0	+12 5	262	+74	Sb	G3	+ 1,752	+ 1,679	1a	150	
4594	37.4	-11 21	268	+51	Sb	G3*	+ 1,180	+ 1,021	1a	50	Southern extension of Virgo Cluster.
4621	39.5	+11 55	267	+73	E5	G7	+ 414	+ 339	1a	125	
4636	40.3	+ 2 57	269	+65	E0	G2*	+ 973	+ 867	1a	75	Abs lines somewhat wide and shallow.
4638	40.3	+11 43	268	+74	E6	G3	+ 1,080	+ 1,011	1a	150	
4649	41.1	+11 49	269	+74	E2	G7	+ 1,389	+ 1,321	1b	50	Observed by Hubble.
4660	42.0	+11 26	270	+74	E5	G2	+ 1,017	+ 950	1b	30	
4665	42.6	+ 3 20	270	+66	SBa	G3	+ 785	+ 684	1a	50	
4697	46.0	- 5 32	272	+57	E5	G4	+ 1,308	+ 1,177	1a	65	Southern extension of Virgo Cluster.
4698	46.0	+ 8 46	273	+71	Sa	G3*	+ 1,032	+ 955	1a	50	
4742	49.2	-10 12	273	+52	E4	G0	+ 1,321	+ 1,176	1a	50	Southern extension of Virgo Cluster.
4754	49.8	+11 35	276	+74	SB0	G4	+ 1,461	+ 1,398	1a	75	
4762	50.4	+11 30	277	+74	Sa	G2	+ 868	+ 805	2a	50	
4856	56.7	-14 46	275	+47	SBa	G5	+ 1,251	+ 1,095	1a	75	Southern extension of Virgo Cluster.
4866	12 57.0	+14 27	285	+75	Sa	G3*	+ 1,910	+ 1,862	2a, 1b	30	One plate by Minkowski.
4941	13 1.6	- 5 17	279	+57	Sa	F8"	+ 846	+ 729	1a	40	This and next one in southern extension of Virgo Cluster.
4958	13 3.2	- 7 45	279	+54	E7	G3	+ 1,515	+ 1,389	1a	75	
COMA CLUSTER											
4798	12 52.5	+27 41	360	+88	E3	G2	+ 7,673	+ 7,679	1a	50	
*3900	53.2	+27 32	355	+88	S0	G5	+ 7,171	+ 7,177	1a	50	
4850	55.8	+28 14	11	+87	S0	G2	+ 5,984	+ 5,996	1a	100	
4853	56.2	+27 52	3	+87	E1	G2	+ 7,550	+ 7,561	1b	50	Observed by Pease.
*3946	56.4	+28 5	7	+87	S0	G3	+ 6,101	+ 6,107	1a	75	
4860	56.5	+28 24	13	+87	E2	G3	+ 7,858	+ 7,870	1a, 1b	40	
Anon	56.7	+28 8	8	+87	E0	G4	+ 6,868	+ 6,880	1a	65	Very faint member 0!5 n f IC 3960.
4864	56.8	+28 15	10	+87	E1	G5	+ 6,819	+ 6,831	1a	125	
4865	56.8	+28 21	12	+87	E6	G4	+ 4,643	+ 4,655	1a, 1b	50	
4867	56.9	+28 16	10	+87	Sa	G2	+ 4,815	+ 4,827	1a	100	
4869	57.0	+28 11	9	+87	E3	G3	+ 6,703	+ 6,715	1a	100	
4872	57.2	+28 14	10	+87	E4	G5	+ 6,910	+ 6,923	1a	300	
4874	57.3	+28 14	10	+87	S0	G7	+ 7,171	+ 7,183	3a	30	p of two brightest, largest neb near center of cluster.
4881	57.5	+28 31	14	+87	E1	G3	+ 6,691	+ 6,703	1a	50	
4886	57.6	+28 15	10	+87	S0	G2	+ 6,214	+ 6,226	1a	150	
4889	57.7	+28 15	10	+87	E4	G2	+ 6,416	+ 6,428	2a	40	f of two brightest, largest neb near center of cluster.
*4021	57.8	+28 19	11	+87	E0	G3	+ 5,789	+ 5,804	1a	75	
4895	57.8	+28 28	13	+87	S0	G4	+ 8,406	+ 8,422	2a	75	
4896	57.9	+28 35	15	+87	S0	G2	+ 5,820	+ 5,836	1a	150	
4898	57.9	+28 13	9	+87	S0	G3	+ 6,935	+ 6,950	1a	50	
4908	58.4	+28 18	10	+86	E4	G3	+ 8,838	+ 8,853	1a	150	
*4045	58.4	+28 22	11	+86	E2	G5	+ 6,527	+ 6,542	1a	200	
*4051	12 58.5	+28 17	11	+86	E1	G5	+ 4,932	+ 4,947	1a	150	
HERCULES CLUSTER											
6041	16 2.3	+17 50	359	+43	S0	G0	+10,469	+10,592	1a	50	
6044	2.6	+18 1	359	+43	E0	G2	+ 9,936	+10,059	1a	50	
6045	2.7	+17 54	359	+43	Sb	G0	+ 9,935	+10,058	1a	50	
6047	2.8	+17 52	359	+43	E0	G5	+ 9,470	+ 9,593	1a	50	
*1183	3.3	+17 54	359	+43	E1	G3	+10,038	+10,161	1a	75	
*1185	3.5	+17 51	359	+43	Sa	G3	+10,452	+10,575	1a	200	
*1194	16 4.4	+17 55	359	+43	E1	G5	+11,642	+11,765	1a	65	
PEGASUS II CLUSTER											
7499	23 7.8	+ 7 20	53	-48	E5	G5	+11,916	+12,117	1a	50	
7501	7.9	+ 7 21	53	-48	E3	G5	+12,714	+12,915	1a	50	
7503	23 8.1	+ 7 18	53	-48	E1	G3	+13,229	+13,430	1a	65	

Tables I and II are alike in form and contain the following information.

Column 1. The NGC and IC numbers. The latter are indicated by an asterisk. Uncatalogued objects have been designated "anonymous." Their location with respect to known objects is given in the notes. Locations of the fainter objects are shown on identification charts, Plates I and II.

Columns 2, 3. The right ascensions and declinations for the equinox 1950 computed from the NGC.

Columns 4, 5. The galactic coordinates computed from the Lund Observatory tables (Ohls-

TABLE III. REDSHIFTS FROM FAINT NEBULAE IN CLUSTERS

Cluster (1)	Neb No. (2)	1950 R A (3)	1950 Dec (4)	Gal Long (5)	Gal Lat (6)	Redshift $c\Delta\lambda/\lambda_0$ (7)	Corr Redshift (8)	No. Plts (9)	Est Error (10)	Ident Chart (11)	
						km/sec	km/sec				
0025+2223	4	$0^h 24^m.7$	+22°23'	85°	−40°	+47,796	+47,994	1	75	1	48-inch Sky Survey cluster.
	8	24.9	+22 23			+47,479	+47,677	2	40		λ3727 appears in spectrum of No. 8.
0106−1536	1	1 6.3	−15 36	116	−77	+15,440	+15,473	1	60	3	Cluster Haufen A. 1 and 2 form a close pair.
	2	6.3	−15 36			+16,057	+16,090	1	60		Larger and n f one of pair.
0138+1840	1	1 37.9	+18 40	108	−42	+51,773	+51,908	1	75	4	48-inch Sky Survey cluster.
0348+0613	1	3 48.2	+ 6 10	150	−34	+25,662	+25,644	1	100	5	48-inch Sky Survey cluster. Cluster membership in doubt.
0705+3506	1	7 4.4	+35 8	150	+20	+23,690	+23,666	3	50	6	Gemini Cluster. No. 1 is Anon 3, No. 2 is
	2	5.0	+35 4			+23,089	+23,065	2	60		Anon 4 in Mt. W. Contr. 531.
0855+0321	1	8 55.1	+ 3 23	194	+31	+61,241	+61,046	1	100	7	Hydra Cluster.
	2	55.1	+ 3 23			+60,964	+60,769	1	50		λ3727 appears in spectrum of No. 2.
	8+9	55.3	+ 3 22			+60,959	+60,764	3	150		Redshift from the blended spectra of 8 and 9.
0925+2044	1	9 25.7	+20 45	178	+45	+57,612	+57,498	1	100	8	48-inch Sky Survey cluster.
1024+1039	1	10 24.4	+10 39	201	+54	+19,636	+19,489	2	50		Leo Cluster. Identification on Plate VIII, Mt. W. Contr. 426.
1055+5702	2	10 55.1	+57 2	116	+55	+39,914	+40,001	1	100	9	Ursa Major Cluster No. 2.
	3	55.7	+57 2			+41,631	+41,718	1	300		No. 3 is Anon 6 in Mt. W. Contr. 531.
1145+5559	48	11 44.5	+55 59	106	+60	+14,982	+15,076	1	50	10	Ursa Major Cluster No. 1. Baade numbers.
	25	44.7	+55 58			+14,688	+14,782	1	60		
	24	44.7	+56 1			+15,459	+15,553	2	50		No. 24 is Anon 7 in Mt. W. Contr. 531.
	7	45.8	+56 3			+15,572	+15,666	1	60		
1153+2341	1	11 53.3	+23 41	197	+78	+42,844	+42,796	1	100	11	48-inch Sky Survey cluster. 1 and 1A a close pair.
	1A	53.3	+23 41			+42,819	+42,771	1	100		Smaller, fainter, and n one of pair.
1228+1050	1	12 28.4	+10 50	258	+73	+50,402	+50,321	1	200	12	1 and 2 form a double. No. 1 is n p of pair.
	2	28.4	+10 50			+48,788	+48,707	1	200		No. 2 is s f of pair.
1239+1852	4	12 38.7	+18 51	264	+81	+21,094	+21,052	2	50	13	
	5	38.8	+18 52			+22,056	+22,014	1	75		
1253+4422	2	12 53.9	+44 20	83	+73	+59,304	+59,382	1	40	14	48-inch Sky Survey cluster. λ3727 present.
1304+3110	1+1A	13 3.5	+31 9	38	+84	+54,887	+54,917	1	100	15	48-inch Sky Survey cluster. Spectra 1 + 1A blended.
1309−0105	1+2	13 9.3	− 1 4	284	+61	+52,458	+52,362	1	300	16	48-inch Sky Survey cluster. Spectrogram quality poor.
1431+3146	1	14 30.6	+31 47	16	+66	+39,046	+39,142	2	50	17	Bootes Cluster. No. 1 is Anon 9 in Mt. W. Contr. 531.
	4	30.6	+31 49			+39,496	+39,592	1	65		
1513+0433	1	15 13.1	+ 4 33	334	+47	+28,300	+28,333	1	60	18	Cluster in Shane cld. A. J., 59, 285, 1954.
1520+2754	1	15 20.0	+27 51	10	+55	+19,522	+19,643	1	65	19	Corona Borealis Cluster.
	15	20.2	+27 52			+20,984	+21,105	1	100		
	3	20.3	+27 55			+23,812	+23,933	2	65		
	2	20.3	+27 54			+20,775	+20,896	3	50		No. 2 is Anon 10 in Mt. W. Contr. 531.
	5	20.4	+27 52			+20,840	+20,961	1	75		
	6	20.5	+27 53			+21,841	+21,962	1	150		
	8	20.6	+27 51			+22,088	+22,209	1	75		
	9	20.6	+27 51			+22,380	+22,501	1	75		
1534+3749	1	15 34.4	+37 48	27	+53	+45,706	+45,865	1	100	20	48-inch Sky Survey cluster.
	4	34.4	+37 42			+46,114	+46,273	1	75		
	5	34.8	+37 51			+45,557	+45,716	1	200		
2322+1425	8	23 22.0	+14 24	63	−44	+12,514	+12,727	1	75	21	48-inch Sky Survey cluster. No. 8 is NGC 7649.
	7	22.2	+14 24			+13,434	+13,647	1	50		

son 1932) and based on the galactic pole R.A. $12^h 40^m$, Dec. +28° (1900).

Column 6. Hubble's estimate of nebular type.

Column 7. Spectral types, except where emission patches in nebulae were observed. These have been indicated "Em," denoting an emission-type spectrum.

Column 8. Measured redshifts, $c\,\Delta\lambda/\lambda_0$, expressed on the convenient scale of velocities. All have been reduced to the sun and, when necessary, corrected for the curvature of the spectrograph slit.

Column 9. Redshifts corrected for the solar motion with respect to the local group, obtained by adding 300 cos $(l-55°)$ cos b km/sec to the values in column 8.

Column 10. Number of plates and dispersion. The number of plates from which the redshift was derived is shown by the Arabic numeral; the order of the dispersion at λ4350, by the letter. Included under "a" are dispersions ranging from 350 to 500 A/mm; under "b" those from 170 to 230 A/mm; "c" indicates a dispersion of 110 A/mm; and "d," a dispersion of 70 A/mm. About 85 per cent of the observations were made with the "a" dispersion.

Column 11. The estimated error of the redshifts which is not a formally computed value. Formal analysis of the errors is discussed in the text.

After the correction for solar motion with respect to the local group was made, there remained in Tables I and II twelve nebulae with negative displacements. Eight are in Table I, and of these seven are members of the local group, within which Hubble's law of the redshifts is inoperative. The eighth is the nearby nebula NGC 253.

The four negative values in Table II are all from members of the Virgo cluster. They are not unexpected, as the range in velocity within this cluster is large enough for some few negative values to occur.

The arrangement of Table III differs in some details from that of Tables I and II, mainly because the nebulae are faint and uncatalogued. The present practice is to identify a cluster of nebulae by the 1950 position of its center, as in column 1, and to assign a number to the observed cluster member, as in column 2.

Column 1. Contains the 1950 right ascension and declination of the center of the cluster. The first two figures are the hours, the next two figures the minutes, of right ascension. The sign of the declination is then shown and is followed by four figures giving the degrees and minutes of declination.

Column 2. The number assigned to the observed individual cluster nebula. When two figures are shown, both objects were on the slit and the measured redshift is from their blended spectra. Identifications for the objects are shown in Plates I and II.

Columns 3, 4, 5, 6, 7, 8. Contain the same data as columns *2, 3, 4, 5, 8, 9* of Tables I and II.

Column 9. The number of plates. The dispersion for all plates is of the order of 370 A/mm at λ4350.

Column 10. Same data as column 11 of Tables I and II.

Column 11. The number of the identification chart shown in Plates I and II. Charts have been provided as the only permanent means of identifying the objects observed. With one exception the direction is north at the top. For chart 20 east is at the top, north at the right. Estimates of relative brightness cannot be made from the charts as the exposure times, emulsions, and telescopes are in many cases not the same.

Nebula No. 8 in Cl 2322+1425 is the only catalogued object in the table. It has been identified as NGC 7649.

TABLE IVA. MEAN SPECTRAL TYPES FOR THE DIFFERENT GROUPS OF NEBULAE

Type	Number	Spec.	Type	Number	Spec.
Eo−7	178	G 3.7	Sb+SBb	102	F 9.6
So+SBo	117	G 2.2	Sc+SBc	65	F 6.1
Sa+SBa	84	G 1.4	All	546	G 1.4

TABLE IVB. PERCENTAGE OCCURRENCE OF EMISSION λ3727

Type	Sample	λ3727	Type	Sample	λ3727
Eo−7	82	18%	Sb+SBb	66	80%
So+SBb	52	48%	Sc+SBc	41	85%
Sa+SBa	37	62%	All	278	54%

The apparent photographic magnitudes of several nebulae in Table III are fainter than 19.5 and required extended exposures on fast blue plates. As fainter nebulae are observed, the spectroscopic observations are becoming more difficult

Notes to Plate III continued.

No. (5). The Fo-type spectrum of an Sc nebula with small dispersion. Absorption lines are not narrow as in (3). Hydrogen is strong and the emission feature λ3727 is seen at the far left. H and K are near their normal position, as the redshift of NGC 1003 is small.

No. (6). Cl 1520+2754, Nebula No. 5 in the Corona Borealis Cluster. Only the narrow spectrum in the center is that of the nebula. The uncorrected redshift is +20,840 km/sec. The wide emission feature to the red of λ3889 is a night-sky band.

No. (7). Cl 1431+3146, Nebula No. 1 in the Bootes Cluster. H and K are shifted to the region of λ4471. The uncorrected redshift is +39,046 km/sec. Only the narrow spectrum at the center is that of the nebula. The faint wide background spectrum is from the night sky.

No. (8). Cl 0855+0321, Nebulae Nos. 1 and 2 in the Hydra Cluster. The narrow spectrum of Nebula No. 1 is below; the narrow spectrum of No. 2 is above. The strong, wide spectrum is that of the night sky, which almost blots out the nebular spectra. Nebula No. 2 has a bluer color index than 1. The emission feature, λ3727, is present and can be seen just to the red of the *He* comparison line λ4471. The nebular type of this object is probably Sb. Nebula No. 1, below, is an elliptical. H and K are not easily discernible as they are partially filled in by the spectrum of the night sky. They appear to the red of the *He* comparison line λ4713. The uncorrected redshift of Nebula No. 1, as measured from the absorption features H and K, is +61,241 km/sec; that for number 2, as measured from the emission feature λ3727, is +60,964 km/sec.

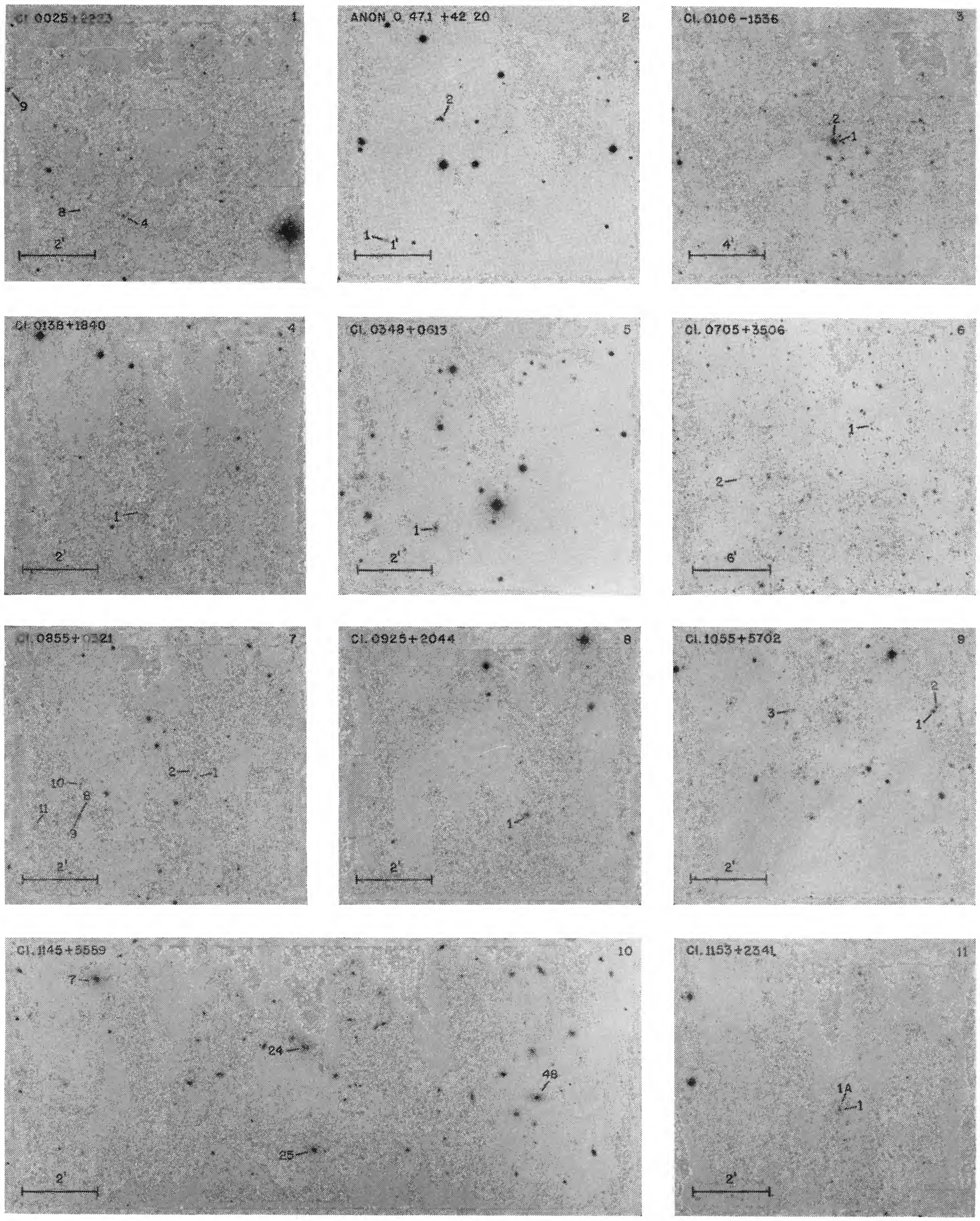

Plate I. Identification Charts for Faint Nebulae

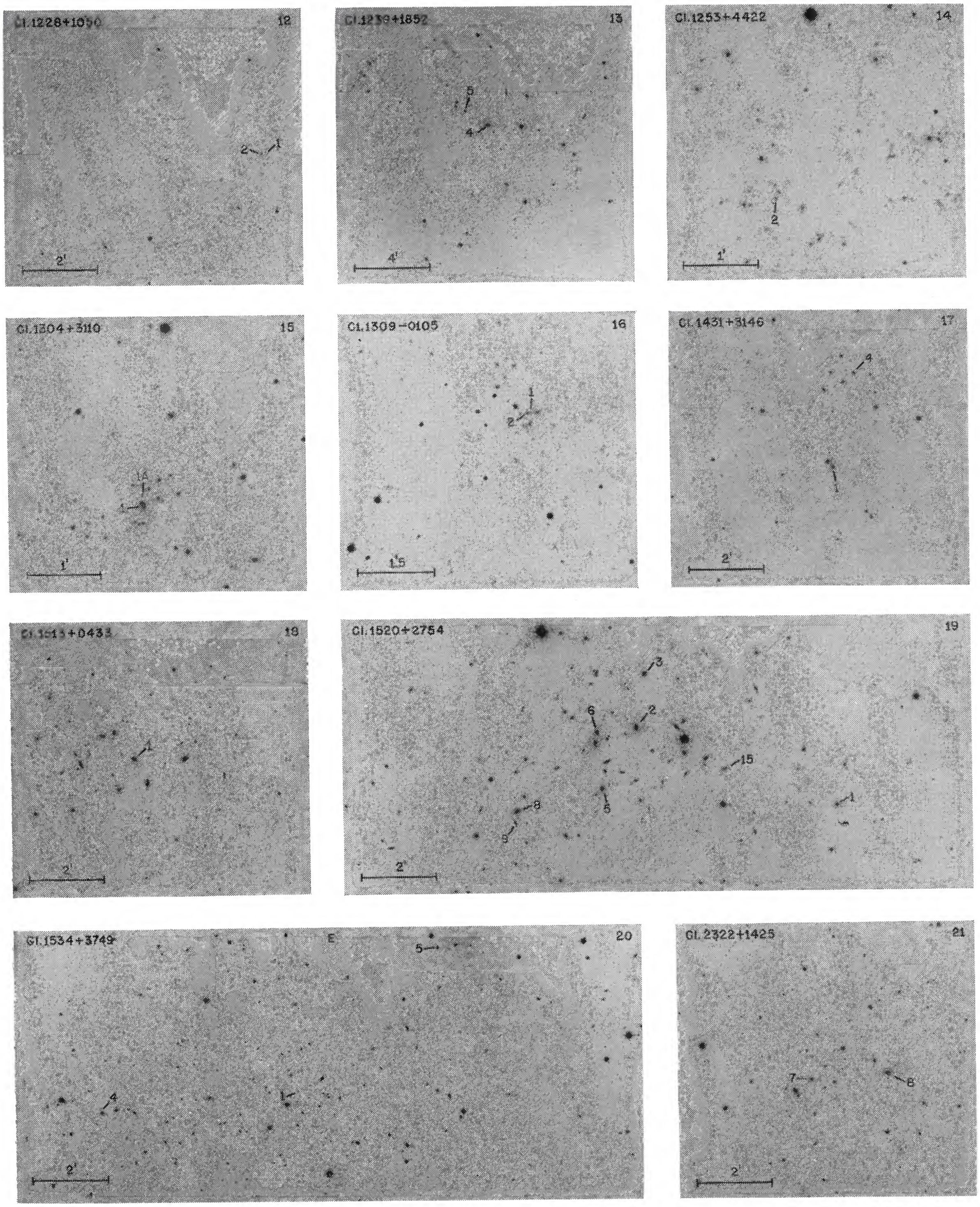

Plate II. Identification Charts for Faint Nebulae and time-consuming. Interference from the night-sky spectrum is already seriously large; its greater intensity on more extended exposures would almost completely obliterate the weak spectrum of a very faint nebula.

Also contributing toward longer exposures will be the greater redshifts of faint nebulae. Largest displacements so far measured move the H and K lines to the region of λ4700. Greater displacements will move them beyond the long wave-length limit of fast blue emulsions, and necessitate use of the slower panchromatic emulsions.

What seems at the present time to be the most promising method of obtaining larger redshifts is the observation of the emission line λ3727. While this feature appears frequently in the spectra of nebulae with relatively blue color indices, the identification of such objects in faint clusters has proved uncertain. Within the limits of the Hydra Cluster three such objects were found from inter-comparison of blue and yellow direct photographs. Each of these was tested as a possible candidate for cluster membership. Although λ3727 was observed in the spectrum of all three, the wave-length displacement showed that only one of the three was a member of the cluster. The other two were foreground nebulae and considerably less distant. In spite of this uncertainty, however, observation of an emission line is advantageous for several reasons: (1) identification of an emission line is more positive than for an absorption feature; (2) the night-sky spectrum builds up an emission feature and tends to make it stand above the background spectrum; (3) an emission feature will register on a relatively shorter exposure; (4) the error of measurement is considerably smaller. These advantages are illustrated in the spectrum of the two faint members of the Hydra Cluster (Plate III, No. 8) where a blue and a red nebula were observed simultaneously. Emission λ 3727 shows in the spectrum of the blue nebula while absorption H and K is present in the spectrum of the red. The redshift for both objects is the same.

Although the spectroscopic observation of still fainter nebulae is costly in the matter of telescope time, the present plan is to make observations in one, or possibly two, very faint clusters. A first attempt to obtain a readable spectrum from a member of a faint cluster has, in fact, been made. Although not successful, it did indicate that, at the 200-inch, exposure times for a nebula of apparent magnitude about 20.5 will be of the order of 50 hours or more.

PART II. LICK LIST OF REDSHIFTS

Program. Upon completion of a nebular spectrograph for the Crossley reflector in 1935, a program of spectroscopic work, mainly on the brighter extragalactic nebulae, was initiated. The decision to undertake such work resulted directly from advances made at Mount Wilson (Hubble 1929; Hubble and Humason 1931; Humason 1931) in this field, which at that time was almost virgin territory for spectroscopy. The present section gives the principal Lick observational results in the form of a table of redshifts, with extensive notes describing in more detail the various spectral features.

The initial Crossley observing lists were closely correlated with the work at Mount Wilson, where Hubble gave invaluable advice, guidance, and help in the selection of nebulae to be observed. The original list of nearly 200 objects comprised three groups. The first two were assembled from the Shapley-Ames catalogue, the third from then unpublished material by Hubble. These groups were as follows:

Group I: all catalogued nebulae, unobserved spectroscopically, north of the 100-inch limit of observation: 47 nebulae with $\delta > +64°$;

Group II: previously unobserved bright nebulae: 35 with $m_{pg} < 11.6$ and $\delta > -30°$;

Group III: nebulae for which Hubble had made estimates of apparent magnitudes of the brightest, resolved stars: 116 spirals.

By March, 1942, spectrograms had been obtained for all of the 82 nebulae in groups I and II, and for many of those in group III. After the war, work was resumed in November, 1945, on a revised and shorter group III list kindly provided by Hubble. He had concluded, from more and better 100-inch plates, that many of the spirals on the original list are beyond its limit of resolution for individual stars, and the number of resolved spirals was reduced to 66. By 1950 the 148 nebulae on the three lists had been observed. During 1935 to 1950, however, there occurred new developments and interests that are reflected in the present twofold greater list of 300 redshifts (Table V). Examples of extra-program observations are redshifts for: (1) possible new members in the groups around the Galaxy and the nearer giant spirals M 51, M 81, and M 101; (2) brighter nebulae in the nearer groups and clusters; (3) nebulae of intermediate brightness observed primarily for sense of spectroscopic rotation and measurement of inclined

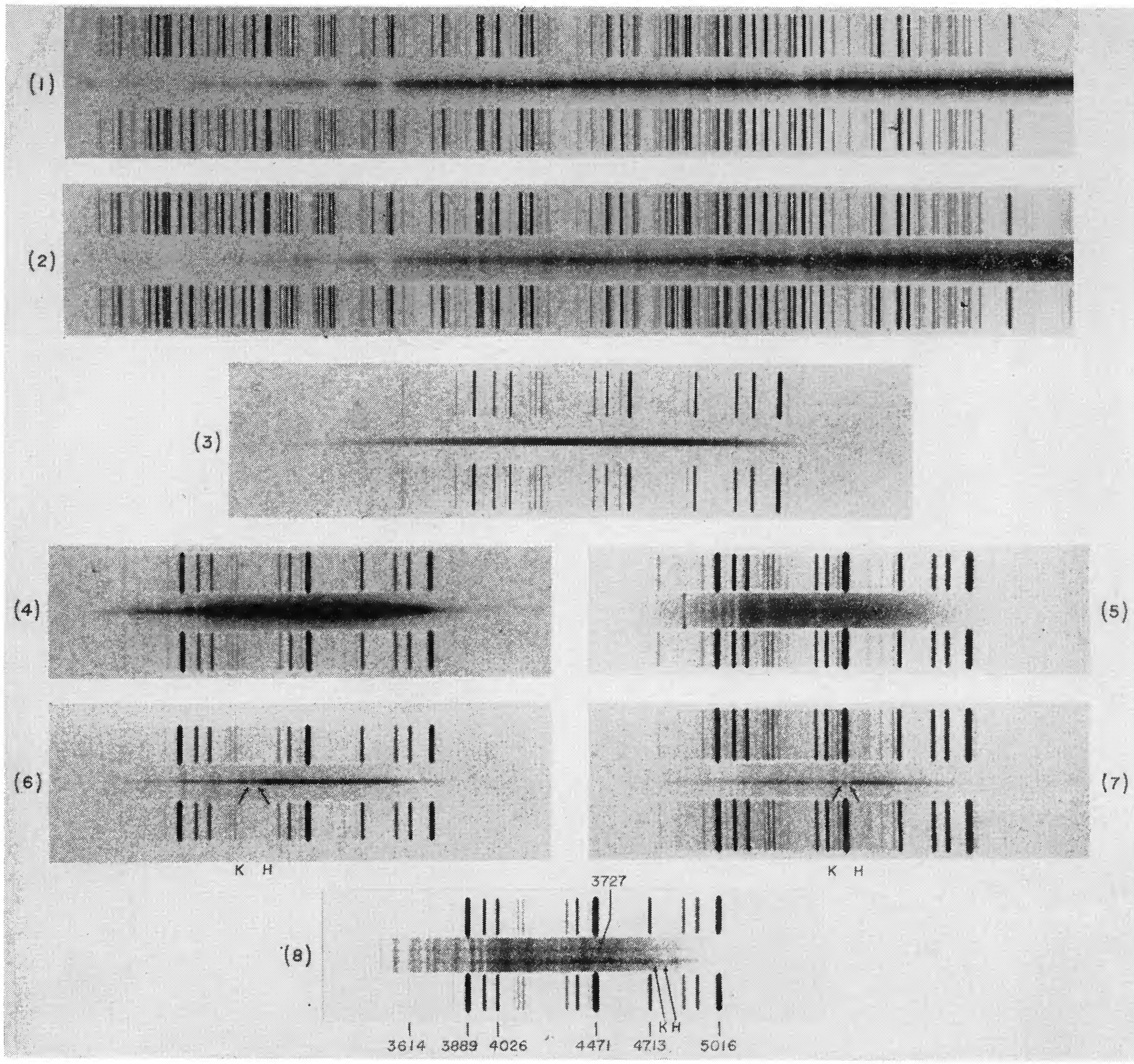

Plate III. Mount Wilson-Palomar Spectra of Extragalactic Nebulae

Observational Data and Notes

No.	Object	Neb. Type	Spect. Type	Orig. Disp.	Exp. Time
1	NGC 221	E2	G3	70 A/mm	505^{m}
2	NGC 224	Sb	G5	70 A/mm	1320
3	IC 342	Sc	F0	185 A/mm	45
4	NGC 4365	E2	G5	370 A/mm	55
5	NGC 1003	Sc	F0	370 A/mm	55^{m}
6	Cl 1520+2754	E	G3:	370 A/mm	60
7	Cl 1431+3146	E	G3:	370 A/mm	168
8	Cl 0855+0321, No. 1 Cl 0855+0321, No. 2			370 A/mm	380

Notes. Numbers 1 and 2 are prism spectra obtained with the 100-inch telescope. The dispersion is at $H\gamma$; the comparison spectrum is *Fe*. All of the others are grating spectra obtained with the 200-inch telescope. The comparison spectrum is $He+H$.

No. (1). Absorption lines in the spectrum of NGC 221 are wide but well defined. The spectra of most elliptical nebulae are very similar in character.

No. (2). In NGC 224 the absorption features are not well defined, and are approximately twice as wide as those in the spectrum of NGC 221. These characteristics appear in the spectra of many Sb nebulae.

No. (3). In the spectrum of IC 342 the hydrogen lines $H\beta$ and $H\gamma$ are bright. Other absorption features are narrow and sharp. Spectra of many Sc nebulae are like that of IC 342.

No. (4). Small dispersion spectrum of an elliptical nebula. On a larger scale this spectrum would be like that of (1).

Continued on page 113.

spectrum lines; (4) objects of special or unusual interest, such as those of uncertain nature in low galactic latitudes, or of peculiar character noted on Crossley or 20-inch astrograph plates.

There were originally two main objectives of the cooperative program. The first was an investigation of the luminosity function on the basis of residuals in the redshift-magnitude relation for all the brighter nebulae having $\delta > -30°$ and $m_{pg} < 12.1$. The second was a solution for the motion of the Galaxy and of the velocity dispersion among the nearer nebulae whose distances were to be estimated, for removal of the redshift term, from apparent magnitudes of brightest resolved stars. During the earliest stage of the Lick program, Hubble published a detailed discussion, based mainly on Mount Wilson material, of the luminosity function of nebulae (Hubble 1936b, 1936c) as well as a preliminary solution, which included some of the first Lick redshifts, for the motion of the Galaxy (Hubble 1939).

Since 1939 ideas concerning those two objectives have changed considerably. More recent developments indicate that study of the luminosity function by means of redshifts and magnitudes may be useful mainly for determining its form for the brighter and intermediate luminosities, because of observational selection. For the galactic motion, the situation is also changed, but for a different reason. This is the recent realization that, for many of the nearer spirals beyond the local group, resolution into brightest, non-variable stars is difficult even with the 200-inch (Sandage 1954a).

Although the original objectives of the Lick nebular spectroscopic program have to some extent become superseded by these recent developments, the spectrograms of the relatively large number of intermediate- and late-type spirals are useful for other purposes. Among these are: (1) spectrographic rotations, for estimates of periods, masses, and direction of rotation, (2) redshifts for estimates of relative distances and of velocity dispersions of multiples, groups, and clusters, and (3) spectral characteristics such as energy distribution, occurrence of emission radiations, and visibility of absorption lines. Data in category (3) may become useful for broad studies of stellar content, particularly of the relative abundance of Baade's stellar population Types I and II in different parts of the same nebula and among nebulae of different classes. For a number of nebulae, preliminary results have been published, or the spectroscopic data communicated to others who requested them for special purposes; references to such cases are contained in the Notes accompanying Table V.

Spectrograph. Although details of the initial operation and later improvement (Mayall 1935; Mayall and Wyse 1941) of this instrument have been described, there are some general remarks that may be made about its performance as the result of experience acquired during 20 years. In the first place, its location at the primary focus of the 36-inch $f/5.8$ Crossley reflector has been advantageous because of: (1) optical efficiency, resulting from absence of one or more auxiliary mirrors that may lose light by reflection and scattering, distort images, and brighten the sky background; (2) convenient scale of 38″.6/mm that is suitable for bright and medium-bright nebulae whose brightest parts—nuclear region and inner spiral structure—have apparent diameters from about 1′ to 15′, which is a range conveniently covered by the maximum slit length of 6′; (3) mechanical and operating conditions, such as fewer difficulties from flexure in a supporting structure that works more nearly vertically than horizontally, ease of setting the slit in various position angles, less risk of disturbance during long exposures, and reduced possibility of damage to the spectrograph by the observing platform. No difficulties have been experienced as the result of operating the spectrograph at the prime focus in such routine actions as adjusting the slit for width, length and position angle, keeping the slit in the focus of the main mirror, locating an off-axis guide star, changing plate holders, exposing the comparison spectrum, or finding faint objects.

Observing Technique. For a number of nebulae in Table V the slit was placed on faint or invisible condensations, which in many cases proved to be emission patches. Such objects are particularly useful for the measurement of redshifts in the spectra of late-type spirals, because the latter often have absorption lines that are difficult to see and, if measured, yield results of low accuracy. Whenever possible, therefore, the slit was given the proper length and orientation in position angle to include both the nuclear region and some condensation judged likely to show emission lines.

In this connection, the operation of placing the slit on a very faint or invisible object deserves consideration. The first requirement is a direct photograph showing the faint object whose spectrum is desired. Next, there is selected a nearby reference star that can be seen in the field on the slit, and its position with respect to the faint object is determined. In principle, either rectangular or polar coordinates may be used, but in practice position angle and distance have regularly been used with the Crossley nebular spectrograph. The reason is that it has been easier to detect, during long exposures, displacements due to differential refraction and instrumental flexure, between object and guide star, which may be more than a degree off-axis. Thus, even if the guide star is kept fixed on the crosswire intersection, the object sometimes moves to the edge, and possibly out of, the slit. But if the slit is oriented on the line joining object and nearby reference star, the latter becomes visible. When this relative motion occurs, the reference star is again centered in the slit, and the position of the crosswire intersection re-adjusted until it coincides with the bright apex of the comatic image of the guide star.

Visibility of Faint Objects. The problem of seeing very faint objects becomes all-important if a moderate-sized telescope is used to obtain, in the nearer spirals, slit spectrograms of the brighter components, such as star clouds, emission patches, globular star clusters, brightest stars, or novae, all of which usually are fainter than the 15th magnitude. Bowen (1947) has investigated the optical conditions that determine the visibility of very faint objects in the field of a reflector. He concluded that maximum visibility occurs when the field is viewed with a magnification of 30× for each inch of telescope aperture. In addition to meeting this optical condition, the Crossley nebular spectrograph incorporates an instrumental feature that has proved invaluable in setting the slit on images of threshold visibility. This is provision for viewing the slit from behind with a power of approximately 1000×, which is nearly Bowen's figure for the Crossley. Thus a very faint object appears in a field that is dark except for the narrow line of night-sky light coming through the slit. By this means, viewing conditions approach those in experiments made many years ago by H. D. Curtis (1903) and by H. N. Russell (1917), who investigated the limiting visual magnitude for stars. Moreover, the optical system for viewing the slit from behind consists only of a small collimating lens and total reflection prism, whereas that for viewing the slit from the front involves reflection from the slit jaws and passage through a larger collimating lens and three total-reflection prisms; for both systems there is a common viewing telescope at the side of the tube. Under these conditions, and with all air-glass surfaces coated with non-reflecting films and the curved, polished stellite slit jaws aluminized, objects nearly one magnitude fainter can be seen behind the slit than in front. The limiting visual magnitude is about 17, for good seeing and transparency; depending on their color indices, stars of $17\frac{1}{2}$ to 18 photographic magnitude may be seen, but for safety in such cases, the slit usually has been set on them by the use of a reference star and polar coordinates. Objects in the range from 15 to $17\frac{1}{2}$ photographic magnitude generally were centered and kept in the slit only by intermittent use of the rearward slit viewing system, in combination, of course, with an off-axis guide star.

Measurement of the Spectrograms. All the plates were measured by making micrometer-wire settings on spectrum lines, with a measuring engine, Toepfer Serial No. 445, having a screw of 0.5 mm pitch. When sufficient plates had been measured to indicate the range in settings on comparison lines for a fiducial position of the plate on the screw, averages were formed and a standard dispersion table was computed in the usual way by the Hartmann formula. Wave lengths for lines in the nebular spectra were determined by successive approximation, with starting values obtained from laboratory, solar, or stellar sources. Since the spectra of spirals show a high degree of compositeness (Plate IV), the normal or unshifted wave lengths of the spectral features may be expected to show considerable variation, and there is evidence in the measurements for real differences amounting to several angstroms. It was not found possible, however, to relate in any systematic way different wave lengths of the same feature with some other characteristic, such as nebular type. Instead, a system of mean wave lengths was deduced for emission and absorption features by applying to the initial values average systematic corrections determined from residuals in km/sec from the preliminary means for each plate. The results are given in Table VI, where the second decimal has little significance beyond that of a guard figure. This table omits the wave lengths found for some infrequently-measured spectral features, generally shortward of 3900; these are blends whose components are so variable in intensity that their average wave lengths are too uncertain for consistent redshift determinations.

The most frequently-measured absorption features were the H and K lines of *Ca* II, and blends in the vicinity of the G-band and $H\delta$; in emission, 3727 of [*O* II] generally was the predominating feature (Mayall 1939; Humason 1947), but for

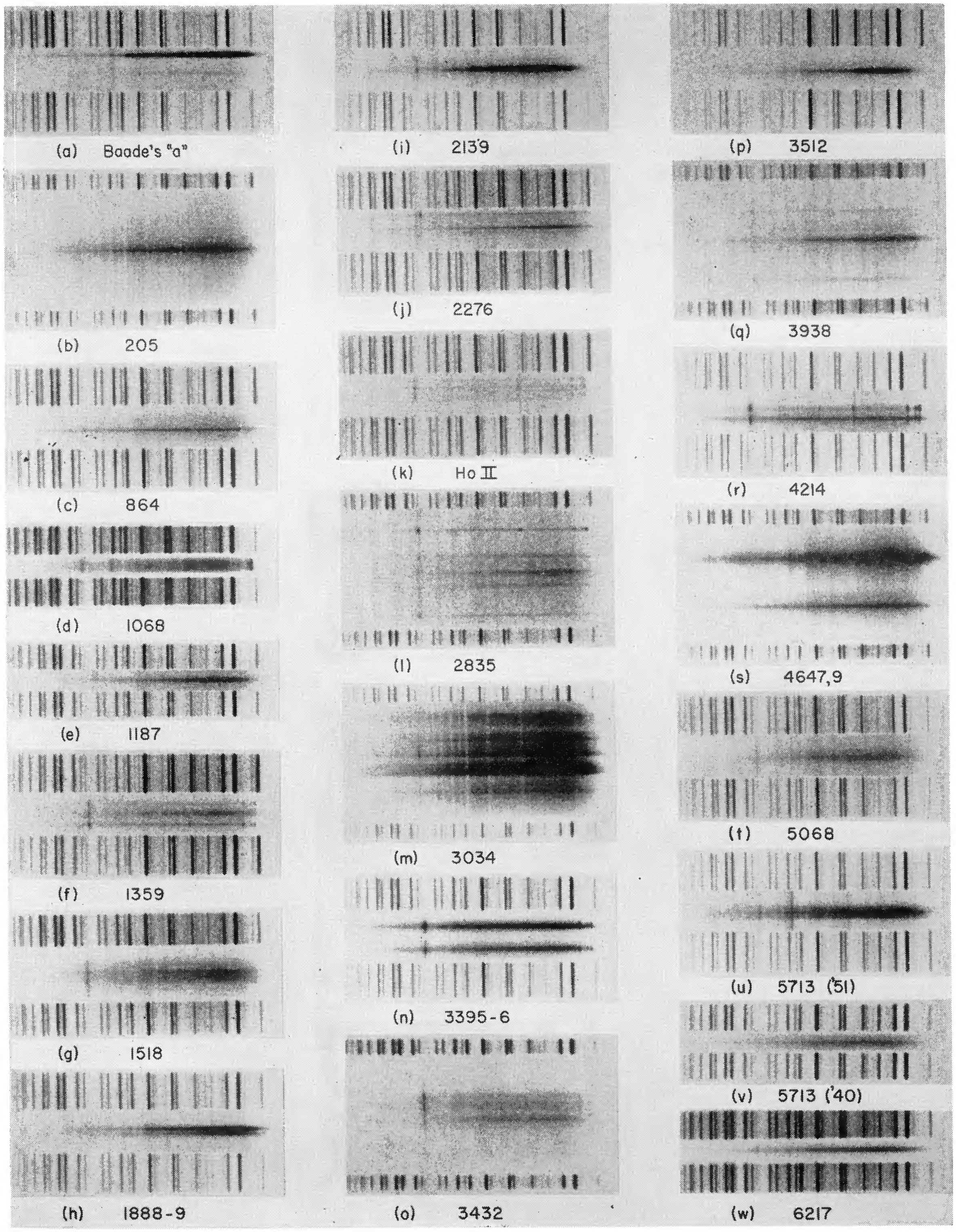

Plate IV. Representative Spectra of Extragalactic Nebulae. Enlarged 8.8× from the original negatives on which the linear dispersion is 430 A/mm at $H\gamma$, with slit lengths ranging from 1′ to 6′. The comparison spectrum consists of spark lines due to *Pd*, *Pb*, *Sn* and *Cd*, with the shortest (left) and longest (right) wave lengths of 3460 *Pd* and 5085 *Cd*. In the nebular spectra the most prominent shortward emission is 3727 [*O* II], while the longward ones are $H\beta$, 4958 and 5006 [*O* III]. The H and K absorption lines of *Ca* II are conspicuous in NGC 1888–9(h) and in 4649(s, upper spectrum), those of hydrogen in 205 and in 3034.

the emission patches bright hydrogen lines, the [*Ne* III] wide pair at 3967 and 3868, and the [*O* III] lines near $H\beta$ were also measured whenever possible. At the time each spectral feature was measured, it was assigned a weight, ranging from $\frac{1}{2}$ to 3, which was intended to include allowance for such factors as intensity, width, blending, and dispersion, in so far as they might affect the reliability of the measured redshift. The number of lines measured, and the sum of their weights, are given for each plate in Table V. In those cases where only one or two lines were measured, their identification is given in the Notes to the table.

Accuracy of the Measurements. Although formal probable errors of the mean redshift from individual lines were computed for some of the earlier plates, their values were considerably smaller, generally by factors of 2 or 3, than the differences between the means for duplicate plates of the same nebula. Under these circumstances, with single-plate probable errors evidently much smaller than obscure systematic errors, and obtainable from only a few lines per plate, it seems inappropriate to use a precision index that implies numerous residuals distributed according to a normal error function. Instead, average deviations (A.D.) have been computed for each plate, on the assumption that they may give a more realistic indication of the accuracy of the tabulated redshifts. These values of A.D. in column (11) of Table V are distributed as follows:

A.D. (km/sec)	No.	A.D. (km/sec)	No.
0– 20	32	121–140	22
21– 40	81	141–160	10
41– 60	80	161–180	11
61– 80	81	181–200	2
81–100	58	201–220	2
101–120	28	221–240	2
		Total	405

The range is from 2 to 234 km/sec, and the mean 72 km/sec; for 99 per cent of the plates the A.D. is less than 200 km/sec, and for 81 per cent, less than 100 km/sec. These figures show that the internal precision is not high by stellar radial-velocity standards; but, percentagewise for nebular redshifts, the accuracy is satisfactory for all but the few nearest nebulae, particularly those in the local group. For them, higher dispersion, or more extensive low-dispersion spectrographic observations are desirable, and a program (Humason 1954) has recently been completed to provide such data of relatively high accuracy.

Although the foregoing discussion is intended to give some idea of the internal accuracy of the redshifts in Table V, it leaves unanswered the question of the external or systematic errors. These, of course, are best investigated by comparison of independent sets of observations. The Mount Wilson-Palomar two-fold greater list of redshifts in Tables I and II provides the necessary material to examine the systematic errors, on the basis of more than 100 nebulae observed in common at Mount Wilson and at Mount Hamilton, and the detailed comparison is given after Table V.

Spectral Characteristics. For reasons related to the original Crossley program that included a large number of resolved spirals, Table V contains a relatively high percentage of late-type normal and barred spirals, those in Hubble's classes Sc and SBc. Their spectra frequently show emission radiations in varying intensity for different objects and for different regions of the same object, absorption features ranging from some easy to see to others very difficult to detect, and continua suggestive of moderately early to late spectral type. That is to say, the spectra give more the impression of diversity than of uniformity. This wide range in spectral characteristics of late-type spirals has already been foreshadowed by previous work, especially from spectral types (Humason 1936, Fig. 1) and from colors measured photoelectrically by Stebbins and Whitford (1937, 1952). Many of these spectral types and colors, however, refer to small areas located, in general, around the brighter nuclear regions. This was especially the case for the Mount Wilson spectrograms, which were obtained for many of the nebulae at the Cassegrain focus of the 100-inch where the scale is eight times greater than that of the prime focus of the Crossley. As a result, the two series of spectroscopic observations represent coverage by slit lengths measured in a few seconds of arc in one case (Mount Wilson), and in a few minutes of arc in the other (Lick). Under these different circumstances, estimates of spectral type for the same nebula may be appreciably different, since they would refer respectively to small nuclear regions and to larger portions of the main bodies. A striking example of this effect is that already reported for M 33 (Mayall and Aller 1942), with estimated spectral types of A7 for the 10″ diameter nucleus, and G0 for the innermost, surrounding spiral structure of 6′ diameter. Moreover, for many of the Crossley spectra of principal parts of spirals it would be difficult, or possibly misleading, to give estimates of spectral types, because different absorption features in the same spectrum often indicate different types, while the frequent occurrence of emission radiations in patches or throughout the spiral adds to the confusion. For these two reasons—variation and compositeness in spectral characteristics—no column of spectral types is included in Table V. Instead, some supplementary information is given in the Notes for those nebulae whose spectra show abnormal features, such as barely visible, unusually broad, or exceptionally strong absorption or emission lines. Plate IV shows a number of fairly typical spectra of spirals, as well as some of the extremes of absorption- and emission-line intensities and widths.

Table of Redshifts. Table V contains nearly all the observational results obtained from the Crossley spectrograms. Omitted data are the detailed measurements of spectrum-line inclinations with the sense of spectrographic rotation, previously reported in preliminary form (Mayall 1948a) and more complete information regarding the distribution and occurrence of emission radiation; these data will be given in later papers.

In addition to the column descriptions and Notes for Table V, given below, there are a few general remarks that may be made about the basic material. As in many extended programs, the early observations are considerably inferior in quality to the later ones. Thus, plates taken before 1942 are in general weaker and more grainy than those obtained after 1945, when the remarkably fast and fine-grained Eastman IIa-O emulsion came into regular use. For a number of nebulae the earlier plates were replaced, or supplemented, with later ones taken with shorter exposure and a narrower slit. For most objects re-observed in this way the improvement in plate quality was very worth while as shown in Plate IVu and v, NGC 5713. Although it would be satisfying to replace nearly all the older plates with new ones, to do so would require an amount of observing time disproportionate with respect to expected new results.

Finally, the fact should be noted that some of the earliest plates were obtained with a straight slit, so that correction of the measurements for prismatic curvature is necessary. Table V includes redshifts from 25 straight-slit plates, for which there are 13 corresponding curved-slit plates. The average systematic difference, curved *minus* straight, is +36 km/sec, with a range from −115 to +186 km/sec. Although the mean value is thus not accurately determined, a correction of +36 km/sec to the straight-slit results for M 31 and M 32 appreciably improves the agreement with the curved-slit results, and with the Mount Wilson results based on more spectra of greater dispersion (Table I). Accordingly, the observed redshifts in Table V obtained from straight-slit plates have been corrected by +36 km/sec.

Detailed data for the columns of Table V are as follows:

Column 1. NGC or IC number, when available; otherwise, a more detailed description or location given in the Notes, with charts in Plate V for the few faintest nebulae.

Column 2. Nebular type assigned by Hubble, as quoted in Pettit's (1954) list of photoelectric magnitudes and colors; where these types differ from those in Pettit's paper, they represent unpublished, later revisions by Hubble; those in brackets [ ] are by Sandage.

Columns 3, 4, 5. Date, exposure time, and emulsion; for the latter, IES = Imperial Eclipse Soft, generally H and D 850, but with a few 1200; Ilf = Ilford; Agf = Agfa Spectral Blau Ultra Rapid; and Ia-O, 103a-O, IIa-O = Eastman spectroscopic emulsions for the astronomical level of intensities.

Columns 6, 7, 8. Slit width, length, and position angle; an asterisk (*) with the slit-length figure denotes early plates obtained with a straight slit, while the same symbol with the position angle indicates that the slit was along the major axis; in a number of cases, supplementary information regarding the orientation of the slit is given in the Notes.

Columns 9, 10, 11. Number of lines measured, their total assigned weight, and average deviation; when 3727 [*O* II] was present in measurable strength, this fact is indicated on the figure for the number of lines by an asterisk (*) when the emission appears to be generally present throughout the nuclear region or main body, and by a dagger (†) when it is localized in one or more emission patches; the same figure *underlined* means the lines are rotationally inclined.

Column 12. Residuals for (a) individual plates, when two or more plates were used to obtain a mean redshift for column (13) with the weights in column (10), and (b) for individual condensations referred to the mean or nuclear-region redshift, when several objects were measured in the same nebula; in both cases, parentheses signify that the results were not used for the deter-

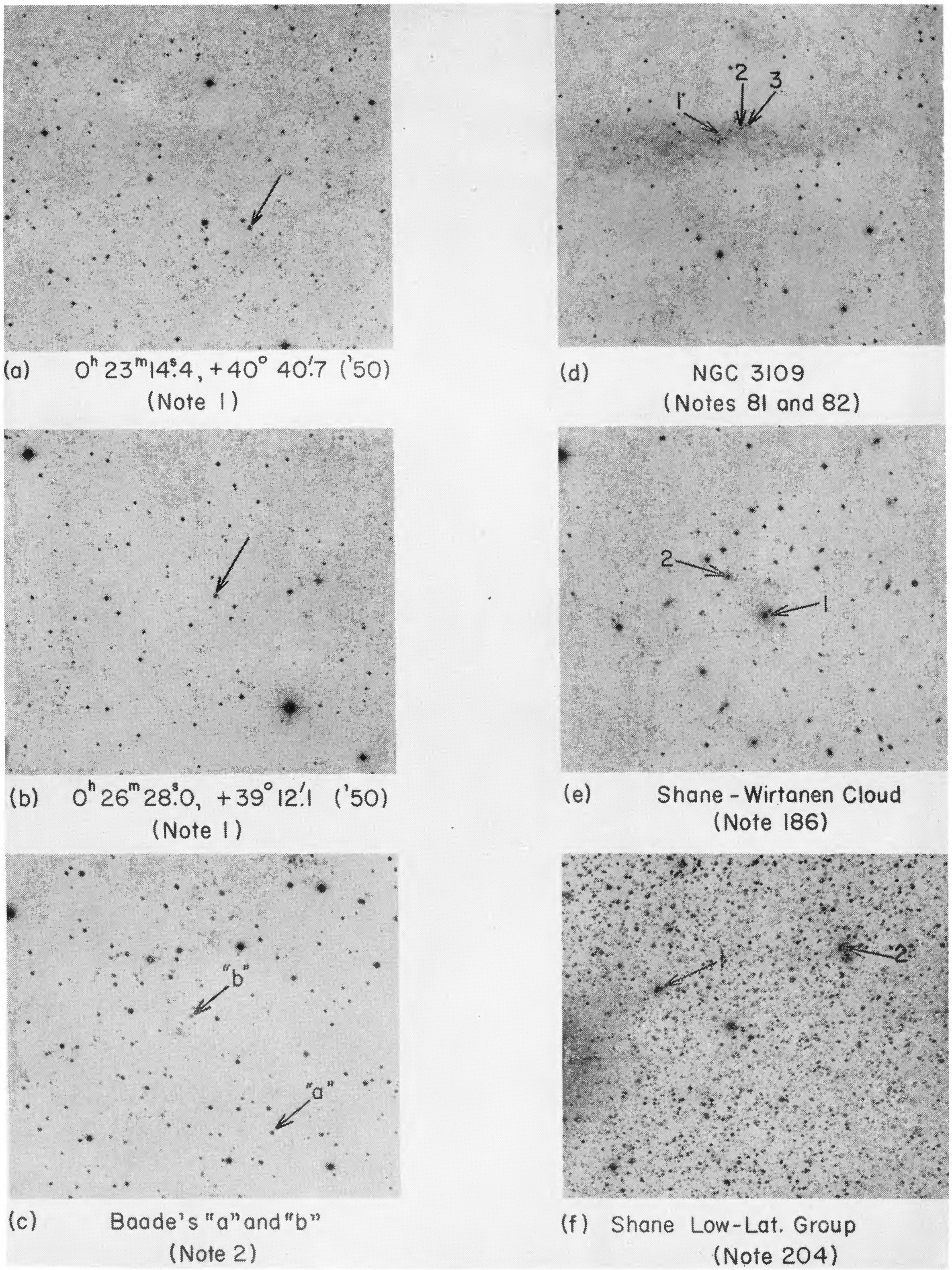

Plate V. Identification charts of nebulae and emission patches for which the descriptions may be insufficient in the Notes to Table V. For each chart north is up, east is left, and the field size is approximately 13′×16′.

Table V. Redshifts of 300 Extragalactic Nebulae.

NGC *IC (1)	Neb. Type (2)	Date Mean UT (3)	Exp. Hr. (4)	Emul. Type (5)	W (6)	Slit L (7)	PA (8)	Lines No. (9)	Wt. (10)	AD (11)	Pl. Res. (12)	Redshift c·Δλ/λ₀ (13)	Galactic Long. (14)	Lat. (15)	100 Cos A (16)	Corr. Redshift (17)	Note No. (18)
Anon	[E2]	52 Aug 26.4	6.7	IIaO	5"	1'	90°	3	3	94		+12418	86°	-21°	+80	+12658	1
Anon	[E1]	52 Aug 18.4	6.0	IIaO	4	1	90	5	4½	76		+11029	87	-23	+78	+11263	1
134	[Sc]	51 Oct 22.2	3.5	IIaO	5	3	50*	3	3½	10		+ 1681	296	-83	- 6	+ 1663	
Anon	[Sb]	51 Sept 7.4	7.0	IIaO	4	2	9½	4*	4½	82	+ 12	+16841	88	-23	+77	+17072	2
		51 Sept 27.4	8.0	IIaO	4	1	90	2*	3½	11	- 15						
Anon	[Sa]	46 Sept 21.3	8.0	IIaO	5	1	85	1*	...	...	- 54	+27128	88	-23	+77	+27359	2
		46 Sept 23.3	9.0	IIaO	5	2	85	1*	...	...	+ 55						
185	Ep	41 Sept 18.4	7.8	IIf	6	3	106	5	6½	22	+ 11	- 241	89	-14	+81	+ 2	3
		41 Sept 23.4	5.5	103aO	6	3	90	5	5½	56	- 13						
205	SBo	36 Sept 26.5	2.0	IES	6	1	90	4	4	19	- 79	- 233	89	-21	+78	+ 1	
		48 Aug 30.3	4.5	IIaO	4	6	165*	8	6½	53	+ 49						4
210	Sb	36 Nov 13.2	3.0	IES	6	1	90	3	3	205	+225	+ 1768	85	-76	+21	+ 1831	
		49 Dec 22.2	2.0	IIaO	5	3	170*	3	4½	29	-150						
214	Sc	41 Nov 15.3	8.0	IIf	6	2	90	2	4	99		+ 4485	88	-37	+67	+ 4686	5
221 (M32)	E2	35 Sept 24.5	0.5	IES	4	½*	90	3	4½	10	+ 13	- 193	89	-22	+77	+ 38	
		35 Nov 25.2	1.0	IES	4	1*	90	3	4½	2	- 45						
		35 Nov 27.2	0.5	IES	4	1*	90	7	6	59	+ 9						
		48 Sept 11.4	3.0	IIaO	4	6	155*	3	3	29	+ 32						
224 (M31)	Sb	35 Sept 23.5	1.0	IES	4	½*	90	7	6	97	- 38	- 290	89	-20	+78	+ 44	6
		35 Oct 4.2	1.0	IES	4	1*	90	3	4½	16	- 34						
		35 Nov 25.2	1.5	IES	4	1*	90	3	4½	34	+ 49						
		35 Nov 27.2	0.8	IES	4	1*	90	4	5½	57	+ 14						
		36 Sept 25.4	0.8	IES	6	1	90	3	5	18	- 22						
		36 Nov 19.1	0.8	IES	6	1	90	3	5	13	+ 25						
		36 Nov 19.1	0.3	IES	6	1	90	3	5	31	+ 15						
		47 Nov 9.3	7.5	IIaO	5	2	71	4	5	58	...	(- 316)					7
255	Sc	49 Dec 12.7	6.0	IIaO	4	3	90	4*	4½	129		+ 1921	93	-74	+22	+ 1987	8
278	Sb	36 Aug 24.6	1.5	IES	6	1	90	8*	6½	68	+ 3	+ 656	91	-15	+78	+ 890	
		37 Aug 12.4	3.2	IES	6	1	90	7*	6½	125	- 2						9
289	[SBc]	51 Nov 3.2	4.0	IIaO	5	3	156*	3	3½	119		+ 1928	245	-85	- 8	+ 1904	
*79	[E1]	51 Nov 4.3	5.0	IIaO	5	1	90	3	2½	234		+12567	117	-77	+10	+12597	10
428	Sc	36 Dec 9.2	5.4	IES	6	2	109*	1†	2	14		+ 1078	105	-61	+31	+ 1171	11
514	Sc	49 Nov 25.2	5.0	IIaO	4	3	119	3	2½	99		+ 2602	105	-50	+42	+ 2728	
520	Irr	36 Sept 4.4	5.0	IES	6	1	140*	5	5	140		+ 2084	109	-58	+31	+ 2177	
578	Sc	49 Nov 18.2	4.5	IIaO	4	3	84	3	2½	15		+ 2017	157	-78	- 4	+ 2005	
604	Gas. Neb.	51 Sept 25.3	2.0	IIaO	4	1	90	12†	9	53	+ 28	- 244	102	-31	+58	- 70	12
		51 Oct 22.3	0.5	IIaO	4	1	90	12†	10½	47	0						
		51 Dec 22.2	0.5	IIaO	4	1	90	10†	9	38	- 30						
		51 Dec 23.1	0.5	IIaO	4	1	90	12†	10	36	0						
613	Sb	52 Dec 15.2	2.0	IIaO	5	1	124*	5*	4	107		+ 1558	194	-78	-16	+ 1510	
672	SBc	41 Oct 23.4	8.0	IIf	6	6	75*	3*	3½	86	-118	+ 340	106	-34	+52	+ 496	
		53 Oct 11.4	5.5	IIaO	5	6	75*	6*	5	74	+ 82						
718	Sa	35 Nov 30.2	3.0	IES	4	½*	90	3	3	34	+ 4	+ 1802	118	-55	+25	+ 1877	
		37 Oct 10.4	4.0	IES	6	1	90	3	3	174	- 3						
753	Sc	37 Nov 25.3	4.0	IES	6	1	90	4	6	132	+ 92	+ 4766	105	-25	+58	+ 4940	
		37 Dec 1.3	7.5	IES	6	1	90	3	4½	95	-127						
864	Sb	52 Dec 18.3	4.0	IIaO	5	2	90	6*	5	94		+ 1583	126	-51	+21	+ 1646	13
871	Sc	36 Dec 17.3	4.5	IES	6	1	0*	5*	5½	136		+ 3757	121	-43	+30	+ 3847	
877	Sc	49 Jan 31.2	4.0	IIaO	4	2	134*	3	2½	91		+ 4016	121	-43	+30	+ 4106	
908	Sc	36 Nov 20.3	5.0	IES	7	1	90	4	3½	104		+ 1734	170	-67	-17	+ 1683	
925	Sc	53 Nov 8.4	4.5	IIaO	5	6	105*	3*	3½	98		+ 587	113	-24	+48	+ 731	
Anon	[Irr]	53 Nov 29.3	5.0	IIaO	4	1	134	3*	4	34		+ 4037	124	-36	+29	+ 4124	14

Table V. Continued.

NGC *IC (1)	Neb. Type (2)	Date Mean UT (3)	Exp. Hr. (4)	Emul. Type (5)	Slit W (6)	Slit L (7)	Slit PA (8)	Lines No. (9)	Lines Wt. (10)	AD (11)	Pl. Res. (12)	Redshift $c\cdot\Delta\lambda/\lambda_\circ$ (13)	Galactic Long. (14)	Galactic Lat. (15)	100 Cos A (16)	Corr. Redshift (17)	Note No. (18)
1042	Sc	41 Sept 22.4	4.0	103aO	6"	3'	101°	2	$2\frac{1}{2}$	125		+ 355	152°	-56°	-07	+ 334	
1052	E3	35 Dec 23.2	2.8	IES	4	$\frac{1}{2}$*	90	5*	$4\frac{1}{2}$	36		+ 1523	150	-57	-05	+ 1508	15
1058	Sc	41 Nov 23.3	8.6	IIf	6	2	76	5	6	76		+ 80	115	-20	+47	+ 221	
1068 (M77)	Sb	38 Jan 25.2	1.3	IES	6	1	90	8*	$7\frac{1}{2}$	75		+ 1121	141	-51	+06	+ 1133	16
1073	SBc	41 Nov 17.2	8.5	IIf	6	2	63	3	$3\frac{1}{2}$	52		+ 1874	139	-50	+07	+ 1895	17
1097	SBb	53 Dec 3.3	3.0	IIaO	5	6	145*	3 2	$3\frac{1}{2}$ $2\frac{1}{2}$	101 3	-136 +191	+ 1424	194	-63	-34	+ 1322	18 19
1187	Sc	48 Jan 12.2 48 Jan 15.2	3.0 3.0	IIaO IIaO	5 5	1 3	90 107	3 3	$2\frac{1}{2}$ $3\frac{1}{2}$	167 83	+ 98 - 70	+ 1579	179	-58	-30	+ 1429	20
1232	Sc	36 Nov 15.3	5.0	IES	7	1	90	4	4	67		+ 1820	176	-57	-28	+ 1736	
1300	SBb	47 Jan 22.2 53 Oct 12.4	3.0 4.5	IIaO IIaO	6 4	2 6	90 106	5* 5*	$6\frac{1}{2}$ $5\frac{1}{2}$	39 40	- 28 + 33	+ 1625	175	-55	-29	+ 1538	 21
1331 1332	E2 So	46 Oct 21.4	3.0	IIaO	5	6	115 115*	3 3	2 $2\frac{1}{2}$	38 29		+ 1408 + 1573	180	-53	-34	+ 1306 + 1471	22 22
1359	SBb	48 Jan 11.2	3.5	IIaO	5	2	97	8*	8	54		+ 1992	176	-51	-32	+ 1896	23
1385	Sc	46 Jan 28.2	2.0	IIaO	6	2	90	6	5*	180		+ 2012	186	-51	-42	+ 1886	24
1395	E2	35 Oct 24.5	3.0	IES	4	$\frac{1}{2}$*	90	5	4	86		+ 1820	183	-50	-40	+ 1700	
1398	SBb	36 Jan 21.2 47 Jan 18.2	2.5 2.0	IES IIaO	4 5	$\frac{1}{2}$* 2	90 90	3 3	3 $2\frac{1}{2}$	95 43	- 4 + 5	+ 1524	189	-52	-43	+ 1395	
*342	Sc	38 Dec 16.3	3.5	Agfa	6	1	90	5*	$3\frac{1}{2}$	101		+ 34	106	+11	+62	+ 220	25
1453	E1	47 Jan 16.2	4.0	IIaO	5	2	90	4*	$5\frac{1}{2}$	47		+ 4035	160	-41	-20	+ 3975	
1518	Scp	47 Jan 21.2	3.5	IIaO	6	3	18	8*	$7\frac{1}{2}$	82		+ 1027	184	-43	-46	+ 889	26
1569	Irr	35 Oct 28.4 40 Dec 6.5	4.0 5.9	IES I1200	4 6	$\frac{1}{2}$* 6	117* 118*	9* 9*	9 $12\frac{1}{2}$	51 39	+ 77 - 56	- 58	111	+12	+55	+ 107	27
1637	Sc	45 Nov 8.9	5.5	IIaO	6	1	90	2	2	8		+ 528	167	-30	-32	+ 432	28
1640	SBb	46 Jan 31.2 46 Oct 29.5	4.0 2.5	IIaO IIaO	6 6	2 2	46 46	4* 6	$3\frac{1}{2}$ 6	88 103	- 50 + 29	+ 1676	187	-36	-54	+ 1514	29
*391	Sb	35 Nov 25.4	5.0	IES	4	$\frac{1}{2}$*	90	1*	1	...		+ 1607	101	+22	+64	+ 1799	30
1744	Sc	49 Feb 1.2	4.0	IIaO	5	3	174	4*	4	100		+ 676	194	-33	-63	+ 487	31
1888 1889	Sb Eo	47 Jan 17.2	4.0	IIaO	5	2	70	4	$5\frac{1}{2}$	25		+ 2557 + 2557	181	-23	-54	+ 2395 + 2395	32 32
1961	Sb	52 Nov 25.5	4.8	IIaO	5	2	70*	6*	$4\frac{1}{2}$	147		+ 3870	110	+21	+54	+ 4032	
1964	Sb	46 Oct 31.5	3.0	IIaO	6	2	25*	3	$2\frac{1}{2}$	78		+ 1849	193	-25	-67	+ 1648	33
2139	SBc	46 Oct 30.5	2.5	IIaO	6	2	90	9*	$8\frac{1}{2}$	103		+ 1913	198	-20	-75	+ 1688	34
2146	Sap	49 Nov 25.4	5.0	IIaO	4	3	138*	4*	$4\frac{1}{2}$	24		+ 784	103	+25	+61	+ 967	35
2217	SBa	47 Jan 18.3	2.8	IIaO	5	2	90	5*	6	44		+ 1573	202	-17	-80	+ 1333	
2268	Sc	36 Jan 22.7	7.5	IES	4	$\frac{1}{2}$*	90	4*	4	51		+ 2337	96	+28	+66	+ 2535	
2276	Sc	47 Apr 16.3	5.0	IIaO	5	2	114	3 4†	$4\frac{1}{2}$ 4	66 69	- 48 + 53	+ 2391	95	+28	+68	+ 2595	36
2300	E1	35 Nov 27.5 51 July 27.3	3.8 2.2	IES IIaO	4 4	$\frac{1}{2}$* 2	90 90	3 3	3 5	142 103	+ 94 - 57	+ 2088	95	+28	+68	+ 2292	37
2314	E3	36 Jan 23.4	5.5	IES	4	$\frac{1}{2}$*	90	6	$4\frac{1}{2}$	47		+ 3951	107	+28	+54	+ 4113	
2336	Sbc	36 Dec 9.5	4.8	IES	6	1	90	4	$3\frac{1}{2}$	103		+ 2252	102	+29	+60	+ 2432	
2347	Sb	47 Jan 17.4	3.0	IIaO	5	2	90	5*	5	80		+ 4521	118	+28	+40	+ 4641	
2366	Irr	35 Oct 3.5	2.0	IES	4	$\frac{1}{2}$*	90	10†	10	36		+ 194	114	+29	+45	+ 229	38
2389	Sc	47 Jan 16.4	4.1	IIaO	6	2	90*	6*	$5\frac{1}{2}$	147		+ 3816	153	+23	+13	+ 3858	

Table V. Continued.

NGC *IC (1)	Neb. Type (2)	Date Mean UT (3)	Exp. Hr. (4)	Emul. Type (5)	Slit W (6)	Slit L (7)	Slit PA (8)	Lines No. (9)	Lines Wt. (10)	AD (11)	Pl. Res. (12)	Redshift $c\cdot\Delta\lambda/\lambda_0$ (13)	Galactic Long. (14)	Galactic Lat. (15)	100 Cos A (16)	Corr. Redshift (17)	Note No. (18)
2441	Sc	42 Jan 14.4	7.5	103aO	8"	2'	157°	4	4	89		+ 3623	109°	+36°	+47	+ 3764	
2475	[E3]	50 Mar 15.3	1.5	IIaO	4	2	40	3	2½	45		+ 5019	132	+32	+19	+ 5076	39
2500	Sc	49 Jan 30.3	6.0	IIaO	4	2	62	4*	4½	143	- 55	+ 470	136	+33	+13	+ 509	40
		49 Feb 20.3	4.4	IIaO	5	6	27	6†	6	66	+ 42						41
2523	SBb	47 Apr 20.3	5.0	IIaO	5	2	120	5	6½	140		+ 3448	107	+33	+52	+ 3604	42
2525	SBc	47 Jan 21.5	4.0	IIaO	6	3	18	3	3	99		+ 2064	200	+12	-80	+ 1824	43
2537	Sc	36 Nov 13.5	3.2	IES	6	1	90	3†	2½	40		+ 290	141	+34	+03	+ 299	44
Ho II	[Irr]	53 Apr 21.3	4.0	IIaO	4	1	174	8†	8	30	+ 11	+ 220	111	+34	+46	+ 358	45
		53 May 3.7	6.2	IIaO	4	2	12	7†	7½	31	- 11						46
2551	Sab	36 Nov 20.5	3.5	IES	6	1	90	4	4	26		+ 2296	107	+33	+52	+ 2452	
2613	Sb	42 Feb 12.3	4.1	103aO	6	2	112*	3	2½	58		+ 1555	213	+11	-91	+ 1282	
2633	SBb	36 Dec 18.5	4.8	IES	6	1	90	4*	5	37	+ 15	+ 2228	106	+35	+52	+ 2384	47
		54 Jan 31.5	5.0	IIaO	4	2	175*	4*	5½	70	- 13						48
								1†	2	..	(- 77)						49
2642	SBb	46 Nov 30.5	3.3	IIaO	5	1	90	3	4½	32		+ 4439	198	+23	-74	+ 4217	
*2389	SBo	45 Nov 30.4	5.0	IIaO	6	1	90	6*	6½	100		+ 2632	107	+35	+50	+ 2782	50
2646	SBo	45 Dec 9.4	5.0	IIaO	6	1	90	4	4	45		+ 3546	106	+35	+52	+ 3702	51
2681	Sa	45 Nov 9.5	1.5	IIaO	6	1	90	9	9½	42		+ 736	134	+41	+14	+ 778	52
2683	Sb	41 Apr 19.8	10.0	I1200	6	6	42*	4*	4	78	- 59	+ 335	158	+40	-17	+ 284	
		41 Apr 23.8	9.0	I1200	6	6	42*	5*	4	26	+ 59						
2715	Sc	48 Feb 15.3	5.0	IIaO	6	6	18*	4*	4	48		+ 1158	102	+34	+57	+ 1329	53
2732	So	41 Feb 4.5	5.0	I1200	6	2	67*	3	2½	8		+ 2121	100	+33	+59	+ 2298	
2748	Sc	47 Feb 24.3	5.0	IIaO	5	3	40*	6*	5½	48		+ 1489	104	+35	+54	+ 1651	
2776	Sc	48 May 12.3	4.0	IIaO	5	3	115	4	5½	134		+ 2673	144	+44	+01	+ 2676	54
2784	So	42 Jan 17.4	4.0	103aO	6	2	90	3	2½	52		+ 708	220	+17	-92	+ 432	
2787	SBa	39 Apr 22.2	4.0	IES	6	1	90	3	3½	79		+ 551	111	+39	+44	+ 683	
2805	[Sc]	53 Mar 8.3	6.5	IIaO	6	2	90	7*	6	54		+ 1916	117	+41	+35	+ 2021	55
2835	Sc	48 Jan 13.4	4.2	IIaO	5	6	20*	2	1	175	+ 39	+ 909	220	+20	-91	+ 636	56
								3†	3½	10	-104						57
								1†	1	..	+ 67						58
								3†	3½	60	+ 20						59
								8†	7	93	+ 27						60
2841	Sb	47 Feb 23.2	4.0	IIaO	5	6	150*	5*	6	30		+ 740	134	+45	+14	+ 782	
2903	Sc	50 Mar 12.3	5.0	IIaO	4	6	26*	6*	4	68		+ 645	177	+45	-38	+ 531	61
2950	SBo	54 Jan 13.5	3.5	IIaO	4	2	160	3	4½	32		+ 1339	122	+46	+27	+ 1420	62
2967	Sc	42 Jan 20.4	4.0	IIf	6	2	90	3	2½	67	- 78	+ 2245	205	+38	-68	+ 2041	
		42 Feb 14.3	6.0	103aO	6	2	90	3	2½	83	+ 79						
2976	Sc	47 Feb 22.3	5.0	IIaO	5	6	145*	5†	4	75	- 41	+ 42	110	+42	+43	+ 171	63
		47 Apr 23.3	6.0	IIaO	5	6	145*	5†	5	68	+ 45						63
		Feb 22.3						5†	5	27	- 7						64
		Apr 23.3						6†	6	71	+ 10						64
		Feb 22.3						1†	1	..	- 39						65
		Apr 23.3						1†	1	..	- 33						65
3027	[Sc]	53 Feb 17.4	6.0	IIaO	5	6	120*	1*	1	..	+ 23	+ 1079	105	+40	+49	+ 1226	66
		53 Mar 9.3	6.0	IIaO	5	6	120*	2*	1½	20	- 16						66
		Feb 17.4						1†	1	..	(- 66)						67
		Mar 9.3						1†	1	..	(- 81)						67
		Mar 9.3						1†	½	..	(- 52)						68
		Mar 9.3						1†	½	..	(+216)						69
		Feb 17.4						1†	1	..	(+112)						70
		Mar 9.3						1†	1	..	(+156)						70
3031	Sb	38 Jan 26.5	5.7	IES	6	6	155*	4*	5½	25	+ 20	- 64	108	+42	+45	+ 71	71
(M81)		38 Mar 26.9	17.0	IES	8	6	155*	4*	5½	50	- 34						71

Table V. Continued.

NGC *IC (1)	Neb. Type (2)	Date Mean UT (3)	Exp. Hr. (4)	Emul. Type (5)	Slit W (6)	Slit L (7)	Slit PA (8)	Lines No. (9)	Lines Wt. (10)	AD (11)	Pl. Res. (12)	Redshift c·Δλ/λ₀ (13)	Galactic Long. (14)	Galactic Lat. (15)	100 Cos A (16)	Corr. Redshift (17)	Note No. (18)
		38 Apr 2.8	6.5	IES	8"	6'	65°	4*	5½		+ 3						71
		50 Feb 16.2	3.5	IIaO	4	6	150*	4*	7½		+ 9						
3034	Irr	39 Mar 15.2	4.0	IES	6	6	65*					+ 275	108°	+42°	+45	+ 410	72
(M82)		46 Apr 24.3	6.0	IIaO	6	6	65*										73
		46 Apr 27.3	6.0	IIaO	6	6	65*										74
		46 Apr 28.3	6.0	IIaO	4	6	65*										75
3055	Sc	39 Apr 20.3	5.0	IES	8	3	72*	5*	6	139		+ 1913	203	+44	-61	+ 1730	76
3065	So	47 Feb 25.2	4.0	IIaO	5	6	155	4*	5½	67		+ 2051	105	+40	+50	+ 2201	77
3066	Sb	47 Feb 25.2	4.0	IIaO	5	6	155	4*	4½	84		+ 2132	105	+40	+50	+ 2282	
3077	Irr	36 Dec 22.5	5.0	IES	6	1	90	7*	6½	39		- 158	109	+42	+44	- 26	78
3079	Sc	50 May 7.3	4.5	IIaO	4	3	168*	4*	4½	83		+ 1171	126	+50	+21	+ 1234	79
								4*	4½	79	(+359)						80
3109	Irr	46 Jan 28.4	3.0	IIaO	6	3	111	1†	1	..	- 19	+ 441	231	+24	-91	+ 168	81
		46 Jan 31.4	3.0	IIaO	6	6	90	1†	1	..	+ 19						82
3145	Sb	49 Apr 1.2	4.5	IIaO	6	2	20*	4*	5½	114		+ 3855	221	+35	-80	+ 3615	
Sex Dw	Irr	47 Jan 28.4	3±	IIaO	5	6	20	2†	3	37	+ 46	+ 436	215	+40	-72	+ 220	83
		47 Feb 20.4	5.0	IIaO	5	6	20	3†	3½	18	- 40						
3159	[E2]	54 Feb 5.5	4.5	IIaO	4	2	82	3	4½	179		+ 6950	150	+57	-05	+ 6935	84
3161	[E3]	54 Feb 5.5	4.5	IIaO	4	2	82	4*	4½	56		+ 6204	150	+57	-05	+ 6189	84
3163	[E1]	54 Feb 9.5	5.0	IIaO	4	2	90	4	5	115		+ 6245	150	+57	-05	+ 6230	85
3169	Sa	54 Jan 10.4	3.5	IIaO	4	2	50*	7*	7	76		+ 1312	207	+47	-60	+ 1132	
3184	Sc	40 Mar 13.3	8.0	I1200	6	1	90	2	2	42		+ 395	145	+57		+ 395	86
3190	Sa	41 Jan 29.5	5.0	I1200	7	3	116*	4	5	106	- 68	+ 1380	180	+56	-32	+ 1284	
		41 Jan 30.5	5.0	I1200	7	3	116*	4	6	41	+ 57						
3198	Sc	48 Jan 11.4	6.0	IIaO	5	6	42*	5*	4	87		+ 649	138	+56	+07	+ 670	
3239	Irr	47 May 14.2	3.0	IIaO	5	3	125	2*	1½	11	- 64	+ 880	189	+56	-39	+ 763	87
								8†	7	60	+ 14						88
*2574	[Irr]	47 Feb 14.3	5.5	IIaO	5	1	90	10†	8	69	+ 44	+ 28	106	+44	+46	+ 166	89
		47 Feb 21.3	5.0	IIaO	5	2	131	10†	8	30	- 24						90
								6†	5½	64	- 30						90
3259	Sb	48 Feb 15.5	4.0	IIaO	5	3	18*	5*	6	77		+ 1866	110	+47	+39	+ 1983	
3294	Sc	48 Jan 14.4	5.0	IIaO	5	2	87	3	2½	116	+ 53	+ 1469	150	+61	-04	+ 1457	91
								6†	5	59	- 27						92
3310	Sb	36 Mar 26.3	3.0	IES	4	½*	90	7*	6½	142	- 91	+ 998	124	+55	+21	+ 1061	93
		37 Dec 3.5	2.5	IES	6	1	90	10*	10	107	+ 59						
3319	SBc	49 Apr 27.3	5.0	IIaO	4	2	135	9†	7½	39	(-191)						94
								8†	7	44	(-208)						95
		54 Apr 30.3	5 ±	IIaO	4	3	40*	5*	5	72		+ 826	144	+61	+01	+ 829	96
3338	Sc	48 Feb 13.3	5.0	IIaO	5	3	90*	3	3½	90		+ 1330	200	+58	-43	+ 1201	
3359	SBc	48 Mar 1.2	5.0	IIaO	5	2	14*	4*	4	68		+ 1008	110	+50	+37	+ 1119	97
								2†	3	37	(+ 35)						98
								3†	3½	85	(+134)						99
								3†	3½	56	(-100)						100
3370	Sc	48 Mar 8.2	3.5	IIaO	5	3	150*	5*	4½	78		+ 1400	195	+61	-37	+ 1289	
3389	Sc	48 Mar 3.4	4.0	IIaO	5	3	96*	6*	5½	54		+ 1334	203	+59	-44	+ 1202	101
3395	Sc	48 Mar 3.2	3.0	IIaO	5	3	70	4*	4	30		+ 1751	161	+64	-12	+ 1715	102
3396	Sc							7*	5½	99		+ 1643				+ 1607	102
3403	Sc	48 Feb 16.4	5.5	IIaO	5	3	73*	4*	4	55		+ 1244	100	+42	+52	+ 1400	103
3419	[So]	48 Apr 1.3	2.0	IIaO	5	2	90	7	5½	127		+ 2982	201	+60	-42	+ 2856	104
3430	Sc	48 Mar 2.2	5.0	IIaO	5	3	32*	4*	3	185		+ 1742	162	+65	-12	+ 1706	
3432	Sc	41 Jan 31.5	4.8	I1200	6	6	41*	7*	6½	75		+ 609	154	+65	-07	+ 588	105

Table V. Continued.

NGC *IC	Neb. Type	Date Mean UT	Exp. Hr.	Emul. Type	Slit W	Slit L	Slit PA	Lines No.	Lines Wt.	AD	Pl. Res.	Redshift c·Δλ/λ₀	Galactic Long.	Galactic Lat.	100 Cos A	Corr. Redshift	Note No.
(1)	(2)	(3)	(4)	(5)	(6)	(7)	(8)	(9)	(10)	(11)	(12)	(13)	(14)	(15)	(16)	(17)	(18)
3510	SBc	48 Apr 13.3	6.0	IIaO	5"	3'	165°*	4*	$4\frac{1}{2}$	68		+ 719	170°	+68°	-16	+ 671	106
3512	Sc	48 May 3.3	4.0	IIaO	5	2	90	4*	$3\frac{1}{2}$	80		+ 1502	170	+67	-17	+ 1451	107
3516	SBo	40 Mar 5.2	3.0	I1200	6	1	90	7*	$8\frac{1}{2}$	175		+ 2632	100	+43	+53	+ 2791	108
3556	Sc	46 May 1.8	7 ±	IIaO	6	6	83*	11*	$8\frac{1}{2}$	114		+ 650	115	+56	+28	+ 734	109
3607	So	37 Feb 10.3	3 ±	IES	6	1	90	5	4	78		+ 871	198	+67	-31	+ 778	
3628	Sb	48 Jan 18.4	5.0	IIaO	5	6	103*	5*	5	85		+ 842	210	+65	-38	+ 728	110
3631	Sc	40 May 6.3	5.5	I1200	6	1	90	4	$5\frac{1}{2}$	96	- 9	+ 1087	115	+60	+25	+ 1162	
		42 Mar 21.0	2 ±	103aO	6	2	109	3	3	22	+ 16						
3646	Sc	48 May 4.3	4.0	IIaO	5	3	50*	2	2	28		+ 4425	197	+69	-28	+ 4341	111
								2†	$2\frac{1}{2}$	4	(-329)						112
3672	Sc	49 Apr 22.3	4.5	IIaO	6	6	10*	4	4	110		+ 2045	240	+48	-67	+ 1844	113
3810	Sc	47 Jan 22.4	4.0	IIaO	6	3	90	7*	7	36		+ 1005	221	+68	-36	+ 897	
3887	Sb	39 Apr 15.8	12.0	IES	8	1	90	4	4	42		+ 1163	250	+44	-70	+ 953	114
3893	Sc	40 Mar 4.4	3 ±	I1200	8	1	90	5	6	35		+ 868	113	+67	+21	+ 931	
3938	Sc	47 May 19.3	5.0	IIaO	5	6	37	2	$1\frac{1}{2}$	77	+ 71	+ 874	117	+70	+16	+ 922	115
								2†	$2\frac{1}{2}$	3	- 45						116
								1†	1	..	+ 6						117
3941	SBo	37 Feb 15.4	3.0	IES	6	1	90	7	$5\frac{1}{2}$	55		+ 927	138	+76	+03	+ 936	
3953	SBb	38 Jan 25.4	5.0	IES	6	1	90	3	3	83		+ 1008	107	+63	+28	+ 1092	
3990	[So]	46 May 7.2	4.0	IIaO	4	6	96	4	3	28	+ 13	+ 720	103	+61	+32	+ 816	118
		54 May 6.3	2.0	IIaO	4	3	48*	3	$4\frac{1}{2}$	41	- 8						
3995	Sc	48 Apr 1.4	3.0	IIaO	5	3	27*	6*	7	29		+ 3347	152	+78	-03	+ 3338	119
3998	So	46 May 7.2	4.0	IIaO	4	6	96	3*	5	43	+ 46	+ 1059	103	+61	+32	+ 1155	
		54 May 6.2	2.0	IIaO	4	3	125*	4*	$4\frac{1}{2}$	83	- 50						
4030	Sc	47 Apr 24.3	5.0	IIaO	5	2	100	6	$5\frac{1}{2}$	47		+ 1509	246	+60	-49	+ 1362	120
4064	SBap	50 Mar 23.4	3.0	IIaO	4	2	166	5*	$3\frac{1}{2}$	47		+ 1033	222	+77	-22	+ 967	121
4088	Sc	41 May 20.8	10.0	I1200	6	6	57*	4*	4	142		+ 739	105	+65	+27	+ 820	122
								3*	3	136	(-287)						123
4102	Sa	40 May 7.5	5.5	I1200	6	1	67	7*	8	78		+ 878	103	+64	+29	+ 965	124
4111	So	37 Apr 7.3	4.5	IES	6	6	150*	5*	6	60	+100	+ 870	113	+73	+15	+ 915	
		51 July 8.2	2.0	IIaO	4	2	150*	5*	6	70	-100						
4116	SBc	48 Mar 7.5	4.0	IIaO	5	3	147*	5*	5	65		+ 1304	248	+64	-43	+ 1175	125
4125	E6	39 Apr 22.4	2.9	IES	6	1	90	4	5	120		+ 1485	96	+52	+46	+ 1623	
4128	So	47 June 21.2	3.0	IIaO	5	2	67*	4	5	43		+ 2395	95	+48	+51	+ 2548	
4151	Sa	38 May 26.2	2.0	IES	4	1	90	9*	$13\frac{1}{2}$	42		+ 934	118	+76	+11	+ 967	126
4162	Sc	49 May 3.4	4.5	IIaO	5	3	170*	4	$3\frac{1}{2}$	135		+ 2546	200	+82	-12	+ 2510	
4178	Sc	50 Feb 23.5	4.2	IIaO	4	6	32*	5*	$3\frac{1}{2}$	108	- 11	+ 233	245	+72	-30	+ 143	127
		54 Mar 1.3	3.2	IIaO	4	6	32*	3*	2	55	+ 18						127
		50 Feb 23.5	4.2	IIaO	4	6	32*	3†	$3\frac{1}{2}$	9	(+ 31)						128
		54 Mar 1.3	3.2	IIaO	4	6	32*	6†	$5\frac{1}{2}$	59	(+ 63)						128
4194	[SBop]	53 Dec 14.5	5.0	IIaO	3	2	160	9*	9	36		+ 2585	100	+62	+33	+ 2684	129
4212	Sc	48 Mar 6.8	5.0	IIaO	5	3	48	4	$5\frac{1}{2}$	61		+ 2125	242	+75	-26	+ 2047	130
4214	Irr	54 July 2.3	3.0	IIaO	4	2	152	8*	$9\frac{1}{2}$	56		+ 318	120	+79	+08	+ 342	131
4216	Sb	41 Apr 21.8	14.0	I1200	6	6	20*	3	$4\frac{1}{2}$	54		+ 59	242	+75	-26	- 19	
4236	Sc	39 Mar 14.4	6.0	Agfa	6	1	90	5†	$5\frac{1}{2}$	59		+ 27	93	+48	+53	+ 186	132
4244	Sc	46 May 5.3	6.0	IIaO	6	6	45*	3*	$4\frac{1}{2}$	56		+ 265	118	+78	+10	+ 295	133
4254 (M99)	Sc	40 Mar 5.4	5.5	I1200	6	1	90	4	5	13		+ 2451	245	+75	-26	+ 2373	

Table V. Continued.

NGC *IC	Neb. Type	Date Mean UT	Exp. Hr.	Emul. Type	Slit W	Slit L	Slit PA	Lines No.	Lines Wt.	AD	Pl. Res.	Redshift c·Δλ/λ₀	Galactic Long.	Galactic Lat.	100 Cos A	Corr. Redshift	Note No.
(1)	(2)	(3)	(4)	(5)	(6)	(7)	(8)	(9)	(10)	(11)	(12)	(13)	(14)	(15)	(16)	(17)	(18)
4256	[Sb]	47 Jun 22.3	3.0	IIaO	5″	6′	43°*	3	2½	59		+ 2583	95°	+53°	+46	+ 2721	
4291	E2	39 May 13.3	4.0	Agfa	8	1	90	3	3	67		+ 1903	92	+42	+59	+ 2080	
4293	Sa	47 May 24.3	4.0	IIaO	5	6	74*	2	3	140		+ 750	230	+79	-19	+ 693	134
4365	E2	41 May 16.3	3.5	I1200	6	1	90	3	2½	18		+ 1290	255	+69	-33	+ 1191	
4386	E5	47 Jun 23.3	3.3	IIaO	5	2	140*	4	5½	61		+ 1811	92	+41	+60	+ 1991	
4401	Sc	36 Mar 19.4	5.2	IES	4	½*	90	2†	3	6	+ 68	+ 294	118	+82	+06	+ 312	135
		47 Feb 22.5	3.0	IIaO	5	2	24	9†	7½	61	- 65						135
								3†	3½	32	+ 80						136
4406 (M86)	E3	36 Mar 26.4	2.5	IES	4	½*	90	5	4	66	- 58	- 309	251	+75	-25	- 384	
		37 Dec 7.5	2.8	IES	6	1	90	4	3	86	+ 78						
4486 (M87)	Eo	49 Jun 24.3	2.0	IIaO	4	3	111	6*	6	76	- 26	+ 1196	255	+75	-24	+ 1124	137
		51 July 7.2	2.0	IIaO	4	2	113	4*	5½	32	+ 28						137
4494	E1	37 Dec 1.5	3.0	IES	6	1	90	4	3½	162		+ 1303	210	+86	-06	+ 1285	
4517	Sc	48 Jan 19.5	5.0	IIaO	5	6	80*	8†	6½	63	+ 15	+ 1218	263	+63	-40	+ 1098	138
								3†	4	57	- 24						139
4519	Sc	48 Mar 8.4	3.3	IIaO	5	3	112	4*	4	68		+ 1213	260	+71	-30	+ 1123	140
4535	Sc	40 Mar 12.4	7.8	I1200	6	1	90	5*	6	48		+ 2097	261	+70	-30	+ 2007	141
4536	Sb	47 Feb 25.4	5.8	IIaO	5	3	90	4*	4½	74		+ 1927	265	+65	-36	+ 1819	142
								5†	5	68	(- 83)						143
4552 (M89)	Eo	37 Feb 15.5	2.5	IES	6	1	90	3	3	94		+ 247	261	+75	-23	+ 178	
4559	Sc	46 Jun 2.3	4.5	IIaO	6	6	137*	4*	5½	60		+ 856	160	+87	-01	+ 853	
4565	Sb	38 Apr 6.4	4.0	IES	8	6	140*	3	3	64	- 43	+ 1174	217	+87	-04	+ 1162	
		47 Jan 18.4	5.0	IIaO	5	6	133*	4*	5½	33	+ 24						
4567	Sc	47 Jan 21.5	2.5	IIaO	6	3	162	7	5½	19		+ 2284	262	+73	-26	+ 2206	144
4568	Sc							4	5	122		+ 2413				+ 2335	144
4594 (M104)	Sb	37 Apr 17.3	5.8	IES	6	6	90*	4*	5	24	+ 19	+ 1207	268	+51	-53	+ 1048	
		38 Mar 31.4	7.1	IES	8	6	92*	3	2½	96	- 37						
4605	Sc	39 Mar 15.4	5.0	IES	6	6	118	4*	5	99		+ 140	91	+56	+45	+ 275	145
4618	Scp	40 Mar 6.4	6.0	I1200	8	1	70	7*	8	47		+ 484	93	+76	+19	+ 541	146
4636	Eo	47 Apr 25.3	4.0	IIaO	5	2	100	4	4½	58		+ 954	269	+65	-35	+ 849	
4643	SBo	47 Jun 10.3	3.0	IIaO	5	2	134	6	7	34		+ 1432	270	+64	-36	+ 1324	147
4647	Sc	48 May 6.3	5.0	IIaO	5	6	136	4*	4½	130		+ 1448	268	+74	-23	+ 1379	148
4649 (M60)	E2							3	2½	33		+ 1244				+ 1175	148
4656	Irr	40 Mar 8.4	5.0	I1200	8	1	90	10†	10½	63		+ 721	92	+85	+07	+ 742	149
4666	Sc	47 May 23.3	4.0	IIaO	5	6	44*	4*	7	39		+ 1645	270	+62	-38	+ 1531	
4699	Sb	46 May 6.3	4.0	IIaO	4	3	50*	3	4½	49		+ 1511	272	+54	-47	+ 1370	
4713	Sc	47 May 15.3	4.0	IIaO	5	3	90	8*	7½	64		+ 664	273	+68	-30	+ 574	150
4736 (M94)	Sb	38 May 23.3	5.0	IES	6	6	123*	8*	8	50	- 2	+ 313	86	+76	+21	+ 376	151
		38 May 30.3	14.4	IES	6	6	123*	7*	6½	24	+ 2						151
		23.3						3†	3½	169	(+256)						152
		30.3						2†	2½	11	(+228)						152
		23.3						1†	1	..	(-210)						153
		30.3						1†	1	..	(+ 28)						153
4750	Sb	47 Jan 18.5	3.0	IIaO	5	2	90	5*	6	89		+ 1647	89	+45	+59	+ 1824	
4753	Sop	41 May 17.3	4.0	I1200	6	1	90*	3	2½	12		+ 1364	277	+61	-36	+ 1256	
4762	Sa	38 Jun 2.3	4.6	IES	6	6	30*	3	4½	69	- 94	+ 997	277	+74	-21	+ 934	
		50 Feb 22.5	4.2	IIaO	4	3	30*	3	2½	37	+ 31						
		51 July 9.2	2.0	IIaO	4	2	30*	4	5½	63	+ 62						
4775	Sc	47 May 20.3	4.0	IIaO	5	2	172	3*	2½	77	+ 66	+ 1684	275	+56	-43	+ 1555	154

Table V. Continued.

NGC *IC (1)	Neb. Type (2)	Date Mean UT (3)	Exp. Hr. (4)	Emul. Type (5)	Slit W (6)	Slit L (7)	Slit PA (8)	Lines No. (9)	Lines Wt. (10)	AD (11)	Pl. Res. (12)	Redshift c·Δλ/λ₀ (13)	Galactic Long. (14)	Galactic Lat. (15)	100 Cos A (16)	Corr. Redshift (17)	Note No. (18)
								5†	5	73	- 33						155
4781	Sc	47 May 22.3	4.0	IIaO	5"	3'	118°*	3*	3½	67		+ 895	273°	+52°	-48	+ 751	
4789	[E5]	52 Feb 25.4 53 Apr 6.4	2.0 2 ±	IIaO IIaO	4 4	1 1	90 90	3 2	3½ 1½	73 77	+ 69 -160	+ 8372	123	+88	+01	+ 8375	 156
4793	Sc	49 May 4.4	5.0	IIaO	5	2	55*	6†	6	68		+ 2529	30	+87	+05	+ 2544	157
4848	[pec]	51 Jun 3.3	5.0	IIaO	5	2	150*	3*	4	97		+ 7209	67	+87	+05	+ 7224	
*3949	[So]	51 Jun 7.3	5.0	IIaO	5	2	74*	2	2	14		+ 7526	8	+87	+04	+ 7538	158
Anon	[pec]	51 Jun 27.3	4.0	IIaO	4	1	90	1*	..	..		+13457	62	+84	+10	+13487	159
4861	Irr	47 Jun 18.3	2.5	IIaO	5	1	64	11†	11½	65		+ 793	70	+83	+12	+ 829	160
4889	E4	41 Mar 7.5	4.0	I1200	6	1	90	3	2½	152		+ 6585	5	+86	+04	+ 6597	
4900	Sc	47 May 16.3	3.5	IIaO	5	2	141	9*	7½	69		+ 1054	279	+64	-32	+ 958	161
4902	SBb	48 Feb 13.5	4.0	IIaO	5	3	67	4	5½	70		+ 2758	276	+47	-51	+ 2605	162
*4040	[Spec]	51 Jun 3.3	5.0	IIaO	5	2	150*	5*	4½	131		+ 7515	11	+87	+04	+ 7527	
4907	SBb	51 May 9.3 51 May 30.3	7.0 5.0	IIaO IIaO	4 5	2 2	31 31	1 4	.. 2½	... 37	+100 - 40	+ 5868	12	+86	+05	+ 5883	163
4911	Sb	51 May 28.8	10.0	IIaO	5	2	90	4	5½	48		+ 8006	6	+86	+05	+ 8021	
4921	Sa	51 May 7.3	5.5	IIaO	4	2	90	5	4½	51		+ 5459	7	+86	+05	+ 5474	
Anon	[Sc]	47 May 13.3	4.0	IIaO	5	3	105	2†	3	56		+ 1350	279	+59	-37	+ 1239	164
4952	[E5]	53 Apr 7.2	3.0	IIaO	5	1	30	3	2½	32		+ 5865	21	+85	+07	+ 5886	
4995	Sb	47 May 18.3	4.0	IIaO	5	2	80*	6*	7½	66		+ 1835	281	+55	-40	+ 1715	
5005	Sb	50 Apr 19.3	7.0	IIaO	4	6	70*	6*	7½	46		+ 1041	62	+79	+19	+ 1098	
5033	Sc	46 May 7.4	3.0	IIaO	6	3	0*	5*	6	46		+ 908	58	+78	+20	+ 968	165
5055 (M63)	Sb	38 May 24.8 50 Apr 21.2 50 May 9.3	7.0 2.5 5.0	IES IIaO IIaO	8 4 4	6 3 6	104* 104* 104*	5* 4* 5*	5½ 5 6	75 38 47	- 26 - 50 + 67	+ 538	68	+74	+26	+ 616	
5061	Eo	47 May 17.3	1.0	IIaO	5	2	148	4	5½	46		+ 2065	279	+35	-59	+ 1888	
5068	SBc	47 May 22.3	4.0	IIaO	5	2	155	4*	4	164		+ 570	280	+40	-54	+ 408	166
5198	E1	40 Jun 4.3	3.8	I1200	8	1	90	3	2½	36		+ 2562	68	+69	+35	+ 2667	
5204	Sc	47 Jun 19.3	4.0	IIaO	5	3	71	6†	6½	48		+ 272	80	+58	+48	+ 416	167
5248	Sc	47 Feb 20.6	1.5	IIaO	5	2	90	6	6	33		+ 1232	306	+67	-13	+ 1193	168
5301	[Sc]	50 Apr 18.3	6.0	IIaO	4	6	150*	3	3	53		+ 1702	60	+68	+37	+ 1813	169
5308	So	49 Jun 28.3	4.0	IIaO	4	3	60*	3	4½	14		+ 2035	77	+55	+53	+ 2194	
HoIV	[Irr]	53 May 12.3	5.5	IIaO	5	3	29*	5†	6	21		+ 149	69	+61	+47	+ 290	170
5363	Irr	51 Apr 8.4	6.5	IIaO	4	2	143*	6*	6½	72		+ 1138	310	+62	-12	+ 1102	
5371	Sb	40 May 10.4 51 July 10.3	5.5 3.0	I1200 IIaO	6 4	1 2	90 90	3 5*	2½ 6	147 34	+117 - 49	+ 2633	45	+70	+34	+ 2735	
5468	Sc	47 Jun 16.3 48 May 5.4	3.5 6	IIaO IIaO	5 5	3 3	12 5	1† 5† 4* 3†	1 5½ 3 3	.. 88 73 106	+ 19 + 78 - 27 -104	+ 2856	305	+51	-22	+ 2790	171 172 173 174
5473	SBo	49 Jun 29.3	4.0	IIaO	4	3	80	3	4½	79		+ 2141	66	+59	+50	+ 2291	175
5474	Sc	40 May 12.3 May 27.6	7.0 8.5	I1200 I1200	6 8	1 1	90 90	3* 4*	4 4½	22 106	- 30 + 26	+ 247	65	+60	+49	+ 394	176
5585	Sc	42 Apr 18.3	7.0	103aO	6	2	118	4*	6½	139		+ 304	65	+57	+54	+ 466	177
5633	Sb	47 Feb 21.5	4.0	IIaO	5	2	90	9	8	71		+ 2390	49	+62	+47	+ 2531	
5653	Sc	52 July 28.2	2.5	IIaO	5	3	90	6*	4½	118		+ 3557	16	+67	+30	+ 3647	178

Table V. Continued.

NGC *IC	Neb. Type	Date Mean UT	Exp. Hr.	Emul. Type	Slit W	Slit L	PA	Lines No.	Lines Wt.	AD	Pl. Res.	Redshift c·Δλ/λ₀	Galactic Long.	Galactic Lat.	100 Cos A	Corr. Redshift	Note No.
(1)	(2)	(3)	(4)	(5)	(6)	(7)	(8)	(9)	(10)	(11)	(12)	(13)	(14)	(15)	(16)	(17)	(18)
5668	Sc	47 Feb 24.5	4.3	IIaO	5"	3'	57°	6*	5	88		+ 1665	323°	+55°	-02	+ 1659	179
5676	Sc	48 May 3.4	2.8	IIaO	5	3	49*	3	2½	78		+ 2244	55	+60	+50	+ 2394	
5678	Sc	50 Apr 15.4	5.0	IIaO	4	2	90	4	3½	89		+ 2300	65	+54	+58	+ 2474	180
5713	Sb	40 Jun 5.3	4.0	I 1200	8	1	90	5*	5½	103	+ 87	+ 1965	320	+51	-06	+ 1947	
		51 July 2.3	3.0	IIaO	5	2	78	7*	8½	77	- 56						181
5746	Sb	41 May 23.0	12.5	I 1200	6	6	171*	$\underline{3}$	2½	118		+ 1882	323	+51	-02	+ 1876	
5846	Eo	49 Jun 27.3	2.5	IIaO	4	3	2	4*	5	63		+ 1774	328	+47	+04	+ 1786	182
Comp	E3							3	4½	23		+ 2321				+ 2333	183
5850	SBb	46 Jun 21.3	3.2	IIaO	6	3	113	4*	5½	84		+ 2476	329	+46	+05	+ 2491	184
5857	Sb	50 May 9.3	5.5	IIaO	4	2	132*	3	3½	63		+ 4721	354	+56	+27	+ 4802	185
5866	So	47 Apr 20.4	2.8	IIaO	5	6	136*	6	7	96	- 21	+ 850	58	+52	+61	+ 1033	
		51 July 26.2	2.5	IIaO	4	3	136*	$\bar{6}$	6½	45	+ 23						
5907	Sb	47 Apr 19.4	4.0	IIaO	5	6	160*	$\underline{4}$	5½	34		+ 522	57	+51	+63	+ 711	
Anon	[So]	49 May 23.3	6.0	IIaO	5	1	90	4	5½	113		+10540	341	+48	+18	+10594	186
Anon	[Eo]	49 May 24.3	6.0	IIaO	5	1	90	3	2	60		+10546	341	+48	+18	+10600	186
5949	Sc	42 Jun 18.4	6.0	103aO	6	2	90	3*	2½	98		+ 380	66	+45	+69	+ 587	
5970	SBb	40 May 9.3	7.0	I 1200	6	1	80	3	2½	40		+ 2127	348	+47	+26	+ 2205	187
5982	E4	39 May 13.4	2.0	Agfa	8	1	90	2	4	56		+ 2981	60	+47	+68	+ 3185	188
6015	Sc	46 Jun 4.3	6.0	IIaO	6	6	45*	$\underline{5}$*	5	115		+ 732	63	+43	+72	+ 948	
6027d	Sa	48 May 12.4	2.8	IIaO	5	3	88	3	2½	83	+119	+ 4468	2	+46	+42	+ 4594	189
		51 July 3.3	4.0	IIaO	4	2	83	4	5	54	- 59						189
6027a	Sa							5	4½	39		+ 4036				+ 4162	190
6070	Sc	46 Jun 24.3	5.0	IIaO	6	3	76	3	2½	25		+ 2120	340	+34	+22	+ 2186	191
								5†	4½	61	(-152)						192
6217	Sc	38 Aug 27.4	5.0	IES	6	1	90	2*	4	32		+ 1382	78	+33	+77	+ 1613	193
6239	SBb	46 Jun 22.3	4.0	IIaO	6	3	113*	$\underline{8}$*	8	40		+ 964	35	+39	+73	+ 1183	194
6314	Sa	47 May 16.4	3.0	IIaO	5	2	177*	3*	2½	94		+ 6748	12	+30	+64	+ 6940	
6384	Sb	46 Jun 30.3	5.0	IIaO	6	3	34*	3	4½	35	+ 25	+ 1717	358	+20	+51	+ 1870	
		51 July 8.4	3.5	IIaO	4	2	34*	$\bar{4}$	5½	58	- 20						
6412	Sc	41 Jun 21.3	6.0	IAO	6	2	171	2*	2½	88	- 77	+ 1508	74	+31	+81	+ 1751	195
		46 July 2.3	5.0	IIaO	6	3	170	4*	3	202	+ 64						
6503	Sc	36 Aug 24.3	6.0	IES	6	1½	124*	4*	4	79	+ 25	+ 33	66	+31	+85	+ 288	
		38 July 1.8	10.7	IES	10	6	122*	$\bar{6}$*	4½	46	- 19						
		47 May 15.4	4.0	IIaO	5	3	125*	$\bar{6}$*	6	49	- 6						196
6574	Sb	46 July 3.3	5.0	IIaO	6	2	90	8*	9	43		+ 2387	10	+14	+69	+ 2594	197
6635	[So]	41 Aug 19.3	8 ±	103aO	6	1	90	3	2	110	+ 73	+ 5071	11	+10	+68	+ 5275	198
		46 Jun 29.3	6.0	IIaO	5	1	90	3	2½	31	- 59						
6643	Sc	41 Jun 22.3	6.0	IAO	6	2	41*	5*	3½	124		+ 1682	72	+28	+84	+ 1934	
6654	SBa	41 Sept 23.2	3.0	103aO	6	1	90	4	5½	82		+ 1924	71	+28	+85	+ 2179	
6661	So	46 May 2.4	3.5	IIaO	6	1	83	3	4½	114		+ 4193	19	+13	+79	+ 4430	
6702	E2	49 Jun 27.4	3.0	IIaO	4	2	65*	3	4½	30		+ 4706	42	+19	+92	+ 4982	199
6703	So	49 Jun 24.4	3.5	IIaO	4	3	90	5*	6	28		+ 2394	42	+19	+92	+ 2670	200
6822	Irr	46 July 31.3	5.0	IIaO	5	6	92	11†	11	28	- 6	- 36	354	-20	+45	+ 99	201
								9†	9½	30	+ 9						202
		46 Aug 1.3	4.0	IIaO	5	2	122	5†	5½	24	- 26						203
		46 Aug 2.2	5.0	IIaO	5	2	122	7†	6½	10	+ 17						203
Anon	[Eo]	47 July 14.3	5.0	IIaO	5	1	90	3	2½	26		+ 4794	43	+ 5	+97	+ 5085	204
Anon	[Eo]	47 July 16.3	5.0	IIaO	5	1	90	2	2	30		+ 4708	43	+ 5	+97	+ 4999	205

Table V. Continued.

NGC *IC	Neb. Type	Date Mean UT	Exp. Hr.	Emul. Type	Slit W	Slit L	Slit PA	Lines No.	Lines Wt.	AD	Pl. Res.	Redshift c·Δλ/λ₀	Galactic Long.	Galactic Lat.	100 Cos A	Corr. Redshift	Note No.
(1)	(2)	(3)	(4)	(5)	(6)	(7)	(8)	(9)	(10)	(11)	(12)	(13)	(14)	(15)	(16)	(17)	(18)
*1317	SBo	40 July 31.9	12.0	I1200	6"	1'	90°	5	4½	122		+ 3975	12°	-21°	+68	+ 4179	206
6944	E1	40 Aug 5.0	10.5	I1200	6	1	90	3	3	165		+ 4598	20	-21	+76	+ 4826	207
6946	Sc	48 Aug 6.3	6.0	IIaO	4	2	126	7†	8½	39	- 22	- 70	64	+11	+97	+ 221	208
		48 Aug 10.3	5.5	IIaO	4	2	96	3†	3½	43	+ 54						209
6951	SBb	35 Sept 24.3	6.0	IES	4	½*	90	3	3	134		+ 1364	67	+15	+94	+ 1646	
7137	Sc	46 Aug 4.4	4.0	IIaO	5	2	90	3	3	76		+ 1505	45	-24	+90	+ 1775	210
7218	[Sc]	52 Aug 15.4	4.5	IIaO	5	2	90	5*	5	80		+ 1808	9	-52	+43	+ 1937	
7318a	E2	36 Aug 14.4	4.8	IES	6	1	90	4	4	33	- 9	+ 6724	61	-21	+93	+ 7003	211
		47 July 21.8	7.7	IIaO	5	2	90	3	2½	78	- 43						212
		51 July 7.4	4.2	IIaO	4	2	88	2	4	34	+ 35						212
7318b	SBb	47 July 21.8	7.7	IIaO	5	2	90	3	2	12	- 29	+ 5867	61	-21	+93	+ 6146	213
		51 July 7.4	4.2	IIaO	4	2	88	3	4½	100	+ 12						
7331	Sb	37 Aug 5.4	6.5	IES	6	6	167*	3	4½	94	+ 86	+ 919	63	-21	+93	+ 1198	
		38 July 25.8	12.3	IES	8	6	167*	4̲	5	43	- 77						
7392	Sb	42 Aug 15.3	5.0	103aO	6	3	115*	3	3	36		+ 2941	10	-63	+32	+ 3037	
7393	[Scp]	52 July 31.4	4.5	IIaO	6	3	90*	4	3	83		+ 3813	34	-55	+54	+ 3975	
7469	Sa	41 Aug 2.4	3.5	IIf	6	1	90	5*	5	140		+ 4692	52	-46	+69	+ 4899	214
7479	SBb	36 Aug 20.4	5.5	IES	6	1	6	6*	4½	75	- 82	+ 2425	55	-44	+72	+ 2641	215
		53 Oct 12.2	4.5	IIaO	4	6	6	4̲*	5½	20	+ 68						215
7562	E2	35 Oct 25.2	4.0	IES	4	½*	90	7	5½	65		+ 3806	54	-49	+66	+ 4004	
7585	Sop	41 Aug 1.4	3.5	IIf	6	1	90	3	3	73		+ 3385	44	-59	+51	+ 3538	
7625	Sop	41 Aug 25.4	4.5	103aO	6	1	90	5*	5½	41		+ 1828	64	-42	+74	+ 2050	216
7640	SBc	39 Aug 16.4	16.2	Agfa	6	6	169*	9†	12	92	(+ 90)						217
								2†	4	8	(+137)						218
								3†	4½	59	(+109)						219
								5*	6	83	+ 31	+ 423	73	-19	+90	+ 693	220
		53 Oct 9.3	6.0	IIaO	5	6	169*	8̲*	7	79	- 24						220
7671	So	36 Aug 23.4	5.0	IES	6	1	90	3	2½	140		+ 4129	62	-46	+69	+ 4336	
7679	So	45 Nov 4.2	2.6	IIaO	5	1	90	11*	13	81	- 33	+ 5101	56	-54	+59	+ 5278	221
		45 Nov 5.2	2.6	103aO	5	1	90	6*	7½	38	+ 39						221
7714	[Spec]	54 Nov 21.2	4.0	IIaO	4	3	85	9*	9	78		+ 2833	58	-56	+56	+ 3001	222
7715	[SBc]							5	3	173		+ 2795				+ 2963	223
7723	SBb	35 Oct 28.2	5.0	IES	4	½*	90	4*	4	160	- 57	+ 1973	41	-68	+36	+ 2081	224
		50 Aug 12.4	3.8	IIaO	5	2̲	70	2	3	150	- 91						225
		53 Oct 28.7	7.5	IIaO	5	6	27*	6̲*	6	80	+ 84						226
7727	Sa	47 July 23.4	3.3	IIaO	5	2	90	5*	6½	97		+ 1877	41	-68	+35	+ 1982	
7742	Sb	35 Sept 25.3	6.0	IES	4	½*	90	5*	4½	114	- 43	+ 1748	67	-49	+64	+ 1940	
		35 Oct 24.3	6.0	IES	4	½*	90	6*	5½	46	+ 36						
7769	Sc	36 Aug 27.4	5.0	IES	6	1	90	4*	4	187		+ 4349	74	-40	+72	+ 4565	227
7770	Sb	41 Aug 27.2	4.5	103aO	6	1	90	3*	4½	236		+ 4338	74	-40	+72	+ 4554	228
7771	SBb	41 Aug 26.4	4.5	103aO	6	2	72*	8̲*	7½	45		+ 4276	74	-40	+72	+ 4492	229
7793	Sc	41 Sept 27.3	3.0	103aO	6	3	10	5*	4½	27		+ 177	330	-78	+02	+ 183	230

NOTES

Note No.	NGC *IC	

1. Anon — Faint field nebulae observed in connection with a search for possible far outlying globular clusters associated with the Andromeda nebula (Mayall and Eggen 1953); positions for 1950 are:

   [E2]: $0^h 23^m 14^s.4$, $+40° 40'.7$ (Plate Va);
   [E1]: 0 26 28.0, +39 12.1 (Plate Vb).

2. Anon — Faint field nebulae observed in connection with a program to obtain radial velocities for emission patches associated with the Andromeda nebula (Mayall 1950), since Baade had found them to be relatively blue on color-filter photographs taken in his survey of the spiral for emission objects (Baade 1945 and 1951); the object of smaller redshift carries Baade's discovery designation in M31 as "a" s pr ext I_2/II_2, the one of larger redshift, "b" s pr ext I_2/II_2; for the

Note No. NGC *IC

latter only a fairly strong 3727 could be measured on the spectrograms at a wave length of about 4065A (Plate IVa); enhanced auroral line at 3914; positions for 1950 and identifying configurations are (Plate Vc): Nebula "a," $0^h\,34^m\,53^s.4$, $+39°\,33'.8$; brighter star 55″ NE; actually "a" consists of two Sb's in contact; Nebula "b," $0^h\,35^m\,08^s.9$, $+39°\,38'.3$; fainter star 18″ NW, brighter star 58″ W, and fainter, diffuse nebula 48″ SE.

3. 185 Strong auroral spectrum superimposed.

4. 205 Hydrogen lines unusually strong (Plate IVb).

5. 214 Only H and K measured.

6. 224 Nucleus, drifted length of slit for all plates.

7. 224 On major axis, $14'.0$ s pr nucleus; absorption lines in unresolved nebulosity.

8. 255 Absorption lines broad and indistinct.

9. 278 Strong hydrogen absorption lines.

10. *79 Brightest member in group discussed by Shapley and Boyd (1940).

11. 428 Only 3727 in two emission patches 42″ NW and 48″ SE of center, on major axis.

12. 604 Brightest emission patch in M33; plates taken to check earlier velocity that indicated departure from rotational velocity curve (Mayall and Aller 1942).

13. 864 Narrow nuclear spectrum; early-type continuum, faint H and K, with 3727, $H\delta$, $H\gamma$, and $H\beta$ in emission (Plate IVc).

14. Anon Brightest (n pr) of close pair of "disrupted galaxies" described by Zwicky (letter Oct. 16, 1953); redshift measured from emission lines $H\beta$, $H\gamma$, and 3727, the latter also being present in the fainter (s f) component; position for 1950 is $2^h\,36^m.4$, $+18°\,9'$.

15. 1052 Spectrum previously described (Mayall (1936) in connection with performance of spectrograph.

16. 1068 Emission spectrum (Plate IVd); broad, bright bands studied spectrophotometrically by Seyfert (1943); apparent absence of absorption H line of *Ca* II, although K line is present, is due to superposition of emission from the longward component of the wide pair 3868 and 3967 of [*Ne* III].

17. 1073 Slit on central bar.

18. 1097 North-preceding part of double nucleus.

19. 1097 South-following part of double nucleus.

20. 1187 Nuclear absorption lines of poor visibility; $H\beta$ and $H\gamma$ in emission (Plate IVe).

21. 1300 Slit on bar.

22. 1331, 1332 Slit simultaneously on both nebulae.

23. 1359 Slit on bar and two emission patches; strong emission spectrum (Plate IVf).

24. 1385 Early-type absorption spectrum, with $H\beta$ in emission.

25. *342 Early-type continuous nuclear spectrum with $H\beta$ in emission and absorption lines nearly invisible; the plate listed is the only one of four suitable for measurement of redshift; the others are:

1941 Sept. 29.4, 4^h, IIf, 6″×1′, 90°; nuclear continuous spectrum that shows only $H\beta$ in weak emission.

1941 Nov. 19.3, 8^h, IIf, 6″×3′, 98°
1941 Nov. 22.3, 6^h, IIf, 6″×6′, 35° } Slit on nucleus and oriented to cover several condensations in the spiral; no emission lines show on these plates.

The probable absence of condensations having strong emission lines is also indicated by a slitless grating spectrogram, kindly taken by G. H. Herbig, which included the whole of this unusually large spiral (Shapley and Seyfert 1935).

Note No. NGC *IC

26. 1518 Early-type spectrum (Plate IVg) with broad hydrogen absorption lines; one part of nebula shows faint emission at $H\beta$ and the [*O* III] chief nebular lines (N1 and N2); slit oriented on brightest part, which may be a bar making a small angle with the major axis.

27. 1569 Emission spectrum; preliminary result published (Mayall 1935).

28. 1637 Only H and K in nuclear spectrum.

29. 1640 Slit on bright central bar for both plates.

30. *391 Only 3727; observed to determine whether galactic or extragalactic (Baade 1931).

31. 1744 Slit on central bar.

32. 1888, 1889 Slit on both members of close pair; spectra measured as of one object since lines in both nebulae have very nearly the same redshift (Plate IVh).

33. 1964 Has a foreground star 3″ following nucleus (Hubble, letter Jan. 9, 1947).

34. 2139 Slit on bright central bar; fairly strong 3727 and night sky spectrum (Plate IVi).

35. 2146 Spectrum reproduced by G. de Vaucouleurs (1950), who used inclination of 3727 to determine sense of rotation with respect to spiral structure.

36. 2276 Slit oriented through nucleus and emission patch 42″ NW (Plate IVj); the smaller redshift is from absorption lines in the nucleus, the larger from emission lines in the patch; the difference of 101 km/sec probably is entirely accidental and is not due to rotation, because the spiral is nearly normal to the line of sight.

37. 2300 The inclusion of this elliptical nebula with resolved nebulae (Hubble 1936b, Table II) was due to a misidentification; the object listed by Hubble is 2276.

38. 2366 Irregular nebula in M81 group investigated by Holmberg (1950); brightest emission patch in s pr end; preliminary result published (Mayall 1935).

39. 2475 Slit on both members of close pair 2474–75; weak exposure with clouds shows only spectrum of brightest component in measurable strength.

40. 2500 Slit on nucleus and double condensation 57″ SW.

41. 2500 Slit on nucleus and double emission patch 33″ NE.

42. 2523 Slit on bright central bar.

43. 2525 Slit on nucleus and through several very faint condensations, none of which show emission lines.

44. 2537 Brightest emission patch approximately 22″ NW of center.

45. HoII Brightest emission patch approximately in center of system; pB star 20″ SE; nebula is a dwarf in the M81 group described by Holmberg (1950).

46. HoII Row of three faint emission patches near SE side of system; star 30″ NW of central patch (Plate IVk).

47. 2633 Nuclear spectrum, absorption lines only.

48. 2633 Slit on bar; nuclear spectrum of absorption lines plus 3727.

49. 2633 Faint emission region in arm that crossed slit 55″ N of nucleus; only 3727 measurable and, since the nuclear spectrum lines

Note No.	NGC *IC	
		are inclined, its velocity was not used in the mean redshift.
50.	*2389	Spectrum confused with faint foreground star that is close to nuclear region in which both absorption and emission lines occur.
51.	2646	Absorption lines broad and faint.
52.	2681	Plate overexposed; early-type spectrum with strong hydrogen lines.
53.	2715	Absorption lines broad and faint.
54.	2776	Slit on nucleus and through faint condensation 65″ NE, which shows no emission lines.
55.	2805	Nuclear absorption lines, and emission lines from area where slit crossed spiral arm approximately 35″ W of nucleus; nebula is among those listed by Holmberg (1950) as possible members of the M81 group; the redshift rules out membership.
56.	2835	Nucleus, absorption $H\delta$ and $H+H\epsilon$; redshift is mean of all measures (Plate IVl).
57.	2835	Emission patch 135″ SW nucleus.
58.	2835	Emission patch 40″ SW nucleus (3727 only).
59.	2835	Emission patch 60″ NE nucleus.
60.	2835	Emission patch 135″ NE nucleus.
61.	2903	Hydrogen absorption lines wide and strong; faint condensation $7'.8$ SW of nucleus on major axis shows no emission lines on a plate taken 1950 Mar 13.3, 6^h, IIa-O, slit $4''\times2'$ in position angle 130°.
62.	2950	Slit on faint central bar that appears to make an angle of about 45° to the major axis.
63.	2976	Spiral in M81 group studied by Holmberg (1950); central region, possibly nucleus; redshift is mean of all measures since differences between those for nucleus and patches are too small to be of significance for rotation.
64.	2976	Bright emission patch 68″ NW of center.
65.	2976	Faint emission patch 80″ SE of center.
66.	3027	Central bar in nuclear region; redshift does not include measures of 3727 in emission patches, since their velocities indicate appreciable rotation, i.e. 3727 is inclined in the system as a whole.
67.	3027	Faint emission patch 95″ NW; faint foreground star almost superimposed; only 3727.
68.	3027	Very faint emission patch about 45″ NW where arm crossed slit; only 3727.
69.	3027	Very faint emission patch about 70″ SE; only 3727.
70.	3027	Faint emission patch about 110″ SE where arm crossed slit; only 3727.
71.	3031	Plates by H. W. Babcock; that of Apr 2.8 was taken with the slit on the minor axis.
72.	3034	Redshift is the result of a large number of measurements of velocity in different points in the nebula, made for investigation of its rotation; the value listed gives a symmetrical distribution of differential velocities in the nebula; the detailed measurements will be published separately.
73.	3034	Slit centered on SW end of nebula; strong auroral spectrum recorded.
74.	3034	Slit centered on NE end of nebula.
75.	3034	Taken with the narrowest slit, this plate shows to best advantage the uncommonly strong hydrogen absorption lines, which indicate a spectral type around A5 (Plate IVm).
76.	3055	Weak exposure that shows $H\beta$, $H\gamma$, and 3727 as emission features.

Note No.	NGC *IC	
77.	3065	Exposed simultaneously with 3066; there is some indication that a stronger exposure might show this wide pair connected by 3727, which is present in considerable intensity throughout both nebulae.
78.	3077	Irregular nebula in M81 group studied by Holmberg (1950); early-type spectrum with N1, N2, $H\beta$, $H\gamma$, and 3727 in emission.
79.	3079	Nuclear region, with very broad, poorly-defined absorption lines, probably inclined by rotation.
80.	3079	Condensation approximately 60″ SE that shows 3727 as the only faint emission; there probably is a real difference in velocity between the nucleus and this condensation, but the lines are so poor and difficult to measure that the amount is quite uncertain.
81.	3109	Only 3727 in several very faint emission patches (Plate Vd; 1, 2, and 3).
82.	3109	Only 3727 in two very faint emission patches (Plate Vd; 2 and 3).
83.	Sex dw	Faint emission patch in dwarf system found by Zwicky (1942), but previously mentioned by Hubble (1941) and by Baade (1940). Patch observed is on SE edge of system and may be identified by proximity to a faint, probably foreground, star approximately 10″ NW.
84.	3159, 3161	Exposed simultaneously; faint absorption lines in 3161; the redshifts of these two nebulae and of 3163 indicate membership in the group including 3158 as the brightest object.
85.	3163	Plate shows trace of spectrum, with approximately the same redshift, of a faint companion 15″ E.
86.	3184	Weak plate, only H and K measurable in absorption spectrum of nucleus.
87.	3239	Slit on central region, possibly nucleus, and bright emission patch; two lines measured are 3727 and emission $H\beta$.
88.	3239	Brightest emission patch 60″ SE of central condensation (nucleus?), and 50″ E of a fairly bright foreground star.
89.	*2574	Brightest emission patch in system, whose redshift indicates that it is a dwarf member of the M81 group studied by Holmberg (1950); plate also shows, at extreme end of slit, emission spectrum of fainter patch 30″ E of bright patch.
90.	*2574	Slit on brightest patch and another faint one 33″ SE.
91.	3294	Slit on nucleus and brightest emission patch.
92.	3294	Brightest emission patch 35″ W of nucleus; difference in redshifts probably not significant for rotation, because patch is nearly equidistant from major and minor axes.
93.	3310	Early-type continuum with strong 3727, and $H\gamma$ and $H\beta$ in emission.
94.	3319	Slit on two emission patches SW of central bar; larger and brighter of two patches.
95.	3319	Smaller and fainter of two patches.
96.	3319	Slit on central bar; fairly strong, broad hydrogen absorption lines; difference in velocity between bar and patches probably due to rotation.
97.	3359	Nucleus in patchy central bar; fairly strong hydrogen absorption lines.
98.	3359	Emission patch near end of bar approximately 30″ S of nucleus.
99.	3359	Emission patch approximately 10″ N of nucleus.

Note No.	NGC *IC	
100.	3359	Emission patch near end of bar approximately 55″ N of nucleus.
101.	3389	Very broad, indistinct hydrogen absorption lines.
102.	3395, 3396	Slit simultaneously on both nebulae; strong, early-type continuum with numerous emission lines (Plate IVn).
103.	3403	Very broad faint absorption lines.
104.	3419	Strong hydrogen absorption lines and early-type continuum.
105.	3432	Very strong 3727 with early-type continuum, and $H\gamma$ and $H\beta$ in emission (Plate IVo).
106.	3510	Broad, poor absorption lines.
107.	3512	Absorption lines of poor visibility (Plate IVp).
108.	3516	This nebula is one of the uncommon, highly concentrated type whose nucleus shows a spectrum of very broad bright bands; it is one of those studied spectrophotometrically by Seyfert (1943).
109.	3556	Redshift is for approximate center of system; $H\beta$ and $H\gamma$ present in faint emission.
110.	3628	Slit on brighter nuclear region north of dark lane.
111.	3646	Only H and K in nucleus.
112.	3646	Emission $H\beta$ and 3727 in emission patch 70″ SW of nucleus; patch fell on extreme end of slit, so difference in redshift is not very reliable; nevertheless, the SW end probably is approaching with respect to center.
113.	3672	Faint nebular spectrum confused with strong night-sky spectrum; redshift uncertain.
114.	3887	Nucleus only; absorption lines are faint and redshift is uncertain.
115.	3938	Only H and K in nucleus; slit across nucleus and two outlying emission patches (Plate IVq).
116.	3938	$H\gamma$ and 3727 in emission patch 90″ SW nucleus.
117.	3938	Only 3727 in emission patch 130″ NE of nucleus.
118.	3990	On slit simultaneously with 3998; faint auroral spectrum superimposed.
119.	3995	Early-type continuum with strong 3727; $H\beta$ and 3868 [*Ne* III] in faint emission; absorption lines of poor visibility.
120.	4030	Slit on nucleus and emission patch in arm 40″ SE of center; redshift is mean of all lines measurable in nucleus and patch, since slit was oriented only about 30° from minor axis; spectrum is progressively out of focus toward $H\beta$ because of presence of emulsion lump at end of plate.
121.	4064	Slit on bright central bar; broad and faint absorption lines.
122.	4088	Nuclear region; absorption lines broad and faint.
123.	4088	Condensation in arm approximately 110″ NE of nucleus; difference in velocity probably is real and due to rotation, but amount is uncertain because of poor quality of lines.
124.	4102	Slit along bright, elongated central region.
125.	4116	Slit along bright central bar, which makes only a small angle with major axis; broad, nearly invisible absorption lines, with $H\beta$ and $H\gamma$ in emission in small, bright nucleus near center of bar.
126.	4151	This nebula is the brightest of those uncommon, highly concentrated spirals whose nuclei show emission bands. It has been extensively observed; for its principal spectral features (Mayall 1934), for a possible difference in redshift determined by a grating (Adams and Humason 1936), for a check on the constancy of $\Delta\lambda/\lambda_0$ with λ_0 (O. C. Wilson 1949), and for detailed emission-band profiles (Seyfert 1943).
127.	4178	Bright central bar; redshift from absorption-line spectrum.
128.	4178	Emission patch approximately 100″ SW of center of bar; difference in velocity between bar and patch is so small that its interpretation as rotational motion is uncertain.
129.	4194	This highly concentrated peculiar spiral, observed with three-prism dispersion, shows a strong, early-type continuum with broad hydrogen absorption lines beginning with $H\delta$; emission features are: strong 3727, and much weaker 5006 and 4958 [*O* III] and $H\beta$ and $H\gamma$.
130.	4212	Slit on nucleus and condensation 40″ NE, which appears to be a foreground star projected on faint nebulosity of the spiral.
131.	4214	Slit on two brightest patches in bright central bar; strong emission-line spectrum (Plate IVr).
132.	4236	Brightest emission patch in SE end, approximately $5'.5$ from center of system; redshift may be affected by rotation.
133.	4244	Redshift is for approximate center of system.
134.	4293	Only H and K measured; auroral spectrum superimposed.
135.	4401	Brightest of two emission patches approximately 125″ SE of center of system, which is catalogued as 4395; the two lines measured are 3727 and $H\gamma$.
136.	4401	Fainter of two emission patches approximately 50″ SW of brighter one.
137.	4486	Slit on nucleus and ray structure NW; scale of Crossley almost too small for good separation of spectra of nucleus and ray; also, the ray continuous spectrum is so narrow that it is uncertain whether there are any faint absorption features that have the same redshift as the nucleus; however, the ray spectrum is different in not showing 3727; the structure and Humason's spectra of this nebula have been discussed by Baade and Minkowski (1954) in connection with its identification as a radio source.
138.	4517	Slit on two emission patches on north side of central part of dark lane; brighter and preceding of two.
139.	4517	Fainter and following of two; a bright foreground star is 20″ NW of this patch; 3727 may be faintly present, and slightly inclined, across full length of slit.
140.	4519	Slit on nucleus and several condensations, which do not show emission.
141.	4535	Nuclear absorption spectrum, with broad, faint lines.
142.	4536	Slit on nucleus and emission patch; redshift is for nucleus only, since rotation may affect result for patch.
143.	4536	Emission patch approximately 75″ E of nucleus.
144.	4567, 4568	Slit simultaneously on both nebulae.
145.	4605	Strong 3727 and broad, faint absorption lines.

Note No.	NGC *IC	
146.	4618	Slit on central bar; strong 3727 and conspicuous hydrogen absorption lines.
147.	4643	Slit on bright central bar.
148.	4647, 4649	Slit simultaneously on both nebulae (Plate IVs).
149.	4656	Brightest emission patch near center of system and approximately 18″ W of the apparent nuclear region, which is at the SW end of the brighter half of the nebula.
150.	4713	Nuclear region and involved faint emission patch approximately 15″ E of nucleus, which has broad hydrogen absorption lines of poor visibility.
151.	4736	Nuclear region; redshift from absorption lines and 3727.
152.	4736	Brighter part of spiral-arc ring 50″ NW of nucleus; 3727 and emission $H\gamma$ and $H\beta$, which give velocities affected by rotation.
153.	4736	Fainter part of spiral-arc ring 60″ SE of nucleus; only 3727, which gives an uncertain velocity affected by rotation.
154.	4775	Slit on nucleus and emission patch; redshift is average of measurements for both, since spiral is nearly normal to line of sight.
155.	4775	Emission patch 30″ S of nucleus.
156.	4789	Only H and K measured.
157.	4793	Emission in region of arm 30″ NE of nucleus; 3727, $H\gamma$ and $H\beta$ are the emission lines measured.
158.	*3949	Only H and K measured.
159.	Anon	Humason and Zwicky (1947) blue object No. 46; strong early-type continuum with intense 3727 as the only measurable feature.
160.	4861	Bright emission patch in SW end of system; redshift may be affected by rotation.
161.	4900	Slit on short, bright and elongated nuclear region; faint absorption lines.
162.	4902	Slit on central bar.
163.	4907	Slit on central bar; weak plate, only G-band measured.
164.	Anon	Irregular spiral or possible dwarf system at $13^h 2^m.0$, $-3° 18'$ (1950) noted by C. D. Shane on 20-inch astrograph plate; weak spectrum, showing only 3727 and $H\gamma$ in measurable strength, is of emission patch approximately 60″ S of center of system; faint star 30″ NE of patch.
165.	5033	Auroral spectrum superimposed.
166.	5068	Slit on short central bar; broad absorption lines on strong night sky spectrum (Plate IVt).
167.	5204	Peculiar-type spiral in M101 group studied by Holmberg (1950); slit on two emission patches approximately 30″ SW of center of system; patches are 20″ apart and nearly in line with a foreground star, which is distant 50″ in position angle 70° from the nearer patch.
168.	5248	Broad absorption lines, fainter ones of poor visibility.
169.	5301	Weak plate that shows broad, faint absorption lines whose measurement was uncertain.
170.	HoIV	Dwarf nebula in M81 group described by Holmberg (1950); redshift is for slightly brighter of two emission patches located each side of center of system; brighter patch is approximately 50″ NE of center, fainter one 70″ SW.
171.	5468	Emission patch 55″ S of nucleus; weak plate on which only 3727 was measured.
172.	5468	Emission patch 55″ S of nucleus; stronger plate shows numerous emission lines.
173.	5468	Nucleus.
174.	5468	Emission patch 33″ N of nucleus.
175.	5473	Slit on bright central bar, which is nearly the minor axis.
176.	5474	The redshift indicates that this nebula is a member of the M101 group studied by Holmberg (1950).
177.	5585	Slit on nucleus and condensation 50″ SE, which does not show emission lines.
178.	5653	Nucleus and adjacent faint emission patch in this peculiar-type spiral noted by C. D. Shane on a 20-inch astrograph plate.
179.	5668	Slit on nucleus and condensation 35″ NE, which shows weak emission $H\gamma$ and 3727.
180.	5678	Absorption lines are of very poor visibility and were difficult to measure.
181.	5713	Slit on three condensations in center of nebula; the central one that shows 3727, $H\gamma$, and $H\beta$ in emission may be the nucleus; auroral spectrum superimposed (Plate IVu); early plate taken with wider slit and longer exposure is much inferior (Plate IVv).
182.	5846	Slit on 5846 and close companion; 3727 very faint in 5846.
183.	5846	Companion 40″ S of 5846.
184.	5850	Slit on faint central bar; 3727 very faint in nuclear spectrum.
185.	5857	Slit on elongated nuclear region, which corresponds closely with major axis; lines may be inclined, but inclination is uncertain because of weak plate.
186.	Anon	These two nebulae are in a cloud described by Shane and Wirtanen (1950); the 1950 position for the two objects, which are separated by 123″ in position angle 45°, is $15^h 20^m.4$, $+8° 47'$; the first one listed appears to be the brightest and largest in this clustered region of the cloud (Plate Ve, 1), and there are two fainter nebulae near it in the following relative locations: one 15″ NW, the other 45″ SW; preliminary values of the redshifts were quoted by Shane and Wirtanen (1950).
187.	5970	Slit on central bar, which nearly corresponds to major axis.
188.	5982	Only H and K used for redshift; wide slit and dark plate obscure other lines.
189.	6027d	Brightest nebula in compact group described by Seyfert (1951).
190.	6027a	Second brightest nebula in compact group described by Seyfert (1951).
191.	6070	Slit on nucleus and emission patch; redshift from nuclear spectrum of absorption lines.
192.	6070	Emission patch 70″ NE of nucleus; differential velocity probably partly due to rotation, since patch is not far off major axis.
193.	6217	Nuclear spectrum of early-type continuum with absorption lines of very poor visibility; redshift from 3727 and the K line (Plate IVw).
194.	6239	Redshift from strong emission spectrum of patchy, central bar.
195.	6412	Slit on nucleus and condensation 35″ N, which shows no emission lines except possibly a very faint 3727; absorption lines of poor visibility, with only 3727 and H line measurable in nucleus for redshift.
196.	6503	Auroral and dawn spectra confused with nebular spectrum.

Note No.	NGC *IC	
197.	6574	Absorption lines broad and faint; early-type continuum with $H\gamma$ and $H\beta$ present as very faint, broad emission features.
198.	6635	This low-latitude object, in a Crossley-plate field devoid of nebulae of comparable and fainter magnitude, was observed to determine its nature; the redshift shows it is extragalactic.
199.	6702	Humason's (1931) published redshift of +2250 km/sec, based on a poor plate by Pease, refers to 6703.
200.	6703	A spectral feature measured as 3727 is extremely faint, but its redshift agrees closely with those from other lines.
201.	6822	Hubble's (1925) gaseous nebula V.
202.	6822	Hubble's gaseous nebula X (IC 1308).
203.	6822	Hubble's gaseous nebulae I and III, measured as one object since the emission lines extend from one object to the other.
204.	Anon	Brightest member in low-latitude group of nebulae at $\alpha = 19^h\,55^m.1$, $\delta = +40°\,17'$ (1950) noted by C. D. Shane on a 20-inch Astrograph plate; the object is $5'.4$ NW of the bright star +39°3968 (Plate Vf, 1).
205.	Anon	Second brightest member in same group described in preceding note; the object is $5'.9$ NE of BD +40°3948 and 25″ NE of another pB star (Plate Vf, 2).
206.	*1317	This nebula was observed to check its extragalactic nature, because it is in a Crossley-plate field lacking in nebulae of comparable brightness.
207.	6944	This object is the considerably brighter member of a pair of nebulae in a Crossley-plate field lacking in nebulae of comparable brightness.
208.	6946	Brightest emission patch 250″ NE of nucleus; near location of the third supernova found in this spiral (Mayall 1948b).
209.	6946	Fainter emission patch 165″ SW of nucleus.
210.	7137	Faint absorption lines difficult to measure.
211.	7318a	Preceding member of close pair in Stephan's quintet of nebulae.
212.	7318a	Slit simultaneously on 7318a and 7318b.
213.	7318b	Following member of close pair in Stephan's quintet.
214.	7469	This spiral has a bright, semi-stellar nucleus whose spectrum shows broad emission bands on an early-type continuum; it has been studied spectrophotometrically by Seyfert (1943).
215.	7479	Slit on central bar.
216.	7625	Early-type continuum with faint absorption lines.

Note No.	NGC *IC	
217.	7640	Bright emission patch approximately 225″ SE of nuclear region; a brighter star is 20″ NE of this patch.
218.	7640	Very faint emission patch in arm approximately 52″ SE of nuclear region.
219.	7640	Faint emission patch in arm approximately 23″ NW of nuclear region.
220.	7640	Nuclear region; redshift is from 3727 and absorption lines.
221.	7679	This highly concentrated nebula has an early-type continuum with strong hydrogen absorption lines; the emission lines are 3727, $H\beta$, and N I of [O III].
222.	7714	Slit simultaneously on nuclear regions of both members of close pair; strong early-type continuum with numerous emission lines, from which the redshift was determined.
223.	7715	Faint spectrum of apparently broad and faint absorption lines, which give a low-precision redshift.
224.	7723	Weak spectrum of semi-stellar nucleus that shows broad and faint absorption lines, with a very faint 3727.
225.	7723	Slit on nucleus and faint central bar; only blended $H+H\epsilon$ and K measured in the nucleus.
226.	7723	Slit on major axis as estimated from elliptical outline of faint outer parts of spiral; nebular spectrum of faint absorption lines and 3727 confused with strong night-sky spectrum that least affects $H+H\epsilon$, which appears to be slightly inclined.
227.	7769	Spectrum shows hydrogen absorption lines of poor visibility and a very weak 3727.
228.	7770	Strong early-type continuum and 3727, possibly inclined; broad and faint H and K lines were measured with considerable uncertainty, which accounts for the large A.D.; nebular type in Pettit's (1954) list probably interchanged with that for 7771.
229.	7771	Slit on patchy central bar, which shows no emission except for a weak 3727 in the nucleus; nuclear spectrum is an early-type continuum with hydrogen absorption lines becoming conspicuous from $H\delta$ to the ultraviolet.
230.	7793	Slit on nucleus and condensation approximately 95″ SW, which shows only a very faint 3727; this spiral has been studied photometrically by Shapley and Mohr (1938).

mination of the redshift in column (13), generally because of the possibility of rotation affecting the measurements.

Column 13. The observed redshift, $c\,\Delta\lambda/\lambda_0$, expressed in km/sec, in accordance with current Mount Wilson-Palomar practice (Bowen 1953); this procedure has the advantage of giving observational results in familiar and convenient units, without involving the moot question of radial motion; for, if the redshifts are velocities of recession, second-order corrections become appreciable for the larger velocities, and these corrections are different depending on whether or not relativity theory is used.

Columns 14, 15. Galactic longitude, l, latitude, b, generally taken from the Shapley-Ames catalogue, or computed from Ohlsson's tables (1932) based on the Harvard pole at $\alpha = 12^h\,40^m$ and $\delta = +28°$ (1900).

Column 16. $100 \cos A$, where A is the angle from the nebula to an apex at $l = 55°$ and $b = 0°$; these coordinates, and a solar motion of 300 km/sec, represent rounded-off values differing less than their probable errors in the preferred solution of Humason and Wahlquist (1955) for the solar motion referred to the local group nebulae; the tabulated numbers multiplied by 3 therefore give the solar-motion corrections applied to the observed redshifts in column (13) to give the corrected redshifts in column (17).

Column 17. Redshift corrected for solar motion and given to the nearest km/sec only in case subsequent small corrections are applied; the general order of accuracy is indicated by the A.D. in column (11).

Column 18. Numbered notes that give additional information regarding more accurate locations in case of uncatalogued or very faint nebulae, detailed spectral characteristics when these appear to be of unusual or special interest, slit orientation with respect to features in the projected nebular image, and references to published reports or descriptions that contain supplementary information.

Systematic Differences in the Redshift Lists. A comparison of Tables I and II with V shows that 114 nebulae were observed in common at Mount Wilson-Palomar and at Lick. For these nebulae

TABLE VI. MEAN WAVE LENGTHS OF SPECTRAL FEATURES

Absorption	Rel. Wt.	Emission	Rel. Wt.
3770.48 $H\iota$	16	3728.16 [*O* II]	405
3798.60 $H\theta$	24	3868.58 [*Ne* III]	26
3835.57 $H\eta$	32	3968.70 [*Ne* III]+$H\epsilon$(=)*	2
3888.22 $H\zeta$	26	3969.30 [*Ne* III](1)+$H\epsilon$(2)	4
3933.28 *Ca* II, K	384	3970.09 $H\epsilon$	6
3968.38 *Ca* II, H	301	4101.67 $H\delta$	36
3968.54 H(2)+$H\epsilon$(1)*	10	4340.38 $H\gamma$	79
3969.01 H(1)+$H\epsilon$(2)	37	4362.78 [*O* III]	6
3969.23 H+$H\epsilon$(=)	34	4859.90 $H\beta$	42
4101.25 $H\delta$	120	4957.02 [*O* III], N2	18
4226.84 *Ca* I	8	5006.27 [*O* III], N1	26
4303.52 G band	140		
4340.61 $H\gamma$	36		

* Figures in parentheses denote hypothetical intensities of the unresolved components; for absorption H+$H\epsilon$ they were estimated from the intensities of K and $H\delta$; for emission [*Ne* III]+$H\epsilon$, from 3868 and $H\delta$.

TABLE VII. DISTRIBUTION OF REDSHIFT DIFFERENCES

No.										
					185					
					205					
				214	221					
25				224	278					
				604	IC342					
				1332	2681					
				1569	2903					
				2146	3034					
20				2217	3169					
				2683	3516	1052				
				3031	3556	1097				
				3184	3810	1889				
				3310	4214	SexDw				
15				3941	4216	3190	514			
				3998	4594	3953	1068			
				4102	4736	4111	1395			
				4151	HZ46*	4406	1453			
				4254	5005	5198	2300			
10				4494	5055	5371	2314			
				4552	5248	5633	4291			
				4565	5363	5713	4365	925		
			2787	4636	5846	5746	4762	2841		
			2950	5033	Comp**	5970	5857	4125		
5		2537	3607	5308	6027a	6015	5866	4535		
	1637	4649	4486	5907	6070	6027d	5982	4889		
	2613	5668	6384	6217	6574	6703	7331	5473		
	3893	7679	7469	6702	6946	7318a	7625	5850	6944	
	6661	7793	7479	6822	7727	7585	7742	6643	7318b	
Interval (km/sec)	−151 −200	−101 −150	− 51 −100	− 1 −50	0 +50	+ 51 +100	+101 +150	+151 +200	+201 +250	Lick *minus* MtW-Palomar
Totals	4	5	7	26	28	19	15	8	2	114

* Humason-Zwicky (1947) blue object No. 46.
** Companion to 5846.

Table VII is a histogram of the catalogue numbers, for differences within intervals of 50 km/sec. The frequency distribution is somewhat skewed, with an excess of positive differences obtained in the sense Lick *minus* Mount Wilson-Palomar. These differences range from -177 to $+229$ km/sec, and their mean with respect to sign is $+28.4$ km/sec. This systematic difference means that, on the average, redshifts on Crossley spectrograms were measured greater by 28 km/sec.

To try to find the source of this systematic difference, detailed information regarding wave lengths, measurements of individual spectral features, and plate quality was exchanged. No consistent explanation was obtained from comparison of the particular wave lengths or lines used, but there was found the expected correlation between spectrogram quality and size of difference. When one or both redshifts for the same nebula depended on plates that were weakly exposed or poor for other reasons, differences tended to be large, with a preponderance of positive ones for inferior Crossley plates. For example, the three largest positive differences, $+229$(7318b), $+223$(6944) and $+188$(6643), involve Crossley plates that are respectively underexposed, affected by night sky (10 hours), and dark and grainy (experimental Ia-O emulsion). While similar cases might also be cited for some of the Mount Wilson-Palomar plates to account for some large differences of either sign, there is little advantage to carry the detailed comparison much further. The reason is that a systematic difference of 28 km/sec between the two sets of redshifts represents a nearly negligible quantity when considered in terms of displacement on the plates. For a dispersion of 300 to 400 A/mm in the ordinary photographic region, 28 km/sec corresponds to about one micron, which is close to the limit of measurement, especially for spectral features of inherently poor visibility.

A systematic difference of 28 km/sec also appears small when compared with the redshift estimated errors in Tables I and II and the average deviations in Table V. If the two series of redshift observations are assumed to be of comparable accuracy, with the differences for objects in common treated as residuals, then the probable error of a single difference is ± 62 km/sec.

As a result of the foregoing comparison, no systematic correction was applied to one series of redshifts in order to reduce it to the other. Thus the redshifts used in Part III for the correlation plots are straight means for those nebulae observed in common at Mount Wilson-Palomar and at Lick.

Observational Selection of the Redshifts. Since the relationship between redshift and magnitude has been investigated in Part III separately for the various types of field nebulae, it seems worth while to indicate in some detail how representative the spectrographic data are for the different classes of the brighter nebulae. For this statistical purpose, the Shapley-Ames catalogue may be used, first, because it still is the only available photometry of the brighter nebulae over the whole sky, and second, because it has been shown, initially by Stebbins and Whitford (1937, 1952) and later by Pettit (1954), that its magnitude scale and zero point are substantially correct in terms of modern photoelectric standards. Although some of the catalogue magnitudes differ by 1 to $1\frac{1}{2}$ mag. from the photoelectric ones, and the catalogue zero point appears to require a correction of -0.1 to -0.2 mag., neither of these

TABLE VIII. COMPARISON OF NUMBERS OF REDSHIFTS/NEBULAE FOR $\delta > -30°$

Cat. Mag.	Totals <11.6	11.6 11.7	11.8 11.9	12.0 12.1	12.2 12.3	12.4 12.5	12.6 12.7	12.8 12.9	<13.0 Totals	%
E	19/19	13/13	5/5	6/7	9/10	10/11	20/24	18/23	100/112	89
So	8/8	5/5	4/4	7/9	3/5	9/11	5/6	13/26	54/74	73
Sa	5/5	4/5	4/5	5/6	2/3	11/17	3/6	9/18	43/65	66
Sb	28/28	7/7	8/13	5/12	8/13	6/16	11/25	9/32	82/146	56
Sc	40/40	*13/14	16/22	10/19	13/29	17/36	13/41	12/55	134/256	52
SBo, a	8/8	4/4	4/4	5/7	5/7	1/3	5/11	6/14	38/58	66
SBb	0/0	2/2	3/4	1/3	1/3	3/9	5/7	2/14	21/46	46
Sbc	8/8	1/1	1/1	1/2	4/5	3/3	1/1	1/2	12/15	80
Irr		0/0	1/1	0/1	0/1	2/2	2/4	1/4	14/21	67
All	120/120	*49/51	46/59	40/66	45/76	62/108	65/125	71/188	498/793	63
%	100	96	78	61	59	57	52	38		
MtW+P	97	32	35	30	32	41	49	54	370	
Lick	67	25	20	16	16	27	25	27	223	
Common	44	9	9	6	3	6	9	10	96	

* Includes redshift for NGC 4027 observed only by Struve and Linke (1940).

circumstances is likely to affect seriously the following statistics on the brighter nebulae observed for redshift. The reason is that over the five-magnitude range from approximately 8.0 to 13.0 pg. mag., mean differences between the catalogue and photoelectric magnitudes show no systematic trend. Undoubtedly a complete photoelectric photometry of the brighter nebulae would change the numbers in the following table, but, on the basis of the comparisons that have been made by the photoelectric observers mentioned, there is little reason to expect changes so drastic as to invalidate the statistics. Table VIII gives the numbers of redshifts and of nebulae, arranged according to classifications by Hubble, for intervals of 0.2 mag. in the Shapley-Ames catalogue.

Since the figures to the left and right of the slant lines are numbers of redshifts and of nebulae, respectively, their comparison shows the proportional completeness of the redshift data. Cumulative totals also are included to catalogue magnitudes <11.6 and <13.0, respectively, in the second and in the next-to-last column; for the latter the numbers are expressed in per cent in the last column. The lowest three lines show the number of redshifts determined in the two series, and those in common.

Because the numbers are rather small for nebulae of a given type and magnitude, except possibly for E, Sb, and Sc, the proportional completeness is not accurately established for the data subdivided so finely. There is definite evidence, however, that a larger proportion of the earlier types was observed for redshift, but the preponderance is not by a large factor. Even in the faintest magnitude group, 12.8 and 12.9, the E+So nebulae are better represented than those of types Sb+Sc only by the factor $(31/49)/(21/87) = 2.6$. On a cumulative basis to 13.0 mag., as shown in the last column, the percentage completeness of redshifts for the different types ranges from 46 to 89 per cent, or by a factor of 1.8. But this smaller factor is, of course, due in large measure to the much more complete coverage for the brighter magnitudes.

A more realistic indication of the observational selection in the redshifts according to magnitude and for all types probably is given by the percentages in the fourth line from the bottom of the table. These figures show that the redshift observations are essentially complete down to 11.6 mag., but that near the end of the next whole magnitude interval the spectrographic data fail of completeness by about 50 per cent.

A fair appraisal of observational selection in the redshifts probably would be the statement that Table VIII shows no large gaps in the sampling to 13.0 mag., and that to this limit there are available in round numbers 500 redshifts out of a possible 800, for an overall completeness of 63 per cent. This result is not expected to be greatly changed by more accurate magnitudes for individual nebulae, but eventual inclusion of the 200-odd nebulae south of declination $-30°$ may appreciably revise upward some of the completeness ratios in Table VIII.

PART III. DISCUSSION OF THE SPECTROGRAPHIC AND PHOTOMETRIC DATA

Introduction. The new redshift data have been reported in Parts I and II of the present paper. The measured apparent magnitudes by Pettit (1954) and by Stebbins and Whitford (1952) have been reported elsewhere. Systematic errors exist in these published magnitudes depending upon the ratio of the measuring aperture to the angular diameter of the nebula. This aperture effect has been removed from the published magnitudes by the method discussed in Appendix A. Table A1 of this appendix gives the corrected photographic magnitudes for 576 nebulae for which redshifts are available. These magnitudes are referred to a standard isophote of about 25 mag. per sq. sec. of arc.

Although it is becoming increasingly evident that the nebular distribution is characterized by a predominant tendency to cluster (Zwicky 1938, Neyman and Scott 1952, first of a series; Shane and Wirtanen 1954, first of a series), the present discussion may conveniently be treated on the basis of the much simplified picture of nebulae in the general field with occasional great clusters superposed. On the more elaborate statistical model of complete clustering, this separation into field and cluster nebulae is merely one according to the size of the cluster. On this theoretical picture, clusters with only one member are possible and these would be considered here as truly isolated objects. We shall treat all aggregates containing from 1 to 50 members as field nebulae. All richer aggregates are considered with the cluster data.

The philosophy behind the present discussion is governed by the observational approach. Two numbers, z $(\equiv\Delta\lambda/\lambda_0)$ and m, are observed. Corrections are made to both quantities to free them from effects extraneous to the problem at hand. The redshifts are corrected for the solar motion with respect to the centroid of the local group.

This correction is made because it appears likely that the systematic redshift does not operate within the local group (Hubble 1936a; Humason and Wahlquist 1955) and that the measured redshifts of its members reflect the motion of the sun with respect to these nebulae. The correction for solar motion is described in Parts I and II. The observed magnitudes are freed from the latitude-effect caused by obscuration in our own galaxy by the equations $\Delta P(b) = 0.25 (\csc b - 1)$ for photographic magnitudes and $\Delta V(b) = 0.18 (\csc b - 1)$ for photovisual magnitudes. These heterochromatic magnitudes are further changed to a bolometric magnitude scale by the K correction, which accounts for the effects of redshift. The theory and computation of the K correction for P and V magnitudes is given in appendix B for the case where the Stebbins-Whitford effect (1948) is zero. Discussion of the modification to the value of K due to the presence of this effect is also given. The K correction accounts only for the selective effects caused by the redshift. Other corrections to the magnitudes, such as the so-called energy and number effects, are not made, as was once the custom, since such effects are absorbed into the theoretical equations used for the interpretation of the data.

The sequel is divided into three sections. These contain the [log cz, m] relation for (1) the field nebulae, (2) selected isolated groups, and (3) the nebular clusters. Appendix C contains the calibration of these relations in terms of distance with a provisional value of the redshift parameter H.

The redshift catalogues of Tables I and V, together with the magnitudes in Table A1, provide the data for discussion of the [log cz, m] relation for the field nebulae. Humason's redshift values in Table III and the magnitudes reported in Table XII provide the data for the clusters.

The Field Nebulae. For a linear redshift-distance relation of the form $cz = Hr$, with r defined by

$$\log r = [m - \Delta m(b) - K - M + 5]/5,$$

the relation between $m - \Delta m(b) - K$, called m_C in the following, and z will be of the form

$$m_C = 5 \log cz + (M - 5 - 5 \log H). \quad (1)$$

Here all of the refinements required for a proper definition of distance are glossed over. Both Robertson (1955) and McVittie (1956) treat this problem, and their results are implicitly contained in a later equation used for the cluster data. For the relatively close field nebulae such refinement is unnecessary. Equation (1) neglects another effect. Due to the finite speed of light, we look back in time to events when light now observed was emitted from nebulae at different distances. Thus, the observed pairs [log cz, m] refer to the condition of the universe at *different* cosmic times (see e.g. Robertson (1933) for a definition of cosmic time), the difference being just the light-travel time between the source and the observer. To transform the observed "world picture" to the so-called "world map"—the condition of the universe at any given cosmic time—requires knowledge of the form of the expansion. Formulae based upon the method of Taylor series (Robertson 1955) are employed for this problem. This time effect is not important for distances such that $z \ll 1$, and this is the case for the majority of the field nebulae. Interpretation of the [log cz, m] relation for the nearby field nebulae with the simplified equation (1) is adequate for the present discussion.

The nebulae in the general field have been divided into 7 groups for analysis according to nebular type. Figures 3 to 10 show the correlation between the corrected photographic magnitude $P_C \equiv P - \Delta P(b) - K$ and $\log cz \equiv \log c\, \Delta\lambda/\lambda_0$ for each group. Linear relations of the form $P_C = A \log cz + B$ were fitted to the data by least squares. The linearity of the redshift-distance relation is tested by the closeness of the value of A precisely to 5. Differences in the mean absolute magnitude $\overline{M(m)}$ for the nebular types are obtained from the differences in B, on the assumption that the value of H is unique. Two solutions were made for each group. Both solutions include all the data, but Solution 1 considers A and B as unknowns, while Solution 2 adopts A as 5.000 and treats B as unknown. Table IX gives the resulting solutions and probable errors. The lines drawn in Figures 3 to 10 are those of Solution 2 since this case is the only one compatible with current theories. The computed probable errors are merely formal and are somewhat unrealistic, due to the nature of the scatter in the [log cz, m] pairs.

This scatter is caused by at least four effects. (1) The large spread in absolute magnitude among the nebulae appears in the correlations as a spread in apparent magnitude at a given log cz. Indeed, early attempts (Hubble 1936c) were made to derive the luminosity function for nebulae from the residuals of the [log cz, m] plot, but the results were affected by the highly selective

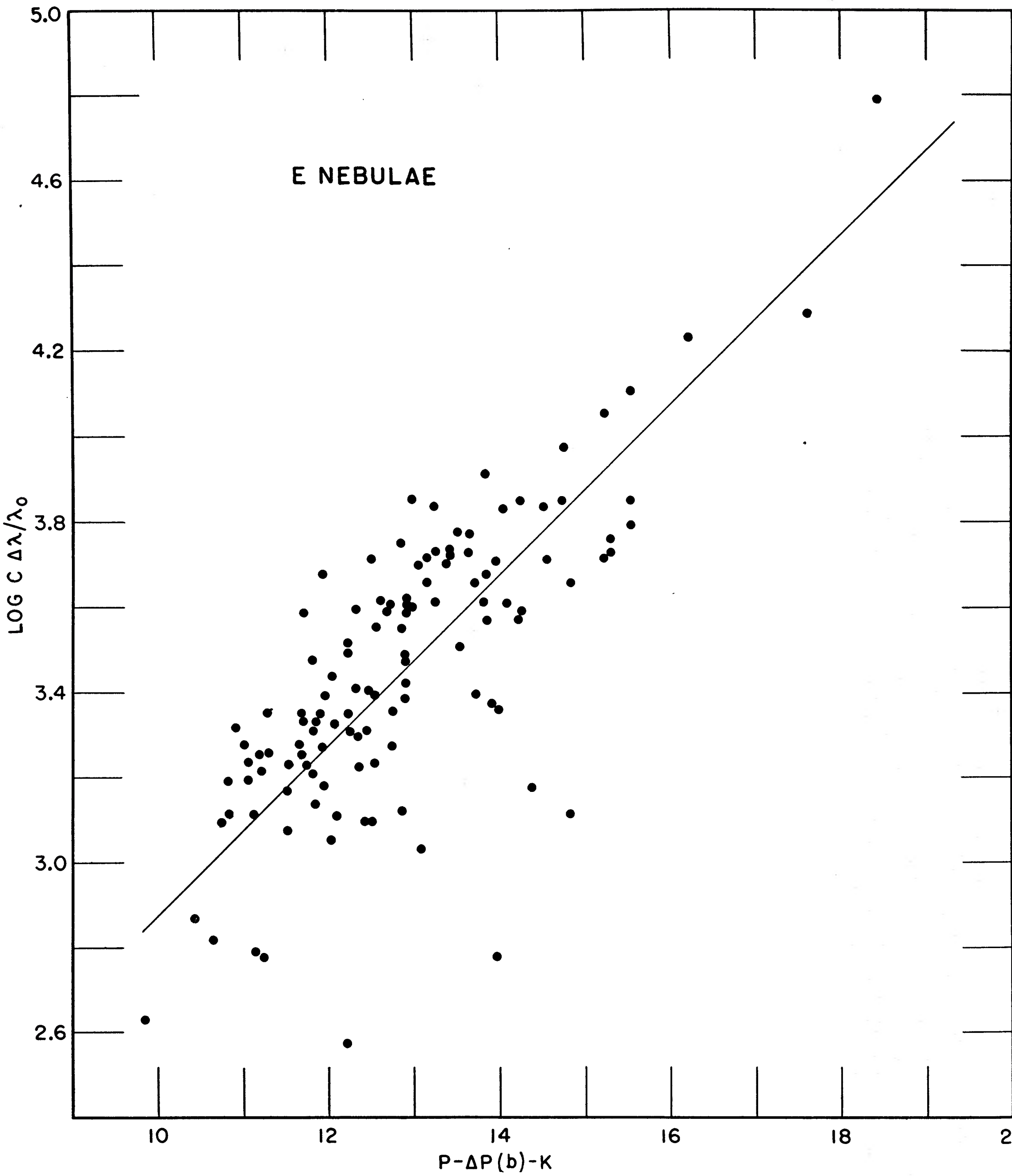

Figure 3. The redshift-magnitude relation for E nebulae in the general field. The apparent magnitudes have been corrected to the galactic pole and for the selective effects of redshifts. The redshifts themselves have been corrected for the solar motion with respect to the local group.

nature of the data. (2) Redshifts represent the sum of the systematic distance effect and the random motion of the nebulae themselves. The exact size of these random motions is not known yet, but they seem to be of the order of 200 to 300 km/sec. When they are of the same size as the distance effect, unsymmetrical deviations from the [log cz, m] relation will occur if the peculiar motions themselves are symmetrical about the distance effect. This circumstance explains part of the large scatter at log cz less than 3.0. (3) The other part of the larger scatter at small *cz* is explained by a selectivity effect favoring the nearer of the intrinsically faint nebulae. Objects such as the dwarf irregulars of low surface brightness are difficult to identify and observe at large distances, and hence these points are missing from the diagrams for larger redshifts than about 1000 km/sec. (4) The values of m and z themselves contain errors of observation, but the discussion in Parts I, II, and Appendix A shows these errors to be small compared with the observed scatter.

Within the total uncertainties of the solutions, all data in the first 8 groups of Table IX are consistent with a linear law. The solution of greatest weight, $N = 474$, gives the computed A as 5.028 ± 0.116 compared with the predicted value of 5.000.

To check the isotropy of the redshift law, correlations were made for nebulae in the north and south galactic polar regions with $|b| \geqslant 30°$. The last two solutions of Table IX, together with Figures 11 and 12, show the result. A significant, and as yet unexplained, difference exists between the two hemispheres. The A values differ from each other, but even more serious is the difference of 0.70 mag. in B between the hemispheres for Solution 2. The southern nebulae appear to be brighter than the northern ones at the same redshift. Part of this difference is probably due to observational selection, since many nebulae in the south galactic polar cap are in high southern declinations not reachable from these latitudes. Table VIII of Part II shows that the redshift catalogues are essentially complete for nebulae brighter than $m_{pg} = 11.6$ north of $\delta = -30°$. South of this declination very few redshifts are available. The scarcity of points in Figure 12 for nebulae brighter than $P_C = 11$ is a result of this selective effect. Comparison of the north with the south galactic hemisphere is therefore biased, since the data for the northern hemisphere are more complete. Counts in the Shapley-Ames catalogue show that 37 nebulae brighter than $m_{pg} = 11.6$ are south of $\delta = -30°$. All of these do not satisfy $b > 30°$S but none satisfy $b > 30°$N. It would be of interest and importance to assemble [log cz, m] data for these bright southern nebulae so that an unbiased test of the isotropy could be made with the field nebulae. Observatories in the southern hemisphere could contribute sig-

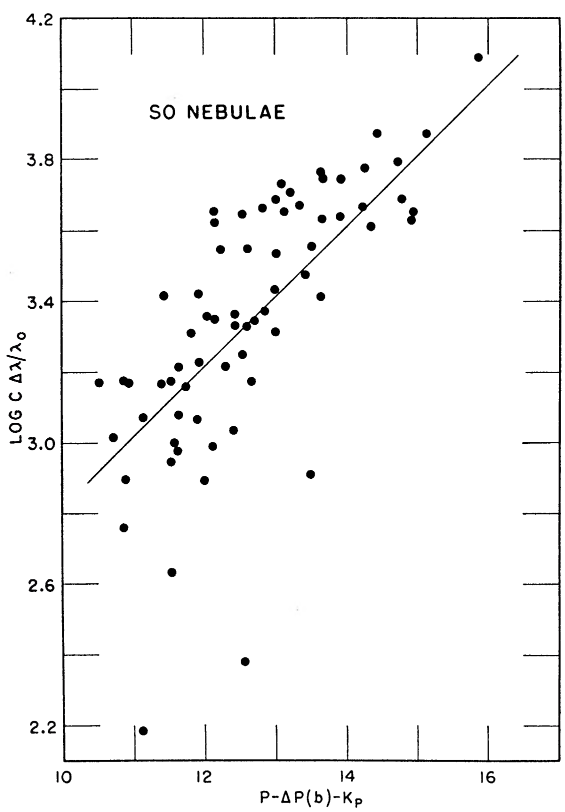

Figure 4. The redshift-magnitude relation for So field nebulae.

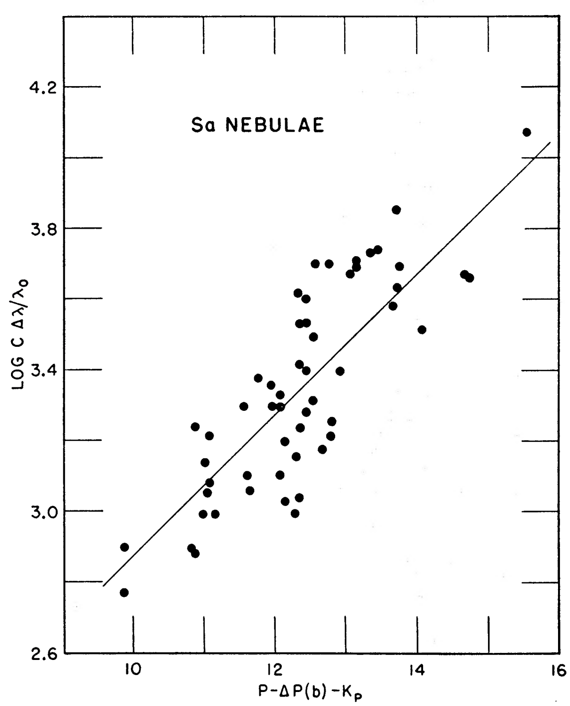

Figure 5. The redshift-magnitude relation for Sa field nebulae.

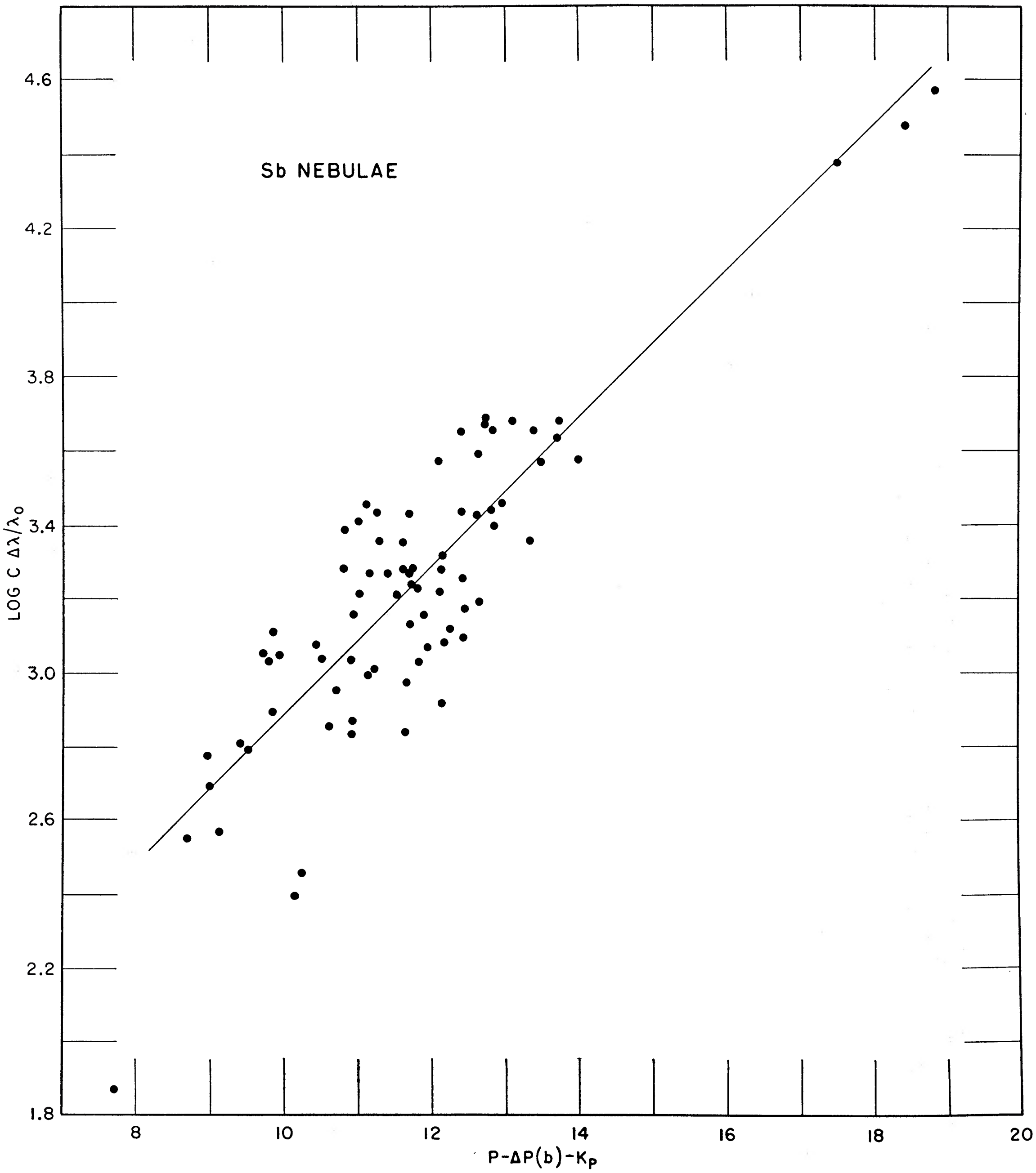

Figure 6. The redshift-magnitude relation for Sb field nebulae.

nificantly toward answering this fundamental question of isotropy.

A small part of the difference in Figures 11 and 12 may be due to photometric difficulties. Many nebulae south of $b = -30°$ are at high southern declinations. This is a difficult region to reach with high photometric precision from Mount Wilson due to the strong Los Angeles lights in the south and west quadrants. No check on this suggestion is possible at present because of the lack of overlap in Pettit's, Stebbins and Whitford's, and Holmberg's magnitude catalogues in the south latitudes.

Whatever the cause of the difference between Figure 11 and 12, strong evidence against appreciable anisotropy of the redshift law is provided

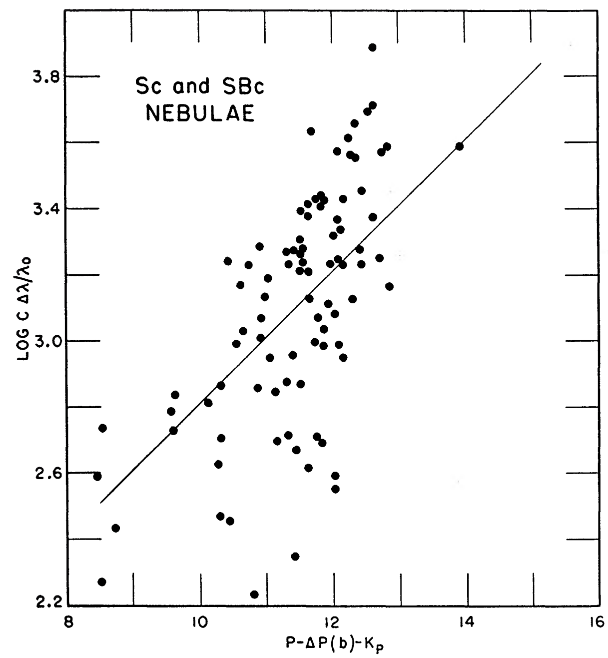

Figure 7. The redshift-magnitude relation for Sc plus SBc field nebulae.

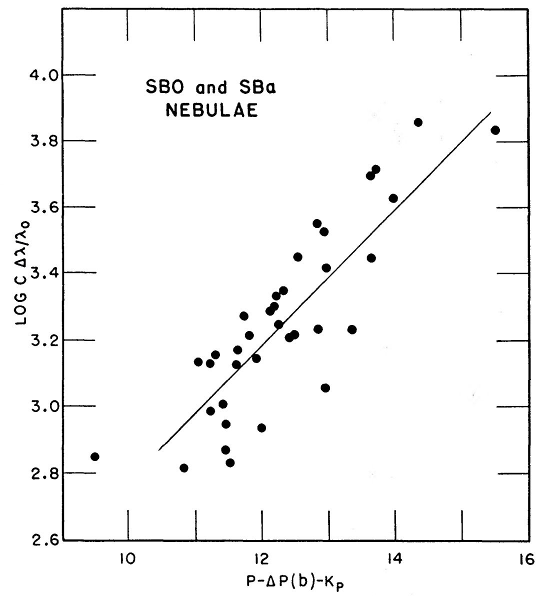

Figure 8. The redshfit-magnitude relation for SBo plus SBa field nebulae.

from the high degree of isotropy in the cluster data. Further work on the field nebulae is required for a satisfactory solution.

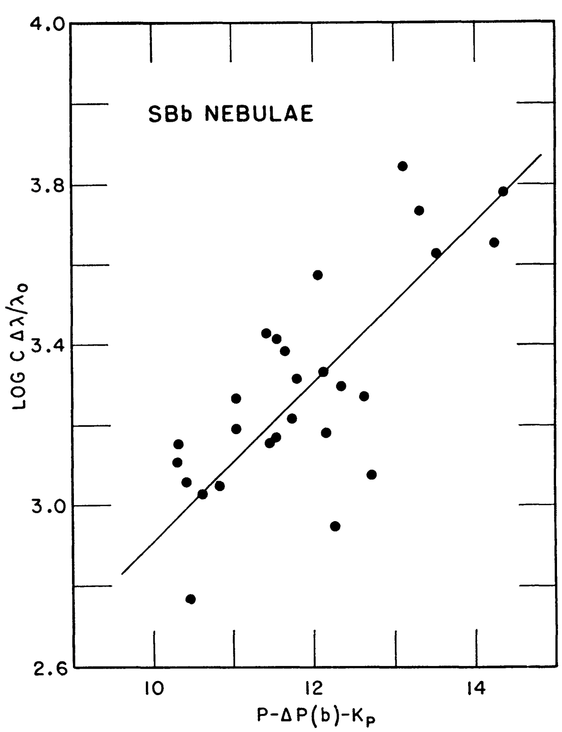

Figure 9. The redshift-magnitude relation for SBb field nebulae.

To the extent that observational selection in the present sample is comparable for the various types of nebulae, differences in their mean absolute magnitudes are reflected in the differences

TABLE IX. SOLUTIONS FOR THE FIELD NEBULAE

	Solution 1		Solution 2		
Neb. Type	*A*	*B*	*A*	*B*	*N*
E	5.882 ±.347	−7.400 ±.246	5.000	−4.375 ±.212	117
So	4.630 ±.378	−2.843 ±.234	5.000	−4.070 ±.253	67
Sa	4.717 ±.312	−3.401 ±.229	5.000	−4.360 ±.243	54
Sb	5.181 ±.337	−4.974 ±.182	5.000	−4.400 ±.175	76
Sc+SBc	4.329 ±.377	−1.931 ±.307	5.000	−4.030 ±.358	90
SBo+SBa	4.854 ±.385	−3.466 ±.252	5.000	−3.950 ±.260	36
SBb	5.618 ±.672	−6.618 ±.261	5.000	−4.570 ±.233	27
All Types	5.028 ±.116	−4.324 ±.129	5.000	−4.235 ±.128	474
All Types $b \geqslant +30°$	5.102 ±.208	−4.250 ±.169	5.000	−3.895 ±.165	257
All Types $b \leqslant -30°$	6.757 ±.412	−10.636 ±.283	5.000	−4.595 ±.219	132

between the values of B from Solution 2 tabulated in Table IX. Table X exhibits these differences, normalized so that $\overline{\Delta M} = 0.00$ mag. for the solution using all data. Tabulated again are

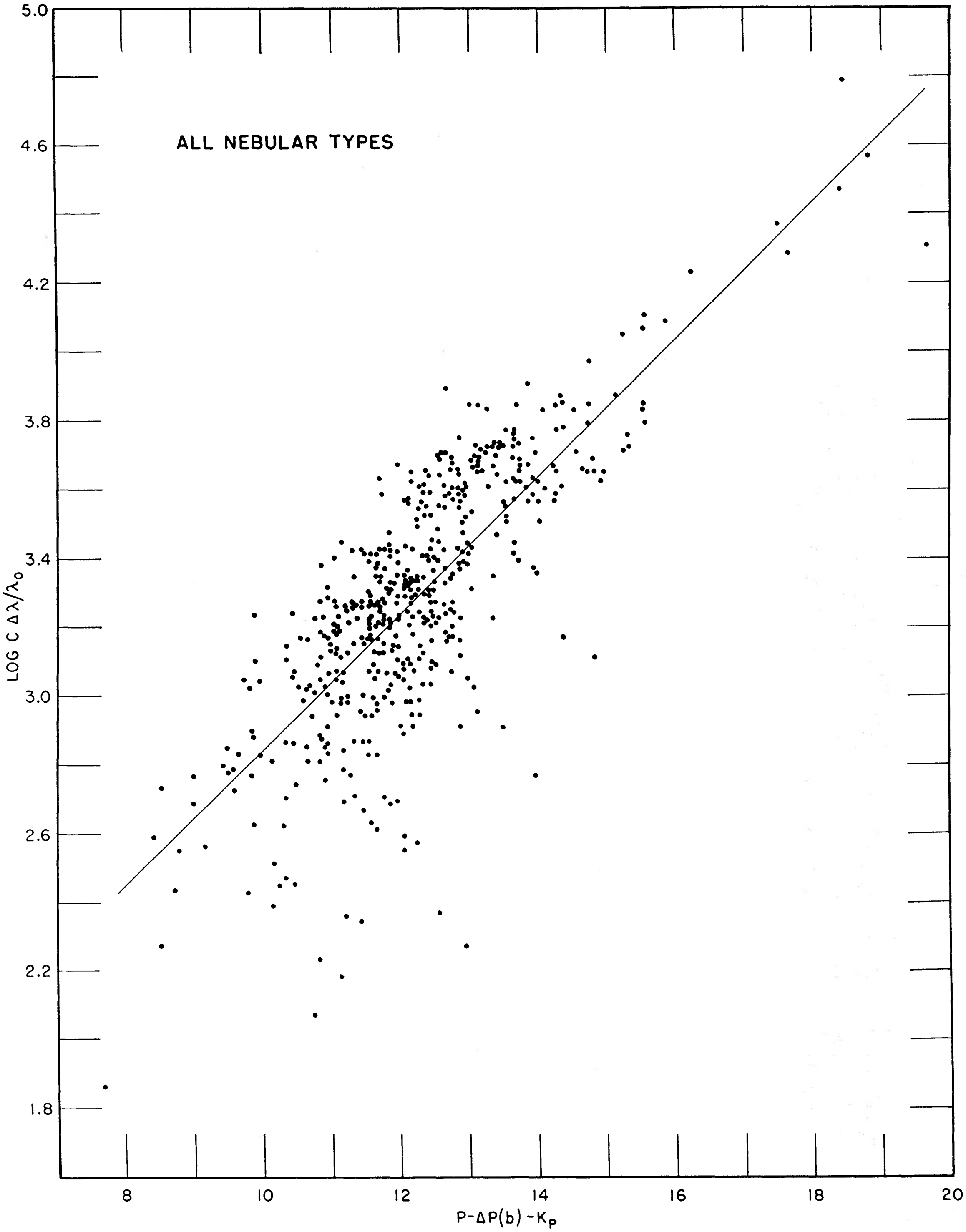

Figure 10. The redshift-magnitude relation for 474 field nebulae of all nebular types.

the number of nebulae N in each group; negative signs for $\overline{\Delta M}$ indicate higher luminosities.

TABLE X. DIFFERENCES IN $\overline{M}$ FOR FIELD NEBULAE

Type	$\overline{\Delta M}$	N
SBb	−.33	27
Sb	−.16	76
E	−.14	117
Sa	−.12	54
All Types	.00	474
So	+.17	67
Sc+SBc	+.21	90
SBo+SBa	+.29	36

According to this table, the SBb are statistically the brightest while the SBo's and SBa's are the faintest. The total range of the differences is 0.62 mag. With the SBb's excluded, for which only 27 nebulae are available, the range becomes 0.43 mag. The sizes of the probable errors for B, ranging from ±0.21 mag. for the E nebulae to ±0.36 mag. for the Sc plus SBc, show that most of the computed differences in $\overline{M}$ are illusory, and that the mean absolute magnitudes of nebulae along the entire sequence of classifi-

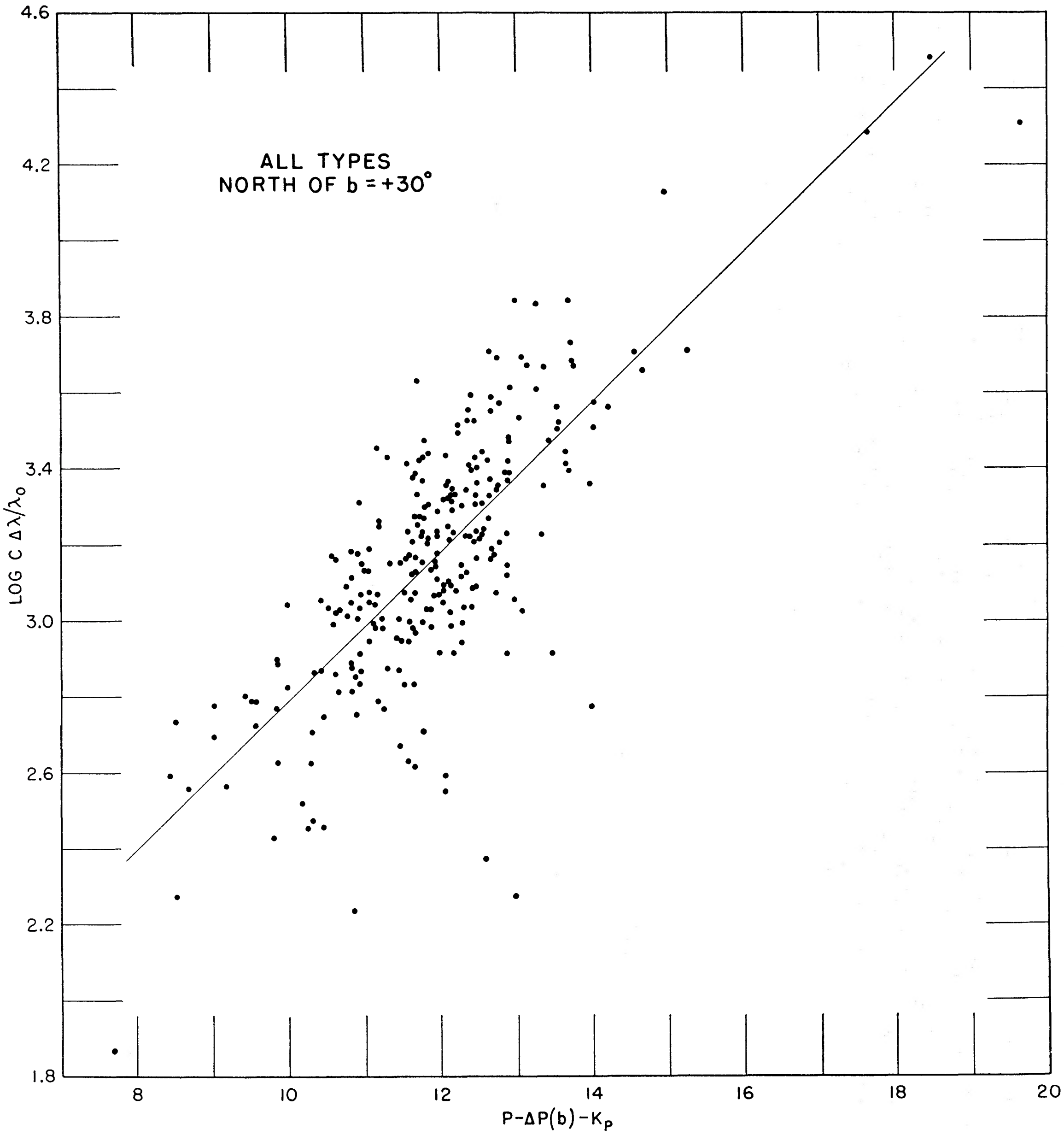

Figure 11. The redshift-magnitude relation for field nebulae of all types north of galactic latitude +30°.

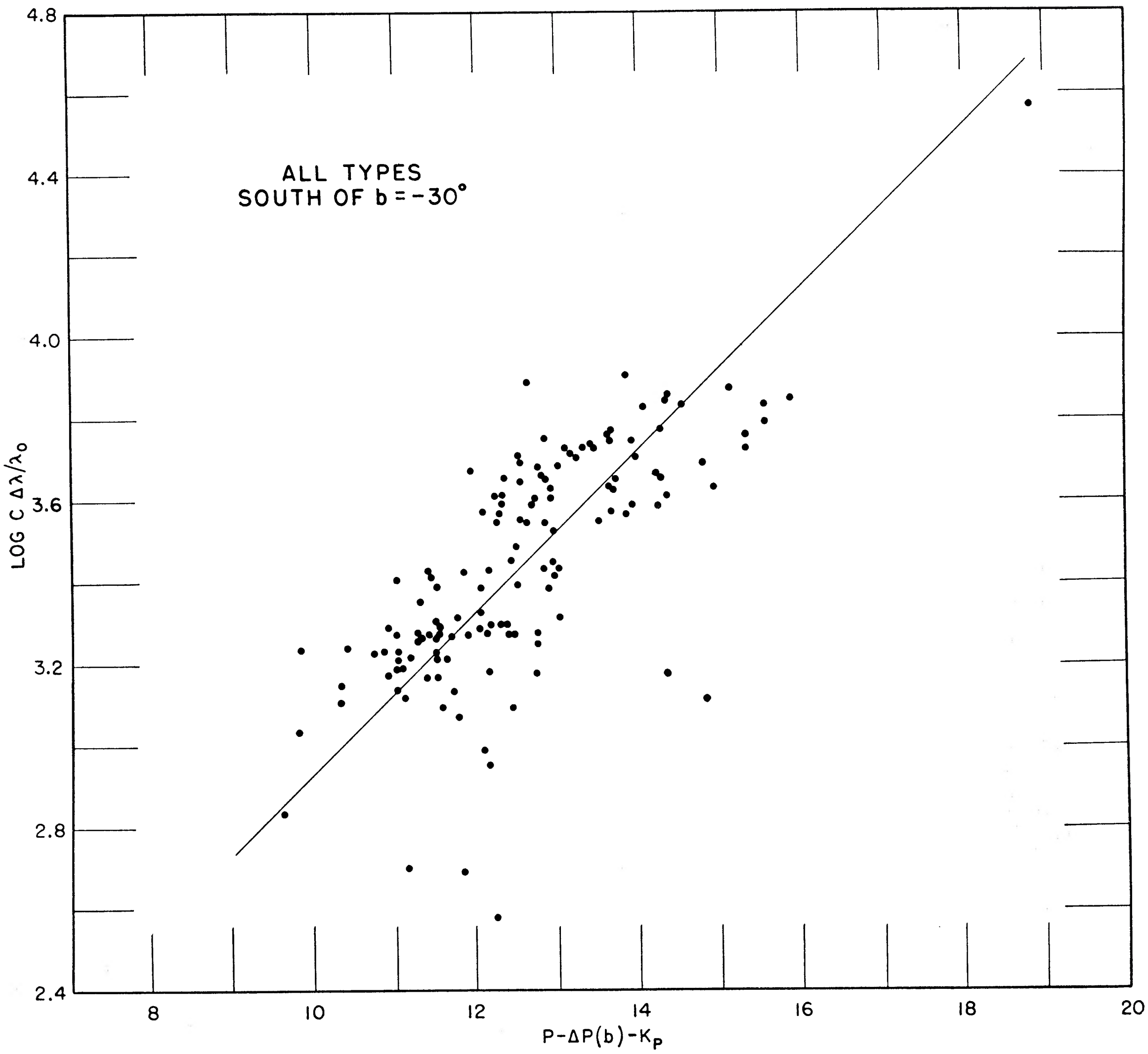

Figure 12. The redshift-magnitude relation for field nebulae of all types south of galactic latitude $-30°$.

cation, excluding the irregulars which show a very large dispersion, are nearly constant for this particular sample. Due to the effects of observational selection, these results may, however, be different for different samples.

Isolated Groups. There exist in space several well-known, isolated, physical groups of nebulae such as the local group, the nearby M81 and M101 groups, the Leo group, and Stephan's Quintet. Many of these aggregates were suspected from the geometrical aspects of the grouping before the redshift data became available. The redshift lists provide a powerful method for confirming such groups and for discovering new ones. While the general problem of the small-scale nebular distribution for nearby systems is not considered here, it is evident that steps toward its solution may now be taken with the present redshift data.

The large scatter in Figures 3 to 12 is primarily due to the spread in the luminosity function for nebulae. If some *a priori* means were available for selecting nebulae with similar absolute magnitudes, this scatter would become smaller and a more refined analysis of the data would be possible. It is reasonable to expect that such a homogeneous nebular sample might be found among the brightest objects in physical aggregates of moderate to large population, since such nebulae would be chosen from a definite part of the luminosity function. This expectation was tested and confirmed by analysis of 27 groups

TABLE XI. DATA FOR REPRESENTATIVE GROUPS OF NEBULAE

Name, Pop., $c\,\Delta\lambda/\lambda_0$	NGC	Pc	$c\,\Delta\lambda/\lambda_0$	Rank
G68	68	14.3	6012	1
20±	72	14.4	7201	2
6785	71	14.5	6816	3
	69	15.6	6862	4
	Anon	15.6	7032	5
G80	80	13.6	5790	1
12	83	14.1	6745	2
6268				
G128	128	12.6	4384	1
5	125	....	5423	
4657	127	....	4228	
	Anon	....	4594	
G194	194	13.2	5237	1
10	182	13.3	5360	5
5298				
G383	383	13.2	5086	1
12	379	13.7	5572	2
5264	380	13.7	4539	3
	385	14.0	5043	5
	384	14.2	4599	6
	388	15.3	5312	7
	386	15.3	5753	8
	375	15.6	6209	9
G507	507	12.5	5121	1
35±	499	12.8	4567	2
4664	495	13.9	4306	4
G564	564	13.7	5923	1
20±	560	13.9	5578	2
5750				
G741	741	12.9	5637	1
9				
G1023	1023	9.5	709	1
6	925	10.1	647	2
513	891	10.2	246	3
	1058	11.4	221	4
	1003	11.5	741	5
G1068	1068	9.8	1082	1
5	1087	11.3	1835	2
1604	1073	11.6	1895	3
Fornax Cl	1380	10.9	1706	1
40±	1404	11.0	1885	2
1631	1399	11.1	1302	3
G1600	1600	12.0	4728	1
8	1601	14.9	4895	
4812				
G2563	2563	13.4	4664	1
20	2562	13.7	4852	2
4758				
G2832	2832	13.3	6895	1
30±	2831	14.6	5104	2
6000				
G3158	3158	13.0	7008	1
20				
G3190	3190	12.0	1252	1
5	3193	12.1	1272	2
1196	3177	....	1118	3
	3185	13.0	1142	4
Leo Gr	3627	9.5	633	1
20±	3623	9.9	588	2
788	3368	9.9	792	3
	3379	10.4	730	4
	3351	10.5	553	5
	3384	10.8	649	6
	3628	....	728	7
	3489	10.9	572	8
	3607	10.9	818	9
	3626	11.0	1362	10
	3810	11.1	880	11
	3377	11.3	595	12
	3412	11.5	735	13
	3593	11.6	427	14
	3389	12.0	1202	15
	3608	12.0	1117	16
	3338	(12.2)	1201	17
	3605	14.0	600	18
G5049	5049	13.7	2600	3
15				
G5077	5077	12.5	2515	1
8				
G5371	5371	11.3	2694	1
5	5353	12.1	2284	4
G5846	5846	11.2	1782	1
10	5813	11.7	1890	2
1808	5838	11.8	1441	3
	5806	12.3	1307	4
	5850	11.7	2412	5
	5831	12.5	1696	6
	5854	12.5	1644	7
	5854 Anon	14.0	2292	8
G6027	6027d	14.7	4568	1
5	6027a		4159	
4364				
G6928	6928	13.1	4994	1
5	6930	13.4	4419	2
4647	6927	15.0	4517	3
	Anon	....	4659	
G7242	7242	13.5	5972	1
15	Anon	....	6272	
6122				
Stephan's	7318a	14.3	6960	1
Quintet	7318b	14.4	6031	2
5	7317	14.8	7014	3
6703	7319	....	6935	4
	7320	....	....	5
	7335	....	6576	.
G7385	7385	13.9	8054	1
13±	7386	14.3	7423	2
7738				
G7619	7619	12.3	3953	1
20±	7626	12.6	3553	2
3836	7562	12.7	4004	3
	7611	13.5	3579	4
	7623	13.9	3659	5
	7617	14.9	4268	6

found with the redshift data. The [log cz, m] relation for the first-ranked member of each group not only has smaller scatter than Figure 10, but it shows preference for high absolute magnitudes. The brightest member nebula for 23 of the 27 groups is at least 0.5 mag. brighter than the mean line of Figure 10. The points for 19 of the 27 groups are at least 1.0 mag. brighter than the mean line, while 8 are more than 1.5 mag. brighter, and 5 more than 2.0 mag. brighter than this line. The increased homogeneity, gained by restricting attention to the brightest nebulae of populous aggregates, is important in the discussion of the cluster data.

Table XI gives the data for the 27 groups studied. Listed in column one are the group designations taken from the NGC number of the brightest member, the estimated group population, and the mean redshift. The remaining columns contain the NGC number, the photographic magnitude corrected for latitude and K effect, the redshift corrected for solar motion, and the rank of the member nebula. Only two of the 27 groups are closer to us than the Virgo Cluster. These are the NGC 1023 and the Leo groups with mean redshifts of +513 and +788 km/sec, respectively. Due to their proximity, these groups will eventually be important in evaluating the redshift parameter H.

The Cluster Data. For a given apparent magnitude, data for the brightest members of the great clusters of nebulae permit the deepest penetration into space. Furthermore, these same nebulae provide the homogeneity of sample so important in the search for a possible second-order term in the redshift law. The [log cz, m] relation can, therefore, be carried farther and be more precisely defined with the cluster data.

Tables II and III of Part I give redshifts for 26 clusters. Photometric data are available for 18 of these from the following sources. (1) Individual members of the nearby Virgo Cluster were measured photoelectrically by Whitford (1936) and by Stebbins and Whitford (1952), and with photographic methods by Bigay (1951). (2) Photoelectric measures were made by Pettit in 9 and by Sandage in 2 of the bright clusters with the 60- and 100-inch telescopes. (3) Magnitudes in the 6 faintest clusters were determined with schraffierkassette methods by Sandage using the 200-inch telescope.

The problem of the measuring apertures is paramount for these photometric data, since any large systematic magnitude error, depending on distance, would invalidate an attempt to find a second-order term in the redshift-magnitude relation. The procedure for aperture correction discussed in Appendix A can be applied with success for nebulae with redshifts less than about 25,000 km/sec. For more distant clusters this procedure fails, because the angular sizes of nebulae become too small for measurement on the 48-inch Schmidt plates. To discuss possible systematic magnitude errors for faint clusters, description of the schraffierkassette measuring technique is necessary.

A schraffierkassette plate contains square images of uniform density obtained by moving a photographic plate in a rectangular pattern by a mechanical device called a jiggle-camera. For large enough squares, the images of stars and nebulae are indistinguishable. After proper calibration, measurement of the densities of the images gives the magnitudes of the objects. Squares of 1, 2, and 4 mm on a side can be made with the present equipment. Thorough tests of this technique and present equipment were made before the start of the current program. First, schraffierkassette plates of Selected Areas 61 and 68, taken with the 200-inch, were measured to check the internal consistency of the method. Residuals from the calibration curves drawn with the standard magnitudes of Stebbins, Whitford, and Johnson (1950) were small; the mean residual without regard to sign was 0.02 mag. This procedure tested only the uniformity of the schraffierkassette images plus the measuring accuracy for the plates. A second test, using diffuse objects of appreciable diameter, was made on selected globular clusters in M31. Plates calibrated with field stars of known magnitude gave magnitudes that did not differ systematically from those of Nassau and Seyfert (1945), with a distribution of residuals whose dispersion was 0.10 mag. These tests were considered satisfactory and the current program was begun.

Schraffierkassette plates were taken for the 6 faint clusters and were calibrated by stars in each field whose magnitudes were determined by photographic intercomparison with S.A. 57 and 68 (Stebbins, Whitford, and Johnson 1950). An average of three independent intercomparisons in two colors was made for these standard stars and the internal magnitude agreement was good. Magnitudes for 4 of the 6 faintest clusters were measured on plates made with jiggle-camera throws of 2 mm. The two faintest clusters 0855+0321 and 0925+2044 were measured from 1-mm squares, since 2-mm images were too faint for satisfactory results.

The question arises of the adequacy of the sizes of these jiggle-camera squares for a check on the aperture effect in these faint nebular magnitudes. Experience, both by Hubble (1936c) and from the tests on the M31 objects, has shown that squares of 2.5 times the apparent diameter of diffuse objects give magnitudes that differ by less than 0.1 mag. from those measured photoelectrically with large apertures. Do squares of 1 and 2 mm for the 6 faint clusters satisfy this criterion? The scale at the 200-inch prime focus is 11″.07 per mm with the Ross $f/3.67$ corrector lens, so that schraffierkassette images of 2 mm are 22″.1 on a side. The nearest of the 6 faint clusters is Bootes (1431+3146) with a redshift of +39,400 km/sec. The diameters of the member nebulae of this cluster are too small to be determined on the 48-inch Schmidt plates, but they may be computed by assuming that ratios of angular diameters vary inversely with the redshift. This procedure assumes a linear law and neglects relativity effects. The apertures that give magnitudes to the standard isophote for the brightest nebulae of the Virgo Cluster are about 10′. Whitford's aperture for NGC 4594 was 7′.5. Since the mean redshift for this cluster is +1136 km/sec, the corresponding angular aperture at the Bootes Cluster is about 17″. A throw of 2 mm is, therefore, inadequate by a factor of $(17 \times 2.5)/22.1 = 1.9$ to give magnitudes for the brightest Bootes Cluster members on the same isophotal system as the nearby clusters. The curves of Appendix A give an estimate of about 0.2 mag. for the aperture effect of the brightest nebula of the Bootes Cluster. This error approaches zero for the 10th brightest nebula because these fainter nebulae average about ⅔ the diameter of the first ranked.

The cluster 0138+1840 is the most distant cluster measured with 2-mm squares. Since the redshift is +51,900 km/sec, the aperture of the standard isophote for the largest nebula would be about 13″. An aperture effect also exists in the measured magnitudes but it is smaller, since the factor is 1.5. For the Hydra Cluster (0855+0321), with a redshift of +60,500 km/sec, 1-mm squares are inadequate to a somewhat greater degree than are 2-mm squares for the Bootes Cluster, since the aperture factor is 2.5. Because of the uncertainty in the size of the effect, no aperture corrections have been made in the tabulated data for these 6 clusters, i.e., the directly-determined magnitudes are given in the data table. In the discussion of the second-order term in the redshift law it is therefore important to remember that the tabulated magnitudes for the 6 faintest clusters are too faint by values ranging from 0.0 to 0.2 mag., depending upon the rank of the cluster member. The existence of this small systematic error is not too serious because the sign of the correction strengthens the second-order trend found in the sequel.

Table XII gives the data now available for the 18 clusters. The first 3 columns are self-explanatory. Column 4 gives the mean redshift, corrected for solar motion, computed from Table II or III of Part I. This redshift is a combination of (1) the systematic distance effect, (2) that part of the internal velocity dispersion remaining in the mean of the redshifts of the cluster members, and

TABLE XII. PHOTOMETRIC DATA FOR 18 CLUSTERS

				P (uncorrected for latitude and K effect)				V (uncorrected for latitude and K effect)			
Name	l	b	$\overline{c\,\Delta\lambda/\lambda_0}$	1st	3rd	5th	10th	1st	3rd	5th	10th
Virgo*	256°	+75°	1,136	9.2	9.8	9.9	10.3	8.3	8.9	9.1	9.4
Perseus*	118	−12	5,433	13.02	14.47	14.49	14.75	12.24	13.24	13.35	13.54
Coma*	10	+87	6,657	12.90	13.31	13.60	14.52	11.69	12.16	12.55	13.60
Hercules	359	+43	10,400	....	14.81	....	15.77	....	13.74	....	14.55
2308+0720	53	−48	12,821	14.85	15.47	16.13	....	13.70	14.22	14.82	....
2322+1425	63	−44	13,187	15.34	15.87	16.22	16.60	14.37	14.87	15.17	15.63
1145+5559	106	+60	15,519	15.88	....	16.89	....	14.77	....	15.78	....
0106−1536	116	−77	15,781	15.20	15.74	16.70	16.80	14.12	15.01	15.77	16.04
1024+1039	201	+54	19,489	16.25	....	....	....	15.08	....	....	....
1239+1852	264	+81	21,533	15.41	16.14	16.32	16.89	14.10	14.86	15.39	15.72
1520+2754	10	+55	21,651	16.57	16.67	16.96	....	15.38	15.66	15.83	....
0705+3506	150	+20	23,365	17.11	....	....	....	16.00	....	....	....
1431+3146	16	+66	39,367	(17.93)	(18.36)	(18.78)	(19.26)	16.57	17.00	17.42	17.90
1055+5702	116	+55	40,360	(18.22)	(18.33)	(18.73)	(19.25)	16.86	16.97	17.37	17.89
0025+2223	85	−40	47,835	18.59	18.80	18.88	19.38	17.04	17.35	17.62	17.90
0138+1840	108	−42	51,908	18.40	18.55	18.84	19.14	17.32	17.65	17.79	18.13
0925+2044	178	+45	57,498	(18.58)	(19.15)	(19.30)	(19.72)	17.08	17.65	17.80	18.22
0855+0321	194	+31	60,526	(19.26)	(19.56)	(19.66)	(20.16)	17.70	18.00	18.10	18.60

* Virgo 1–3–5–10 4594, 4486, 4382, 4374
Perseus 1–3–5–10 1275, 1270, 1278, 1273
Coma 1–3–5–10 4889, 4789, 4921, 4853

TABLE XIII. CORRECTED PHOTOMETRIC DATA FOR 18 CLUSTERS

Cluster (1)	z (2)	ΔP(b) (3) mag.	$K(z, t_0)_P$ (4) mag.	$\overline{P}_C$* (5) mag.	ΔV(b) (6) mag.	$K(z, t_0)_V$ (7) mag.	$\overline{V}_C$* (8) mag.
Virgo	.004	.01	.02	9.16	.01	.01	8.27
Perseus	.018	.95	.08	12.51	.68	.04	11.72
Coma	.022	.00	.10	12.84	.00	.05	11.80
Hercules	.035	.12	.16	14.12	.09	.08	13.09
2308+0720	.043	.08	.20	14.78	.06	.09	13.79
2322+1425	.044	.11	.21	15.04	.08	.10	14.18
1145+5559	.052	.04	.24	15.71	.03	.12	14.70
0106−1536	.053	.01	.25	15.21	.01	.12	14.45
1024+1039	.065	.06	.30	15.88	.04	.15	14.89
1239+1852	.072	.00	.33	15.22	.00	.17	14.19
1520+2754	.072	.05	.33	15.93	.04	.17	14.96
0705+3506	.078	.48	.37	16.26	.35	.18	15.46
1431+3146	.131	.02	.61	17.31	.01	.35	16.21
1055+5702	.134	.05	.63	17.31	.04	.36	16.22
0025+2223	.159	.14	.74	17.39	.10	.44	16.28
0138+1840	.173	.12	.81	17.16	.09	.48	16.49
0925+2044	.192	.10	.90	17.54	.07	.54	16.41
0855+0321	.202	.24	.94	17.84	.17	.58	16.70

* On system of first brightest.

(3) the peculiar motion of the cluster itself. For all but the nearest three clusters, the effect of internal velocity dispersion should be small. For the Virgo Cluster, the spread in the redshifts for the individual members is about 2000 km/sec, which is larger than the systematic distance effect. This makes the adopted mean redshift of +1136 km/sec the most uncertain of the group as far as the systematic distance effect is concerned. No information is available on the size of the peculiar motions of the clusters themselves, but it appears to be small because of the small spread in the [log *cz*, *m*] correlations. Columns 5 to 12 of Table XII give the photographic and photovisual magnitudes of the 1st, 3rd, 5th, and 10th cluster members. The magnitudes for the first 12 clusters are corrected to the standard isophote by the procedure of Appendix A, while the values for the last 6 clusters are directly as measured. For 2 of the 6 faint clusters, both photographic and photovisual magnitudes were measured; for the 4 for which only photovisual values were obtained, the photographic magnitudes were found by applying the color indices for these cluster nebulae determined by Stebbins and Whitford (1952) and by Whitford (1954) to the measured V. Magnitudes so determined are enclosed in parentheses in Table XII.

In analyzing the photometric data we have the choice either of treating the correlation of m with log cz for the 1st, 3rd, 5th, and 10th nebulae separately, or of suitably combining the data into mean values of high weight. The latter method is to be preferred, since it uses all available material and tends to smooth any small differences in the luminosity functions for the various clusters. The magnitudes of the 3rd, 5th, and 10th nebulae were systematically reduced to that of the 1st by subtracting the mean differences of 0.48, 0.80, and 1.29 mag. respectively from the P data, and 0.51, 0.84, and 1.27 mag. respectively from the V data. The resulting mean magnitudes, on the system of the first brightest, were then corrected for latitude and K effect by the values listed in columns 3, 4, 6 and 7 of Table XIII. The final magnitudes, $P_C \equiv P - \Delta P(b) - K_P$ and $V_C \equiv V - \Delta V(b) - K_V$, are listed in columns 5 and 8 of this Table. These constitute the final data for discussion of the [log *cz*, *m*] relation for the clusters.

Interpretation of Cluster Data. Robertson (1938) has shown that, in an expanding universe, the intensity of light received at time t_0 from a source radiating at time t_1 is given by

$$l_{\mathrm{bol}_0} = \frac{L_{\mathrm{bol}\,(t_1)}}{4\pi R_0^2\sigma^2(1+z)^2} \tag{2}$$

where R_0 is the scale coefficient in the line element at the time of observation t_0 and σ is related to the dimensionless radial coordinate. The relation connecting m_{bol} and z is then given by Robertson (1955) as

$$m_{\mathrm{bol}} = 5 \log cz + 1.086\left(1 + \frac{R_0\ddot{R}_0}{\dot{R}_0^2} - 2\mu\right) z + \mathrm{const.} \tag{3}$$

Here, $\dot{R}_0/R_0 \equiv H$ is the Hubble redshift parameter and $\ddot{R}_0$ is the second time derivative of the metric scale factor, both evaluated at t_0. The quantity μ is related to the time rate of change of the absolute bolometric magnitude of the nebulae, plus the rate of change of that part of the K correction due to the Stebbins-Whitford effect, and plus the effect of any intergalactic obscuration. This equation accounts for the difference in the light-travel time for the nearby and distant clusters, by reducing the "world picture" to the "world map."

Following this equation, the data have been analyzed in the form $m_C = A \log cz + Bz + D$ for both P_C and V_C. Least-squares solutions were made for 3 cases: (1) A, B, and D were treated as unknowns, (2) A was considered to be precisely 5, with B and D as unknowns, and (3) A and D were considered unknowns, with $B = 0$. Table XIV gives the results. The goodness of fit

TABLE XIV. SUMMARY OF SOLUTIONS FOR 18 CLUSTERS

Unknown	Case 1	Case 2	Case 3
P data			
A	5.73	5.000	5.029 ±.121
B	−5.62	−1.180 ±.875	0.00
D	−8.55	−5.81 ±.092	−6.03 ±.519
σ_0 (P) mag.	.282	.315	.302
V data			
A	5.72	5.000	4.925 ±.138
B	−6.34	−1.976 ±.895	0.00
D	−9.40	−6.71 ±.094	−6.56 +.590
σ_0 (V) mag.	.292	.323	.344

in each case may be judged by the dispersions of the distributions of the magnitude residuals. These dispersions, σ_0, are also given in this Table. Case 1 fits the data best. Solutions in Cases 2 and 3 are the only ones compatible with equation (3), since in them $A = 5$ by assumption for Case 2 and to within the probable error for Case 3. Case 2 is adopted in the following discussion.

There are at least 4 causes for the observed dispersion σ_0: (1) dispersion in the absolute magnitudes of the nebulae considered (σ_M); (2) scatter in the redshift coordinate due to internal velocity dispersion and to the mean peculiar motions of the clusters themselves (σ_z); (3) scatter due to possible patchy internebular obscuration in the direction of the 18 clusters (σ_F); (4) measuring errors in both m and z (σ_ϵ). The observed σ_0 of 0.32 mag. is compounded of these four separate dispersions. The remarkable smallness of σ_0 shows that σ_M, σ_z, σ_F, and σ_ϵ must each be very small. In particular, this analysis provides little evidence for the existence of patchy internebular absorption in the direction of the 18 clusters. An upper limit of 0.30 mag. is placed for σ_F but the true value is undoubtedly smaller. No information on possible uniform internebular obscuration is contained in the present material, since only deviations from uniformity can be detected by study of the dispersions.

The term of greatest interest is B, because it describes deviations from linearity. The value of B from Solution 2 is only twice its probable error, but two uncertain elements not allowed for in the data should be emphasized. These are: (1) the aperture effect in the faint clusters, and (2) possible uniform internebular obscuration. Corrections for both effects not only preserve the negative sign of B, but they make its absolute value larger. That the aperture effect is indeed present may be seen by separate analysis of the [log cz, m] relation for the 1st and 10th brightest nebulae with the data of Table XII. A larger negative B is found with the 10th ranked nebulae, due to the smaller aperture correction required for the higher-ranked cluster members.

The data are plotted in Figures 13 and 14 with the solid lines drawn from Solutions 2. The difference in the B values between the photographic and photovisual solutions is undoubtedly caused in the following way by the Stebbins-Whitford effect. The computed K corrections in Appendix B are those which would be valid in the absence of the SW effect. If this effect is due to stellar evolution, K will be a function of time as well as of redshift. The correct value to be applied is $K(z, t_1)$ instead of $K(z, t_0)$ as given in Appendix B. The difference between $K(z, t_1)$ and $K(z, t_0)$ is absorbed in μ of equation (3). This difference, when expressed in a Taylor series, enters μ by the term $\delta K/\delta t$. The excess reddening of the Stebbins-Whitford effect requires that $K_P(z, t_1) - K_V(z, t_1) > K_P(z, t_0) - K_V(z, t_0)$ and hence that $\delta K_P/\delta t > \delta K_V/\delta t$. Since μ has the form (Robertson 1955)

$$\mu = 0.46[\dot{M} - \dot{K}(\lambda) - cF(\lambda)]H^{-1}, \quad (4)$$

equation (3) shows that the consequence of this inequality is $B_P > B_V$, as is actually observed. Here $\dot{K} \equiv \delta K/\delta t$ and $F(\lambda)$ is any possible internebular absorption expressed as F mag. per unit distance. If H^{-1} is expressed in 10^9 years and the velocity of light, c, is in light years per year, then F must be expressed as magnitudes per 10^9 light years. Since K and F are functions of wave length, the reason for the observed dependence of B on wave length is clear.

We are now in a position to consider the results

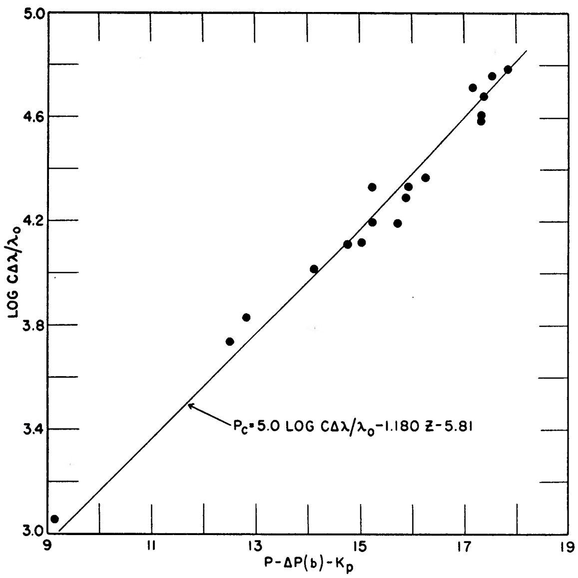

Figure 13. The redshift-P magnitude relation for clusters of nebulae. The apparent photographic magnitudes have been corrected only for the latitude effect and for the selective effect of the redshift. The "energy" and "number" corrections are *not* included in the data but are introduced into the theoretical equations used for the interpretation.

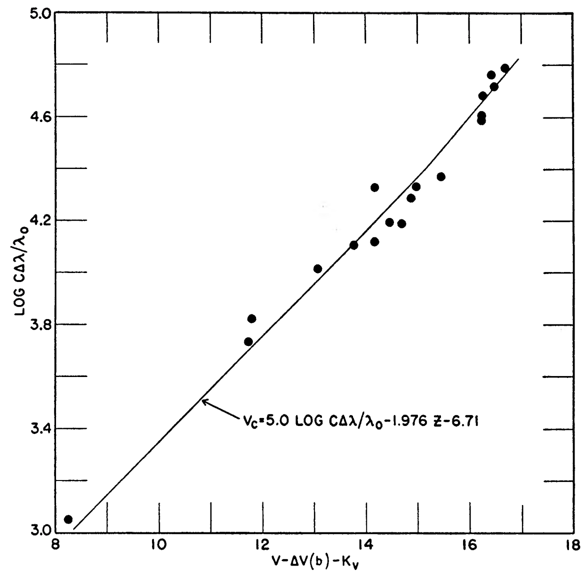

Figure 14. Same as 13 for photovisual magnitudes.

contained in the [log cz, m] relations of Figures 13 and 14. This material suggests the following five major conclusions.

(1) The slope of the [log cz, m] correlation line for small z is as close to 5 as the probable errors of the determination. This conclusion rests upon (a) the small magnitude residuals of the solution for Case 2 with the slope assumed to be 5, and (b) the direct determination of the slope as 5.029 ± 0.121 and 4.925 ± 0.138 for Case 3. This result means that for small z, the redshift-distance relation is linear, on the supposition that there is no general internebular obscuration. If we postulate the existence of general uniform internebular absorption, the redshift-distance relation is non-linear. The absorption, expressed as F mag. per unit distance, must be of just the right amount to cancel the non-linearity of the redshift law so that the observed [log cz, m] relation remains linear. Such an interpretation is highly unlikely but cannot definitely be excluded.

(2) The expansion appears to be isotropic, since no separation of points occurs between the 12 clusters in north galactic latitudes and the 6 southern clusters. This is a stronger test than that for the field nebulae, since the cluster data (1) probably are less affected by observational selection and (2) show smaller scatter about the mean correlation line.

(3) The absolute magnitude of the brightest nebulae in clusters is nearly equal to the very brightest of the field nebulae. This near equality is seen if the line drawn in Figure 13 for the clusters is transferred to Figure 10 for the field nebulae. Such a line defines a limit above which few field nebulae occur. On this basis there appears to be an upper limit to the absolute magnitude of extragalactic nebulae close to that of the brightest cluster members.

(4) The departures from uniformity for any postulated intergalactic obscuration must be distributed with $0.30 > \sigma_F \geqslant 0$ mag.

(5) The second-order term, B, in the redshift law is negative and appears to be statistically significant. Its value is -3.0 for the photovisual data and -2.2 for the photographic data if an allowance is made for an aperture correction of 0.20 mag. at the distance of the Hydra cluster. These values, together with equation (3), give

$$\frac{R_0\ddot{R}_0}{\dot{R}_0^2} = -(3.0 \pm 0.8) + 2\mu_P \qquad (5)$$

$$\frac{R_0\ddot{R}_0}{\dot{R}_0^2} = -(3.7 \pm 0.8) + 2\mu_V \qquad (6)$$

where the subscripts P and V stand for photographic and photovisual wave lengths. If $2\mu_P > 3.0$ or if $2\mu_V > 3.7$, then $\ddot{R}_0$ is positive and the expansion is accelerating; otherwise it is decelerating. For a decision we must evaluate the right member of equation (4) which involves $\dot{M}$ and $\dot{K}$ as the principal unknown quantities.

Estimates of $\dot{M}$ can, at present, come only by appeal to some theory of stellar evolution for systems of Population II. Current ideas for such evolution stem primarily from the work of M. Schwarzschild that has appeared in a series of papers with his collaborators (Oke and Schwarzschild 1952; Sandage and Schwarzschild 1952; Härm and Schwarzschild 1955). Application of these ideas to the particular case of the globular cluster M3 (Sandage 1954b) provides a basis for an estimate of $\dot{M}$. Within the framework of this theory, the observational data show that the M3 stars were formed about 5×10^9 years ago. The theory predicts that the brightest stars in the cluster have moved from their original places on the main sequence in the H-R diagram into the giant region, and subsequently, after burning most of their fuel, have disappeared to faint luminosities. Presumably, the cluster was brighter in early times because of the presence of these bright stars. In the available time of 5×10^9 years, all stars brighter than absolute bolometric magnitude $+3.5$ have evolved from the main sequence. We know with some certainty only the evolutionary tracks for the present time t_0. If we assume that tracks for slightly different luminosities are homologous, i.e. parallel in the log T_e-M_{bol} plane, an evaluation of $\dot{M}$ can be made. The change in the absolute magnitude of the main-sequence break-off point in time t_1 to t_0 is, for small t_0/t_1,

$$\Delta M_{bol} = 2.5 \log \mathfrak{M}_1/\mathfrak{M}_0 + 2.5 \log t_0/t_1 \quad (7)$$

where $\mathfrak{M}_0$ and $\mathfrak{M}_1$ are the respective masses of the stars at the break point. We wish to compute this change in the bolometric magnitude in the last one billion years. If $t_0 = 5 \times 10^9$ yr., $t_1 = 4 \times 10^9$ yr. and with the ratio $\mathfrak{M}_0/\mathfrak{M}_1$ obtained by iteration from the mass-luminosity law, then $\Delta M_{bol} = 0.31$ mag. For homologous evolutionary tracks this value also equals the change of the bolometric magnitude of the entire cluster if we assume that most of the light comes from stars brighter than $M_{bol} = +3.5$. If an appreciable fraction of the total light comes from stars fainter than $M_{bol} = +3.5$, then the ΔM_{bol} for the system will be less than 0.3 mag. This computation gives, therefore, an upper limit to $\dot{M}$. If the case for elliptical nebulae is similar to that of the globular clusters, then $\dot{M} \leqslant 0.3$ mag. per 10^9 yr.

Estimates of $\dot{K}_P$ and $\dot{K}_V$ are more difficult. Precise values must await the results of Whitford's current six-color work with the 200-inch in these distant clusters. Meanwhile, estimates may be made on the basis of his statement (Whitford 1953) that "the observed two-color excess could arise from additional radiation in the distant systems of a quality like that of a Type I G0 supergiant." An energy curve determined from the $I(\lambda)$ for M32 (Stebbins and Whitford 1945) and from the $I(\lambda)$ for supergiant G0 stars (Stebbins and Whitford 1945) permitted direct computation of $K(z, t_1)$ by the procedure described in Appendix B, with the result that $\dot{K}_P \approx +0.3$ and $\dot{K}_V \approx 0.0$ mag. per 10^9 yr. These values agree fairly well with the observed Stebbins-Whitford excess of $\dot{K}_P - \dot{K}_V = +0.40$ mag. for the Hydra Cluster (Whitford 1954).

Finally, to evaluate 2μ we need the value of the redshift parameter H. From the discussion in Appendix C, we adopt $H^{-1} = 5.4 \times 10^9$ years. If the units of $\dot{M}$ and $\dot{K}$ are in mag. per 10^9 yr. and F in mag. per 10^9 l.y., then equation (4) gives $2\mu_P = 5.0\,[0.3 - 0.3 - F_P]$ and $2\mu_V = 5.0\,[0.3 + 0.0 - F_V]$. If $F = 0$, then $2\mu_P = 0.0$ and $2\mu_V = 1.5$. Equations (5) and (6) then give $(R_0\ddot{R}_0/\dot{R}_0^2) \approx -3.0$ for P magnitudes and -2.2 for V magnitudes. The average is -2.6. It is interesting to note that the presence of any general internebular obscuration will give $\ddot{R}_0$ an even more negative value. For as small a value as $F_P = 0.30$ mag. per 10^9 l.y., $R_0\ddot{R}_0/\dot{R}_0^2$ becomes about -5.

The result that $\ddot{R}_0$ is negative has such important cosmological implications that it is well to review the steps in its evaluation and to indicate the uncertainties at each point. The basic data are the $[\log cz, m]$ pairs. Of the two, observational errors are appreciable only in the magnitudes. Call these errors ϵ_P and ϵ_V. The expression for the second order term B, obtained by modifying equations (3) and (4), now becomes

$$B_{P,V} = 1.086\left[1 + \frac{R_0\ddot{R}_0}{\dot{R}_0^2} - 5.0(\dot{M} - \dot{K}_{P,V} - F_{P,V}) + \epsilon_{P,V}/z\right] \quad (8)$$

If we require that $\ddot{R}_0 \geqslant 0$, then the inequality

$$\frac{B_{P,V}}{1.086} - 1 + 5.0(\dot{M} - \dot{K}_{P,V} - F_{P,V}) - \epsilon_{P,V}/z \geqslant 0 \quad (9)$$

must hold. With $B_P/1.086 \approx -2.0$ and $B_V/1.086 \approx -2.7$, as given by the observations, and with $\dot{M} = +0.3$, $\dot{K}_P = +0.3$, and $\dot{K}_V = 0$, equation (9) requires that $|\epsilon_P/z| \geqslant 3.0$ mag. and $|\epsilon_V/z| \geqslant 2.2$ mag. The errors in the magnitudes of the faint clusters with $z \approx 0.20$ must then be

$|\epsilon_P| \geqslant 0.6$ mag. and $|\epsilon_V| \geqslant 0.4$ mag. These values probably are too large to be ascribed to observational uncertainty.

Incorrect estimates of $\dot{M}$ and $\dot{K}$ also affect the sign of $\ddot{R}_0$. Since, however, $\dot{M}$ and $\dot{K}$ enter equation (8) with opposite sign, and since we know that $\dot{K}_P > 0$ because the Stebbins-Whitford effect is an excess reddening and not a bluing, the upper limit to $\dot{M}$ that satisfies equation (9) is large. If $\dot{K}_P = 0$, then $\dot{M} \geqslant 0.6$ mag./10^9 yr. for $\ddot{R}_0$ to be positive. With the more realistic value of $\dot{K}_P = +0.3$ mag./10^9 yr., the upper limit to $\dot{M}$ becomes $+0.9$ mag./10^9 yr. These values seem quite high on any current theory of stellar evolution. While it is obviously true that present ideas on stellar evolution may prove to be either incorrect or non-applicable to the present case, and therefore that the basis of our present estimate that $\dot{M} \leqslant 0.3$ mag./10^9 yr. may be invalidated, nevertheless $\dot{M} \approx 0.9$ mag./10^9 yr. is so high as to appear improbable.

The foregoing analysis therefore suggests that any reasonable estimates of the errors in the measured magnitudes and in the values of $\dot{M}$ and $\dot{K}$ require that $\ddot{R}_0$ be negative and that the expansion is decelerating. This result cannot be considered as established, however, until accurate values of $\dot{K}$ are available from Whitford's current work and until an adequate theory is worked out to explain the Stebbins-Whitford effect. If the excess reddening is a time effect, such a theory must predict from evolutionary tracks in the M_{bol}, $\log T_e$ plane the details of the change with time of the spectral energy curves. Then it should be possible to estimate the value of $\dot{M}$ and the sign of $\ddot{R}_0$ with some confidence.

Although it would be appropriate to end this paper with a definite statement of the possible cosmological models consistent with the present data, such a statement cannot be given at present for the following reason. With the field equations of general relativity, a series of mathematical models are obtained for the character of the expansion. (See, e.g., Einstein 1945 or Bondi 1952.) These models show how the function $R(t)$ depends on time, and they differ from one another according to the sign of the space curvature $(1, 0, -1)$ and of the value of the cosmological constant Λ. Three of the crucial observational items required for a choice between the models are (1) the sign of $\ddot{R}_0$, (2) the value of $1/H$, and (3) independent knowledge of the "age of the universe"—really the time since the beginning of the expansion—from say an astrophysical theory for the age of the oldest stars or from a geological age for the earth. When these three items are known, a weeding out of certain inconsistent models can be made. Unfortunately, the present uncertainty in the value of $1/H$ and the imminent rediscussion of the sign of $\ddot{R}_0$ with Whitford's anticipated results for computing $K(z, t_1)$ make such a discussion inappropriate at the present time.

Acknowledgments. For the Mount Wilson-Palomar lists of redshifts it is a pleasure to express sincere appreciation to Miss Alice Beach, who has participated in the measurement and reduction of the plates and, to a large extent, in the preparation of this complete paper; and also to Mrs. Mary Coffeen, Miss Sylvia Burd, and Miss Wilma Berkebile, whose contributions are greatly appreciated.

For the Lick list of redshifts (Table V), grateful acknowledgment is made to Mrs. C. Roger Lynds (Beverly Turner), who carried out the extensive reduction to a standard system of wave lengths, and to Mrs. Howard C. Cowan, who did the exacting job of typing on the IBM electric typewriter.

Part of the extensive computational work of Part III was done by Mr. Walter Bonsack of C.I.T. and his very efficient help is gratefully acknowledged. Mr. Harold Kinney did his usual fine job in preparing the line drawings for the press. It is also a pleasure to thank Drs. H. P. Robertson and A. E. Whitford for their critical reading of an early draft of Part III.

APPENDIX A. CORRECTIONS TO THE MAGNITUDES FOR APERTURE EFFECT

The total magnitude of an extragalactic nebula is difficult to measure by any technique because of the large angular size of the regions contributing appreciably to the total light. The diameters of nebulae are very much larger than revealed by visual inspection of well-exposed photographs. Nearly all early investigations of nebular magnitudes have been affected by this difficulty, because measures have usually been restricted to the regions of the nebulae seen on photographs. Because the observed magnitudes depend upon the aperture used in the photometry, a systematic error in the magnitudes is introduced that depends upon the nebular diameter itself. This systematic error has the effect of changing the slope of the regression line of redshift vs. apparent magnitude. The error must be removed from the basic magnitude measures before numerical results from the correlations are obtained.

It is clear that the corrections to the tabulated magnitudes in Pettit's and in Stebbins and Whitford's catalogues will be a function of the ratio of the aperture actually used to the angular diameter of the nebula. The determination of this function is the main objective of this appendix.

Hubble's (1930) investigation of the intensity distribution in elliptical nebulae showed the remarkable fact that the intensity function $I(r/a)$, where r is the distance measured along the major axis of the nebula and a is the value of r at $I = I_0/4$, is very nearly the same for 15 nebulae studied. Hubble further showed that the isophotal contours are elliptical. These two results together with the form of $I(r/a)$ permit a derivation of the correction function $\Delta m = f\ (D_p/D_s)$, where Δm is the correction to be applied to the catalogue values of Pettit and of Stebbins and Whitford, D_p is the diameter of the diaphragm used by these observers, and D_s is the diameter estimated from a photograph.

The function Δm could be defined so as to correct the catalogue magnitudes either (1) to the total light of the nebula, or (2) to the light contained within a certain isophote. Ideally the desired quantity would be the total magnitude, but this is more difficult to obtain than the magnitude within a given isophote, for the following reason. The term total magnitude has the meaning of the magnitude approached asymptotically as $r/a \to \infty$. Since the form of $I(r/a)$ is not yet known for $r/a > 50$, we do not have sufficient knowledge of the form of the asymptotic approach. Some investigators have even inferred that such a limiting magnitude does not exist. This conclusion results from extrapolation of Hubble's interpolation formula $I = I_0/[(r/a) + 1]^2$ to large r/a. Since the radial intensity given by this equation does not fall more rapidly than r^{-2}, the total intensity obtained by using this form is a divergent integral and consequently the total light of any given nebula would not be finite. The measures that Hubble considered reliable were taken only to $r/a = 20$. To this point his equation fits the data well. Beyond $r/a = 30$ there is no reason for expecting the interpolation equation to hold. Indeed, E. Dennison's recent photometry (Thesis, University of Michigan 1954) of NGC 3379 shows that beyond $r/a = 20$ the observed $I(r/a)$ falls more rapidly than r^{-2}. G. de Vaucouleurs (1948) has also studied the problem and reaches the same conclusion. His measures for NGC 3379 extend only to $r/a = 22$ which is not as far as $r/a = 50$ reached by Dennison. For the E2 nebula NGC 4649, de Vaucouleurs has carried his measures to $r = 190''$ along the major axis which corresponds to $r/a = 26$. He finds that $I(r/a)$ goes approximately as $r^{-2.3}$ for this object. The decline is steeper than r^{-2} and this agrees with Dennison's measures in NGC 3379 beyond $r/a = 20$. An asymptotic total magnitude therefore probably does exist. However, in view of the present lack of knowledge of $I(r/a)$ beyond $r/a = 50$, a value for the asymptotic magnitude is not reliable. Consequently the correction function Δm will be derived to give the magnitude contained within some standard isophote.

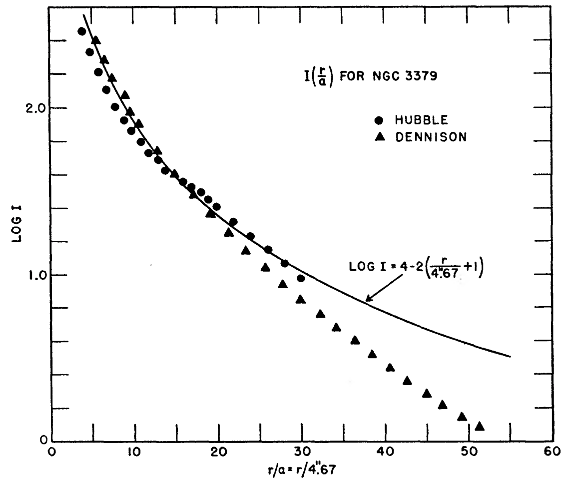

Figure A1. The radial intensity function $I\ (r/a)$ for the Eo nebula NGC 3379 as given by Dennison (1954).

Dennison's results are shown together with those of Hubble in Figure A1. The agreement to $r/a = 20$ is good. Similar agreement exists with de Vaucouleurs' results. Beyond this point, Dennison measures lower intensities than Hubble,

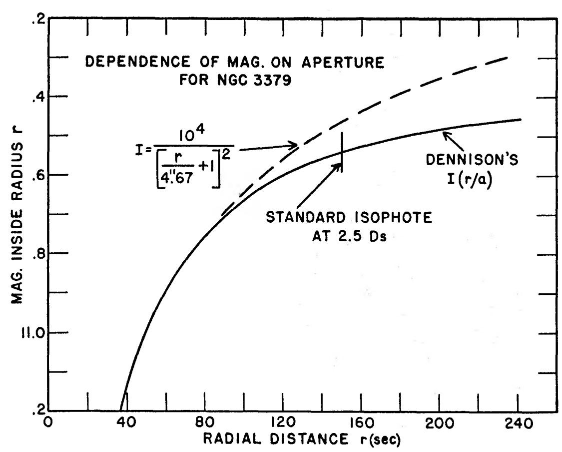

Figure A2. The increase in the apparent magnitude of NGC 3379 as a function of the measuring aperture. The $I\ (r/a)$ function of Figure A1 is adopted.

but the latter considered his own photometry beyond $r/a = 20$ as somewhat uncertain. The unit of intensity in Figure A1 is 27 magnitudes per square second of arc. In the sequel, Dennison's $I(r/a)$ is adopted as standard.

To obtain a general form for Δm we shall assume that the shape (but not necessarily the calibration) of Dennison's $I(r/a)$ function applies to all nebulae. The justification for this assumption lies in (1) Hubble's demonstration that the shapes of the $I(r/a)$ curves for 15 E nebulae studied were nearly identical and (2) in the fact that, except for the Sc and Irr nebulae, the disk of Population II stars which underlies the spiral structure is present in all nebular types and is elliptical in outline. This disk contributes eighty per cent or more to the total light (Holmberg 1950). Therefore $I(r/a)$ for S0 to Sb nebulae is assumed to be like that in E nebulae. The errors introduced by this assumption are small compared with the Δm corrections.

The dependence of the measured magnitude on aperture for the E0 nebula NGC 3379 is obtained from

$$m(r) = \text{const} - 2.5 \log \int_0^r 2\pi r I(r)\, dr \qquad \text{(A.1)}$$

Figure A2 shows the curves $[m, r]$ for the case of Dennison's $I(r)$ and for the case of Hubble's formula extrapolated to large r. This figure shows the difficulty of obtaining the value of the asymptotic magnitude even from Dennison's function. The $[m, r]$ relation of Figure A2 permits the reduction of measured magnitudes to that magnitude which would have been measured if the aperture had been a certain standard size. We must now decide what to use as this standard size.

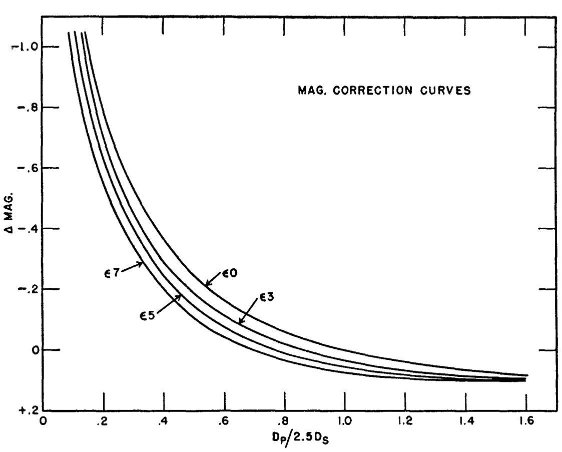

Figure A3. The magnitude correction curves for different apparent ellipticities of projected images as a function of the ratio of the measuring aperture to the apparent nebular diameter.

Images of most extragalactic nebulae on photographic plates appear to have definite boundaries. While it is true that the apparent diameters become larger on plates of longer exposure times, it is also true that plates taken under identical conditions show the same diameters. This fact means that the limit of visual discrimination between a nebula and the sky background occurs at some definite isophote related to the exposure conditions on the plate. Holmberg (1945) has shown that the limit of discrimination also depends upon the gradient of I with r where r is measured in linear units on the plate (say mm). Fortunately this effect on the final Δm function is small and is neglected in what follows.

If a strictly homogeneous set of plates were available, it is clear that a homogeneous set of isophotic diameters could be obtained. A close approach to such a plate collection exists in the plates taken with the 48-inch Schmidt for the Palomar-National Geographic Sky Survey, since every care has been taken for uniformity. With these plates, the diameter D_s obtained by visual inspection will approach a system of isophotic diameters. The diameter of the apparent image of NGC 3379 on these Schmidt plates is $2r = 121''$, or $r/a = 12.9$. Figure A1 shows that $\log I = 1.74$ at this point. This isophote is at 22.6 mag. per square second, which is about 0.6 mag. fainter, on the average, than the light of the night sky.

The standard isophote to which the catalogue magnitudes will be corrected may be chosen arbitrarily, but, for convenience, it should be chosen so that the corrected magnitude will be close to m_{total}. For the purposes of this paper we shall define the standard isophote as that point in the nebula that has a radial distance from the nucleus of 2.5 times the maximum radius visible on the 48-inch Schmidt plates. The value of $2.5\,D_s$ is $302''$ in NGC 3379 and this figure corresponds to $r/a = 32.4$. The calibration of Figure A1 shows that this isophote has a surface brightness of about 25.1 mag./sq. sec.

The choice of the standard diameter of $2.5\,D_s$ now permits the calculation of $\Delta m = f(D_p/2.5\,D_s)$ from Figure A2. If NGC 3379 were measured with an aperture whose radius differed from $r = 151''$, the correction Δm must be applied to the measured value to give that which would have been measured with an aperture of $2.5\,D_s$. The values for Δm may be computed for any value of $r/151$ from Figure A2 by assigning

$\Delta m = 0$ at $r = 151''$. The Δm function is plotted in Figure A3 as the correction curve for nebulae with ellipticities $\epsilon = 0$. The curves for nebulae with ellipticities 3, 5, and 7 were obtained in the following manner. The intensity at every point of each elliptical image was obtained by assuming that the $I(r/a)$ function of Figure A1 applies along the major axis and that the isophotes are elliptical. Numerical integration for the intensity within circular apertures placed upon the elliptical images gave the $[m, r]$ curves similar to the curve in Figure A2 for the E0 case of NGC 3379. The correction curves $[\Delta m, D_p/2.5\, D_s]$ for each ellipticity derived from the $[m, r]$ curves are also shown in Figure A3.

Every nebula for which either Pettit or Stebbins and Whitford have a magnitude and for which a redshift exists was examined on the 48-inch Schmidt plates to obtain the diameter D_s and the ellipticity of the projected image. Pettit as well as Stebbins and Whitford give the aperture D_p to which their magnitude corresponds. Consequently $D_p/2.5\, D_s$ was found for each object and Δm was read from the appropriate curve in Figure A3. This value was applied to the catalogue magnitudes to give the magnitude corrected for aperture effect. In many cases the validity of the corrections could be tested from Pettit's catalogue, since two or more apertures were frequently used on a given object. This permitted two or more independent determinations of the corrected m. Surprisingly consistent values were obtained. Often the agreement was within ± 0.1 mag. The corrected magnitudes for every object used in the field-nebulae correlations are given in Table A1 of this appendix. Magnitudes for individual members of the two great clusters in Virgo and Coma are also included in the table.

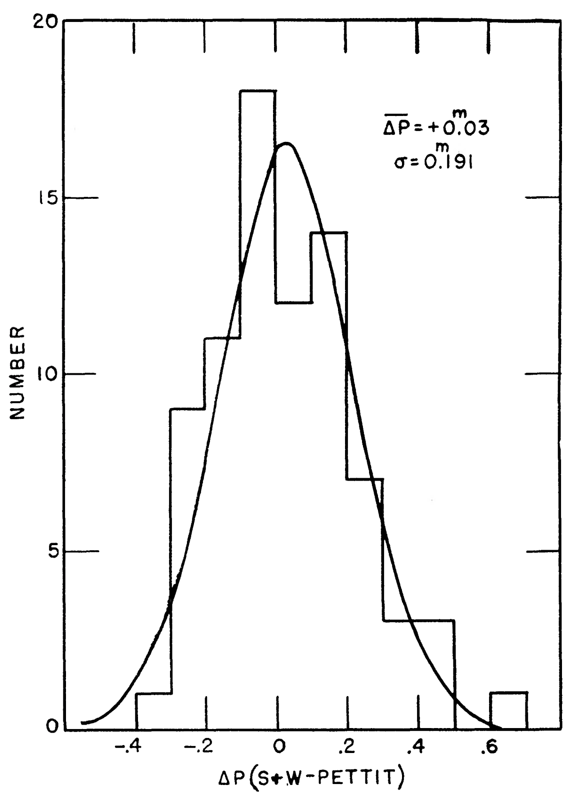

Figure A4. Histogram of the distribution of magnitude differences between Stebbins-Whitford's and Pettit's corrected catalogues.

The success which has been achieved in removing the aperture effect from the magnitudes may be determined by study of the overlap between the catalogues of Pettit and of Stebbins and Whitford. These lists have 79 nebulae in common for which redshifts are available. Of these, 44 have color indices in common. After correction for the aperture effect, the mean residual in magnitude in the sense SW *minus* Pettit is $\overline{\Delta P} = +0.026$ mag. The dispersion of the distribution is $\sigma = 0.191$ mag. The lack of systematic difference and the relatively small size of the random difference shows that, for the purposes of this paper, the two basic catalogues may be used interchangeably. Figure A4 shows the distribution of ΔP between the two lists.

Comparison for color differences of the 44 objects common to Pettit's and to Stebbins and Whitford's catalogues reveals the existence of a color equation. This result was expected, since Pettit's measures were not reduced to a standard system but were left on his natural instrumental system. A least-squares solution of the data gives

$$(\mathrm{CI})_{\mathrm{Pettit}} = \underset{\pm 0.027}{0.018} + \underset{\pm 0.033}{1.056}\, (\mathrm{CI})_{\mathrm{SW}}.$$

Comparison of Pettit's magnitudes, corrected for aperture effect, with magnitudes determined by Holmberg is also possible. For the past several years Holmberg has been measuring the colors and magnitudes of bright nebulae by a laborious but highly accurate photographic method. His final catalogue, based on plates taken with the Mount Wilson 60-inch and 100-inch telescopes, will contain between 250 and 300 nebulae. By private communication Holmberg states that the mean error of his final magnitudes for objects measured to date (1955) is ± 0.04 mag. and the mean error of the final color is ± 0.05 mag. Holmberg also states that comparison of his magnitudes with those of Stebbins and Whitford

TABLE A1. MAGNITUDES FOR 576 NEBULAE CORRECTED FOR APERTURE EFFECT.

NGC	m_{pg}	NGC	m_{pg}	NGC	m_{pg}	NGC	m_{pg}	NGC	m_{pg}	NGC	m_{pg}
7814	11.7	751	14.1	1744	12.1	2787	11.7	3430	12.0	4192	10.5
16	13.2	753	12.9	1832	12.0	2798	13.0	3486	10.7	4203	11.5
23	13.0	772	11.2	1889	14.4	2811	12.4	3489	11.0	4214	10.2
68	14.6	788	12.4	1964	11.4	2831	14.8	3504	11.6	4216	11.1
69	15.9	821	12.0	2139	11.9	2832	13.5	3512	12.9	4220	12.2
71	14.8	864	11.6	2146	11.3	2841	10.0	3516	12.7	4244	10.3
72	14.7	871	14.1	2217	11.8	2855	12.6	3521	9.6	4245	12.3
Note (1)	15.9	877	12.4	2268	12.2	2859	12.0	3556	10.4	4251	11.6
80	13.9	890	12.6	Note (10)	17.1	2865	12.5	3585	11.0	4254	10.2
83	14.3	891	10.8	2276	12.0	2880	12.6	3593	11.6	4258	9.0
Note (2)	19.4	908	10.8	2300	12.2	2903	9.7	3605	14.0	4273	12.2
Note (3)	16.2	925	10.5	2314	13.3	2911	13.6	3607	11.0	4274	10.8
Note (4)	15.8	936	11.1	2336	11.2	2914	14.2	3608	12.1	4278	11.2
128	12.7	972	12.1	2339	12.5	2950	11.8	3610	11.9	4281	12.3
157	11.0	Note (8)	14.1	2347	13.1	2964	12.1	3611	12.8	4283	13.1
160	13.7	1003	12.1	2366	11.5	2974	11.9	3613	11.8	4291	12.4
Note (5)	16.9	1023	10.1	2379	14.6	2976	10.9	3619	12.6	4303	10.0
182	13.4	1052	11.6	2389	13.3	2983	12.6	3623	9.9	4314	11.5
194	13.3	1058	11.9	2403	8.8	2985	11.2	3626	11.0	4350	11.9
210	11.8	1068	9.9	2441	13.0	2986	12.2	3627	9.5	4365	10.9
214	12.8	1073	11.7	2460	12.9	3003	12.0	3640	11.6	4374	10.5
227	13.5	1084	11.1	2500	12.0	3031	7.8	3642	11.6	4394	11.6
Note (6)	19.9	1087	11.4	2523	12.6	3032	12.8	3646	11.8	4406	10.3
Note (7)	18.4	1097	10.4	2525	12.0	3055	12.6	3665	11.9	4414	10.9
255	12.4	1140	12.8	2532	12.9	3065	12.9	3675	10.7	4421	11.8
278	11.5	1156	12.2	2535	13.2	3066	13.5	3681	12.5	4425	13.2
357	13.0	1201	11.7	2537	12.2	3067	12.6	3684	12.3	4429	10.9
375	15.9	1209	12.6	2549	12.1	3077	10.9	3686	11.7	4435	11.7
379	14.0	1232	10.5	2551	13.2	3078	12.1	3726	11.8	4438	11.2
380	14.0	1300	11.2	2562	14.0	3115	10.1	3810	11.1	4442	11.4
383	13.6	1302	11.1	2563	13.7	3147	11.4	3818	13.0	4448	11.7
384	14.6	1316	(10.0)	2608	12.8	3158	13.2	3872	13.0	4449	9.8
385	14.3	1317	(12.1)	2613	10.9	3166	11.2	3893	11.0	4459	11.5
386	15.7	1331	14.9	2633	12.8	3169	11.2	3898	11.7	4461	12.0
388	15.6	1332	11.0	2639	12.6	3184	10.2	3900	12.4	4473	11.3
404	11.4	1359	12.5	2642	(14.0)	3185	13.1	3904	12.1	4474	12.7
428	11.8	1380	11.0	2389*	13.9	3190	12.1	3923	11.3	4477	11.4
474	13.0	1385	11.5	2646	13.1	3193	12.2	3941	11.3	4478	12.3
488	11.4	1395	11.4	2654	12.8	3222	13.8	3945	11.7	4479	13.6
495	14.2	1398	10.4	2655	10.8	3226	12.6	3949	11.3	Note (14)	15.4
499	13.2	1399	11.2	2672	13.2	3227	11.3	3953	10.7	4490	10.0
507	12.8	1400	12.3	2673	14.4	3245	11.8	3962	11.9	4492	13.2
514	12.3	1404	11.1	2681	11.0	3254	12.1	3990	13.6	4494	10.9
520	12.2	1407	11.2	2683	10.4	3277	12.4	3992	10.5	4526	10.6
524	11.6	1426	12.6	2685	12.3	3301	12.2	3998	11.2	4527	11.4
560	14.0	1439	12.9	2693	13.3	3310	10.8	4026	11.7	4546	11.4
564	13.8	1441	13.9	2694	15.5	3338	(12.3)	4036	11.6	4548	10.9
578	11.6	1449	14.6	2712	12.8	3344	10.4	4038-9	10.8	4550	12.6
584	11.4	1451	14.5	2715	11.9	3348	12.0	4051	11.0	4552	11.0
596	12.1	1453	12.9	2716	12.7	3351	10.5	4102	12.3	4569	10.5
628	9.8	1518	12.3	Note (11)	19.2	3359	10.9	4105	(12.0)	4570	11.8
1727*	12.3	1569	11.7	Note (12)	20.3	3367	11.9	4106	(12.4)	4578	12.3
636	12.4	1587	13.2	2732	12.7	3368	9.9	4111	11.6	4589	12.0
672	11.4	1600	12.2	2744	13.8	3377	11.3	4116	12.5	4594	9.1
681	12.8	1601	15.1	2748	12.3	3379	10.5	4125	10.9	4621	11.0
718	12.5	Note (9)	15.1	2749	13.5	3384	10.9	4138	12.4	4631	9.6
720	11.3	1637	11.6	2768	11.0	3389	12.1	4143	12.0	4636	10.6
736	13.6	1640	12.4	2775	11.3	3412	11.5	4150	12.6	4638	12.2
741	13.0	391*	12.9	2776	11.9	3414	12.0	4151	11.2	4647	12.1
750	13.7	1700	12.1	2782	12.5	Note (13)	18.0	4179	11.7	4649	9.9

TABLE A1. MAGNITUDES FOR 576 NEBULAE CORRECTED FOR APERTURE EFFECT.

NGC	m_{pg}	NGC	m_{pg}	NGC	m_{pg}	NGC	m_{pg}	NGC	m_{pg}	NGC	m_{pg}
4660	12.1	4902	11.7	5474	12.1	5898	12.6	6814	12.2	7392	12.6
4666	11.5	4907	14.7	5485	12.6	5899	12.5	6824	12.9	1460*	15.3
4697	10.4	4908	15.1	5493	12.5	5903	12.7	1317*	14.5	7448	12.0
4698	11.6	4045*	15.4	5533	12.7	5907	11.0	6921	14.7	7457	12.3
4699	10.2	4051*	14.8	5548	12.8	5921	11.6	6927	15.6	7469	12.7
4725	10.0	4911	13.6	5557	12.3	5962	12.1	6928	13.8	7479	11.6
4736	8.7	4915	13.0	5566	11.4	5970	12.2	6930	14.0	7499	15.1
4742	12.5	4921	13.6	5574	13.4	5982	12.4	6944	14.4	7501	15.5
4753	10.7	4941	12.0	5576	12.0	5985	11.9	6946	9.8	7503	14.7
4754	11.6	4958	11.5	5585	11.5	6015	11.6	6951	12.5	7507	11.6
4762	11.0	4995	11.9	5614	12.5	6027d	14.8	6954	14.1	7541	12.6
4789	13.3	5005	10.6	5631	12.6	1183*	15.8	6962	12.8	7562	12.9
4793	12.3	5018	12.2	5633	12.9	1185*	14.8	6963	15.2	7576	13.8
HZ46	15.2	5033	(10.6)	5638	12.4	1194*	15.4	6964	14.2	7585	12.7
4800	12.2	5049	13.8	5668	12.2	6070	12.3	7137	13.1	7600	13.0
4814	12.7	5055	9.0	5672	14.1	6181	12.3	Note (17)	15.4	7606	11.6
4826	9.2	5077	12.6	5676	11.7	6207	12.0	Note (18)	16.2	7611	13.6
4850	15.4	5087	12.1	5687	12.8	6217	11.9	Note (19)	16.5	7617	15.0
3946*	15.3	5173	13.8	5689	12.9	6239	12.9	7171	13.1	7619	12.4
4853	14.5	5194	8.6	5713	11.8	6314	14.0	7177	12.0	7623	14.0
4856	11.4	5195	(10.7)	5746	11.3	6340	12.0	7217	11.0	7625	13.2
4860	15.0	5198	13.0	5806	12.4	6359	13.8	7240	15.5	7626	12.7
4861	12.9	5204	11.7	5812	12.6	6384	11.4	7242	14.3	7640	11.7
4865	14.7	5248	11.0	5813	11.8	6412	12.4	7252	13.1	7671	13.8
4866	12.0	5273	12.5	5820	13.1	6482	13.1	7302	13.1	7678	12.5
4867	15.7	5308	12.2	5831	12.6	6503	10.7	7314	11.6	7679	13.2
4869	15.0	5322	11.0	5838	11.9	6627	14.4	7317	15.3	7716	12.9
4872	15.4	5353	12.1	Note (15)	11.3	6635	14.7	7318a	14.8	7723	11.8
4874	13.7	5363	11.2	Note (16)	14.1	6643	11.8	7318b	14.9	7727	11.6
4881	14.8	5364	11.0	5850	11.8	6654	12.5	7319	13.7	7741	12.3
4886	15.2	5371	11.4	5854	12.6	6658	14.1	7331	10.2	7742	12.2
4889	12.9	5377	12.0	5857	13.9	6661	13.2	7332	11.7	7743	12.3
4021*	15.8	5394	13.6	5859	13.2	6674	13.0	7343	14.5	7769	12.5
4895	14.3	5448	12.2	5866	10.9	6702	14.0	7377	12.4	7770	14.5
4896	15.1	5457	8.5	5878	12.4	6703	12.5	7385	14.1	7771	13.1
4900	11.9	5473	12.4	5879	11.9	6710	14.2	7386	14.6	7785	13.0

NOTES TO TABLE

(1) Anon. at 0016 +2946.
(2) Neb. No. 9 in foreground of Cl 0025 +2223.
(3) Anon. M 31 field at 0023 +4042. Mag. by Kron.
(4) Anon. M 31 field at 0026 +3914. Mag. by Kron.
(5) Baade "a" M 31 field. Spr ext I2/II2. Mag. by Kron.
(6) Anon. at 0047 + 4219. Mag. by Whitford and Code.
(7) Anon. at 0047 + 4220. Mag. by Whitford and Code.
(8) Anon. at 0234 + 3412.
(9) Anon. at 0438 + 0409.
(10) Anon. at 0705 + 3506 (Brightest member of Gemini Cluster).
(11) Neb. No. 10 in foreground of Cl 0855 + 0321.
(12) Neb. No. 11 in foreground of Cl 0855 + 0321.
(13) Neb. No. 1 in foreground of Cl 1055 + 5702.
(14) Anon. at 1227 + 1247.
(15) Mag. is for NGC 5846 plus anon. companion.
(16) Mag. is for anon. companion to 5846.
(17) Anon. at 2058 + 1607.
(18) Anon. at 2058 + 1556.
(19) Anon. at 2059 + 1556.

(1952), after applying a correction to the latter for aperture effect, gives a distribution of residuals whose dispersion is about 0.10 mag. Since this dispersion is less than $\sigma = 0.19$ mag. obtained from the foregoing comparison of Pettit's and of Stebbins and Whitford's corrected magnitudes, a direct comparison of Pettit's corrected magnitudes with the precision data of Holmberg is of interest. Holmberg has generously made his manuscript catalogue available for this comparison. The distribution of differences, in the sense Holmberg *minus* Pettit, is shown in Figure A5 for 56 nebulae in common. A normal error function is drawn with $\Delta P = -0.04$ mag. and $\sigma = 0.189$ mag. This comparison of Pettit's values with Holmberg's gives results which are almost

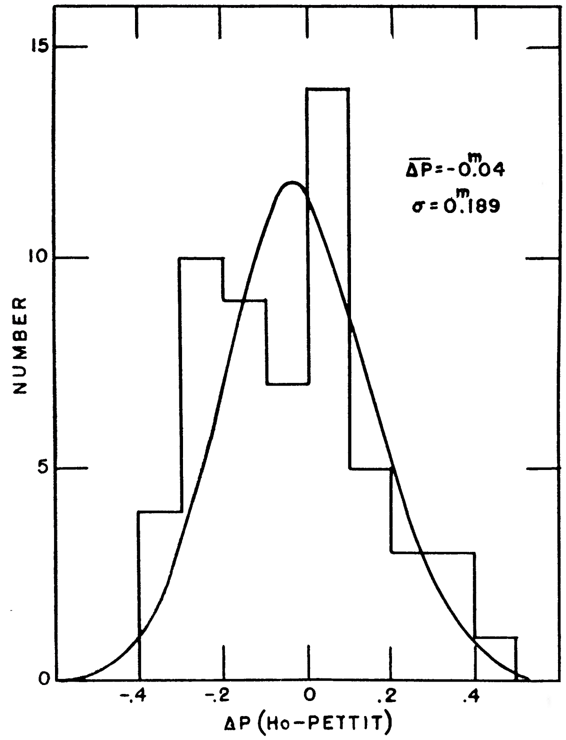

Figure A5. Same as A4 for Holmberg's tabulated magnitudes minus Pettit's corrected values.

identical with those of the comparison of Pettit with Stebbins and Whitford. However, the value of $\sigma = 0.10$ mag. from the comparison between Holmberg and Stebbins and Whitford shows that the accuracy of Pettit's magnitudes is lower than those of Holmberg or of Stebbins and Whitford, because $\sigma_{\mathrm{Ho-P}} \approx \sigma_{\mathrm{SW-P}} > \sigma_{\mathrm{Ho-SW}}$. It is evident, however, that Pettit's accuracy is entirely adequate for the present problem, since no systematic error is revealed by the available tests and since Pettit's inferred mean error is small compared with the spread in absolute magnitude of the nebulae themselves. The agreement of the comparison between the catalogues of Stebbins and Whitford and of Pettit with the comparison between those of Holmberg and of Pettit suggests that the gross systematic aperture effect has been removed from the basic magnitudes. This conclusion depends upon the assumption, however, that Holmberg's data require no correction for the large limiting diameters reached in his photometry.

APPENDIX B. THE *K* CORRECTION

In the various theoretical treatments of the expanding universe it is customary to assume that pairs of numbers, $[z, m_{\mathrm{bol}}]$, characterizing certain properties of extragalactic nebulae, are available from observational astronomy. The first of these numbers is the redshift $\Delta\lambda/\lambda_0$. It is directly obtained by spectroscopic observation. The second is the bolometric magnitude which, unfortunately, is not directly measured but which must be derived from observed heterochromatic magnitudes. The term to convert observed magnitudes to a bolometric scale is called K. Its evaluation is the subject of this appendix.

The bolometric magnitude of a radiating body is defined as the total energy, expressed as a magnitude, received from all wave lengths on a unit area outside the earth's atmosphere. Such a magnitude is never directly measured because of the selective spectral transmission of the atmosphere and response of the detecting device. Hence, bolometric corrections must be computed from the known properties of the source, atmosphere, and receiver. Evaluation of the K correction is made by computing the difference of the bolometric corrections for nebulae with different $\Delta\lambda/\lambda_0$. This difference is caused by the change in the heterochromatic energy received through the acceptance bands of the radiation detector due to the redshift of the nebular spectrum.

We shall first consider the idealized case where all nebulae of a given type with $z = 0$ have the same spectral energy curves, and where these curves do not change with time. This assumption is known to be false from the existence of the Stebbins-Whitford effect (1948), but we shall later see how this idealized theory of the K correction may be modified to fit actual conditions.

Except for a normalizing factor, the bolometric intensity of a radiating source is equal to the total area under the energy-distribution curve $I_z(\lambda)$. Likewise the heterochromatic intensity is that part of $I_z(\lambda)$ contained within the acceptance bands of the receiver. Let $I_z(\lambda)$ be the energy-distribution function, outside the earth's atmosphere, for a nebula with redshift z, $S(\lambda)$ the sensitivity function of the atmosphere, telescope, and detecting device, l_{h} the observed heterochromatic intensity of the nebula, and l_{bol} the bolometric intensity; hence by definition

$$l_{\mathrm{bol}}(z) = \mathrm{A} \int_0^\infty I_z(\lambda)\, d\lambda, \tag{B1}$$

$$l_{\mathrm{h}}(z) = \mathrm{A} \int_0^\infty S(\lambda) I_z(\lambda)\, d\lambda, \tag{B2}$$

where A is a normalizing factor depending on the zero point of the magnitude scale. The bolometric correction $\Delta m(z)$ is defined by

$$l_{\mathrm{bol}}(z) = l_{\mathrm{h}}(z)10^{0.4[\Delta m(z)]}. \tag{B3}$$

The difference in the observed heterochromatic magnitudes due to the redshift is the quantity of interest. From (B3),

$$\frac{l_{\mathrm{h}}(z)}{l_{\mathrm{h}}(0)} = \frac{l_{\mathrm{bol}}(z)}{l_{\mathrm{bol}}(0)} 10^{-0.4K}, \tag{B4}$$

where

$$K \equiv \Delta m(z) - \Delta m(0). \tag{B5}$$

From (B3) and (B5) it follows that

$$m_{\mathrm{bol}}(z) - \Delta m(0) = m_{\mathrm{h}}(z) - K. \tag{B6}$$

Since $\Delta m(0)$, which is the bolometric correction for zero shift, is assumed constant for any given nebular type, this equation shows that the bolometric magnitude is obtained to within a constant from the observed magnitude $m_{\mathrm{h}}(z)$ if K is known.

The value of K for different z may be computed from (B4) with the aid of (B1) and (B2), if $I_z(\lambda)$ and $S(\lambda)$ are known. These functions are obtained as follows. Stebbins and Whitford's six-color curve (1948) for M32, reduced to intensity units, is taken as the standard $I_0(\lambda)$ for elliptical nebulae, since, according to these authors, the $I_0(\lambda)$ for M32 is representative for this nebular type. The sensitivity function $S(\lambda)$ is found from the product of (1) the spectral transmission of the atmosphere (Pettit 1940), (2) the reflection coefficients for two reflections from aluminized mirrors (Pettit, reported by Seares 1943), and either (3) the sensitivity functions for Pettit's (1954) or Stebbins and Whitford's (1948) filters plus photoelectric equipment for magnitudes determined in this way, or (4) the sensitivity functions for the photographic plates plus filters for magnitudes determined with the jiggle-camera at the 200-inch. For jiggle-camera magnitudes only one reflection from an aluminized mirror is involved, since photometry is done at the prime focus, but the transmission function of the Ross $f/3.67$ corrector lens enters instead. However, since the removal of one aluminum reflection and the addition of the glass transmission nearly compensate in the wave-length regions considered, the $S(\lambda)$ computed for Stebbins and Whitford's equipment at the 100-inch is used for the jiggle-camera case. The adopted sensitivity functions are listed in Table B1. The normalization of $S(\lambda)$ in this table is arbitrary, since only the form is required to compute K. Equations (B4) and (B2) give

TABLE BI. SENSITIVITY FUNCTION $S(\lambda)$

$\lambda \times 10^6$ cm	Free	Pettit Blue	Pettit Yellow	Stebbins and Whitford Blue	Stebbins and Whitford Yellow
30	.002	.000			
31	.028	.014			
32	.135	.114			
33	.243	.208		.000	
34	.293	.258		.155	
35	.331	.294		.442	
36	.375	.331		.638	
37	.402	.354		.823	
38	.404	.354		.964	
39	.421	.370		1.120	
40	.441	.387		1.187	
41	.440	.392		1.249	
42	.426	.378		1.266	
43	.408	.349		1.254	
44	.384	.310		1.239	.003
45	.366	.265	.000	1.148	.008
46	.341	.217	.008	1.050	.056
47	.319	.170	.032	.864	.229
48	.300	.129	.077	.627	.455
49	.285	.095	.152	.405	.964
50	.269	.063	.220	.245	1.097
51	.249	.036	.220	.157	1.084
52	.226	.015	.210	.069	1.037
53	.205	.003	.192	.044	.962
54	.183	.000	.172	.013	.875
55	.163		.152	.009	.723
56	.141		.129	.008	.609
57	.111		.101	.000	.405
58	.083		.075		.305
59	.061		.057		.209
60	.042		.042		.165
61	.027		.027		.101
62	.016		.016		.072
63	.011		.011		.037
64	.009		.009		.019
65	.007		.007		.009
66	.005		.005		.000
67	.004		.004		
68	.003		.003		

$$K = 2.5 \log \frac{l_{\mathrm{bol}}(z)}{l_{\mathrm{bol}}(0)} + 2.5 \log \frac{\int_0^\infty S(\lambda) I_0(\lambda)\, d\lambda}{\int_0^\infty S(\lambda) I_z(\lambda)\, d\lambda}. \tag{B7}$$

The second term of (B7) may be computed by simple quadrature, once $I_z(\lambda)$ is known. This function is constructed from $I_0(\lambda)$ by reading the intensity at a given λ and by plotting this intensity at $\lambda_{\mathrm{new}} = \lambda(1+z)$. With this procedure it is obvious that the area under the new curve, $I_z(\lambda)$, has been artificially increased by $1+z$. Consequently the first term in (B7) is $2.5 \log (1+z)$.

Table BII tabulates the K corrections to the photographic (P) and photovisual (V) magnitudes, $K_{\mathrm{P}}(z)$ and $K_{\mathrm{V}}(z)$, computed from B7. The change in the color index, $\Delta(\mathrm{P}-\mathrm{V})$, due to the redshift is also given. This is obtained from $K_{\mathrm{P}}(z) - K_{\mathrm{V}}(z)$, and it is the color change predicted if the assumptions used in deriving K are true. It is known that this predicted color change

TABLE BII. VALUES OF $K_P(z, t_0)$ AND $K_V(z, t_0)$

	E Nebulae Pettit's S(λ)			E Nebulae SW's S(λ)		
z	K_P (mag.)	K_V (mag.)	ΔCI	K_P (mag.)	K_V (mag.)	ΔCI
0.00	0.00	0.00	.00	.00	.00	.00
0.05	.21	.11	.10	.22	.10	.12
0.10	.47	.25	.22	.44	.25	.19
0.15	.71	.41	.30	.66	.41	.25
0.20	.93	.57	.36	.89	.59	.30
0.25	1.16	.76	.40	1.10	.76	.34
0.30		.94			.95	
0.35		1.13			1.13	

	Sb Nebulae SW's S(λ)			Sc Nebulae SW's S(λ)		
z	K_P (mag.)	K_V (mag.)	ΔCI	K_P (mag.)	K_V (mag.)	ΔCI
0.00	.00	.00	.00	.00	.00	.00
0.05	.25	.10	.15	.14	.02	.12
0.10	.50	.23	.27	.30	.06	.24
0.15	.75	.36	.39	.47	.13	.34
0.20	.99	.55	.44	.62	.22	.40
0.25	1.24	.76	.48	.81	.35	.46
0.30		.99			.50	.48
0.35		1.23			.64	.51

is less than that given by the observations, and the excess is known as the Stebbins-Whitford effect (Stebbins and Whitford 1948; Whitford 1954). One proposed explanation of the effect is that a change of $I_z(\lambda)$ with time is involved, which is caused by the evolution of the brightest stars comprising the nebula. If this hypothesis is true, it follows that K_P and K_V will be functions of $t_0 - t_1$, where t_0 is the time of receipt of the light signals emitted by a nebula at t_1.

By the above procedure we have evaluated K at t_0, whereas we actually need the function $K(z, t_1)$, which is the K correction derived from the energy curve extant at time t_1. With our present lack of knowledge of $I_z(\lambda)$ we assume the following expansion for the required function:

$$K(z, t_1) = K(z, t_0) + \frac{\delta K}{\delta t}(t_1 - t_0). \quad \text{(B8)}$$

This equation has the same form that Robertson assumes for the change in the total bolometric magnitude with time, and hence, by a redefinition of Robertson's quantity μ (Robertson 1955), the change in K caused by the Stebbins-Whitford effect can be incorporated into the theoretical equation connecting m_{bol} and z. At the present time this seems to be the best procedure.

In 1948 Merle F. Walker computed K corrections by essentially the same method used here. His results were not published, but he has generously made them available for the purpose of comparison. The agreement between Walker's and the present values of K_P and K_V for E nebulae is fairly good. The average difference is 0.04 mag. Walker also computed K_P and K_V for Sb and Sc nebulae, and these values are also tabulated in Table BII.

One important point made by Walker is that the size of the K correction depends strongly on wave length. By choosing effective wave lengths far enough to the red, the K correction can be made quite small for an appreciable range of z. Walker computed the optimum effective wave lengths for minimum K correction, over the range $z = 0$ to $z = 0.30$, and found them to be $\lambda = 6300$ for E nebulae, $\lambda = 6200$ for Sb nebulae, and $\lambda = 5500$ for Sc nebulae. For these wave lengths the values of K do not exceed 0.1 mag. These results show that a proper choice of wave length will be important for future, more precise evaluation of the [log cz, m] relation and for studies of nebular counts.

APPENDIX C. EVALUATION OF H

The determination of the expansion parameter H is one of the most difficult problems in modern observational astronomy, since each step required for an accurate solution is just on the borderline of possibility. The difficulty, of course, lies in determining distances to resolved nebulae that are far enough away to have significant redshifts and yet are close enough to show distance indicators of suitable precision, such as novae, globular clusters, and the variable and non-variable stars of highest luminosity.

Hubble's calibration of 1936 was obtained from the [log cz, m] relation for the brightest resolved objects in a sample of nearby resolved nebulae. These objects were identified at that time as bright supergiant stars. The absolute magnitudes of those objects were assumed to be known from previous calibration of blue supergiants in M31 and in M33 with respect to the cepheid variables. The zero-point of the period-luminosity law for the cepheids was assumed known from the statistical parallax calibration first by Hertzsprung (1913) and later by Shapley (1918) and by R. E. Wilson (1923, 1939). Evidence accumulated in the past five years has shown the need to examine anew each step of this procedure.

H. Mineur (1945), and later Baade (1952), and Blaauw and H. R. Morgan (1954) have shown the need for revision of the zero-point of the period-luminosity relation for classical cepheids. The correction from Blaauw and Morgan's solution is $\Delta M = -1.4 \pm 0.3$ mag., which is in good agreement with Baade's original estimate. This correction increases the apparent distance modulus for M31 and M33 and revises upward the absolute magnitudes of the brightest stars in these systems.

With the availability of fast red-sensitive emulsions it has only recently been possible to test Hubble's assumption that the bright resolved knots in the spiral arms of nearby spirals are stars. The test procedure has been to take two plates with appropriate filters so as to isolate the $H\alpha$ region on one plate and a neighboring portion of the continuum on the other. Comparison of the two plates distinguishes the emission H II regions from the stars. Reproductions from two such photographs are shown in Plates VI and VII for NGC 4321, the brightest spiral in the Virgo Cluster. Plate VI shows the entire nebula taken with the 200-inch on a 103a-D plate behind a Schott GG 14 filter. This plate and filter combination isolates the spectral region from λ5100 to λ6400 which is free from strong emission lines. Plate VII shows a plate pair for part of a spiral arm of NGC 4321. The left side is from the a-D plate; the right from a 103a-E plate plus RG 2 filter which has a band pass from λ6300 to λ6700. This region contains the $H\alpha$ emission line. From these photographs, the brightest resolved knots in the spiral arm of NGC 4321 are seen to be H II regions instead of resolved stars. Several prominent H II regions are indicated by arrows on the right part of Plate VII. Similar identification of the brightest knots with H II regions has been made in all other resolved nebulae tested. Stars can be resolved in NGC 4321, but they begin to appear about 2 magnitudes fainter than the knots. The arrow on the left part of Plate VII points to two objects that are probably stars. Over the entire nebula about 15 of these objects appear. On blue-sensitive plates they are more conspicuous than on the yellow or red plates. All indications point to identification with stars. These objects begin to resolve in NGC 4321 at $m_{pv} \approx 20.8$, which is considerably fainter than Hubble's (1936b) value of $m_{pg} = 19.0$. Hence, although it will be possible to use the brightest resolved stars as distance indicators, they are faint and must first be isolated from the H II regions. Use of such stars appears to be one good way eventually to determine H with precision. The long-term program now in progress calls first for this separation of the stars from the H II regions in all nebulae north of $\delta = -15°$ that can be resolved with the 200-inch telescope. Next, the absolute magnitudes of the stars will be recalibrated in the nearby systems of M31, M33, NGC 6822, and the M81 and M101 groups by the cepheid criterion before apparent moduli for the resolved systems are found. From these same calibrating systems the dependence of the upper luminosity of the involved stars on the luminosity of the nebulae will be investigated. The resulting distance moduli for the resolved systems, correlated with the redshift, ultimately may give H with fair precision. Although this approach is straightforward, it is obvious that any current discussion of the value of H must be considered provisional. Two ways of estimating the value of H, however, are possible at this time, and, because of its importance, the present evidence will now be discussed.

The well-defined limiting envelope for the field nebulae in Figure 10 indicates that an upper limit to nebular luminosity exists, which, if known, gives H. The brightest system with reasonably well known M_{pg} is the Andromeda nebula, and one calibration method is to assume that this spiral is indeed one of the intrinsically brightest in the sky. Arbitrary as this assumption seems, the resulting value of H agrees with that determined from the resolved stars in NGC 4321, as described in the following paragraphs.

The absolute photographic magnitude of M31 is $M_{pg} = -19.92$, which is obtained from Baade and Swope's (1954) apparent modulus $m - M = 24.25$ and Holmberg's (1950) apparent magnitude $m_{pg} = 4.33$. This absolute magnitude is the asymptotic or total magnitude, since Holmberg's photometry is carried to an isophote of about 27 mag./sq. sec. All magnitudes in this paper, however, refer to an isophote of about 25 mag./sq. sec. Figure A3 of Appendix A shows that the conversion term between these two cases is about +0.10 mag. The absolute magnitude to be used with the present data is, therefore, $M_{pg} = -19.82$. The upper envelope line of Figure 10 for all types of field nebulae gives $H = 211$ km/sec per 10^6 pc if we adopt -19.82 for the absolute photographic magnitude together with 0.25 mag. for the photographic half-thickness of our galaxy. The same criterion applied to the first-ranked cluster data of Figure 13 gives $H = 180$ km/sec per 10^6 pc. The difference in the two values is due to the slightly brighter limiting absolute magnitude for the field nebulae.

The other method of calibration uses the apparent magnitude of the brightest resolved stars in NGC 4321. These stars appear at $m_{pv} \approx 20.8$. The absolute magnitude for brightest stars is obtained by comparison with those in M31 and M33. The brightest non-variable stars appear in these systems at photographic magnitudes 16.0 and 15.6, respectively. With respective apparent

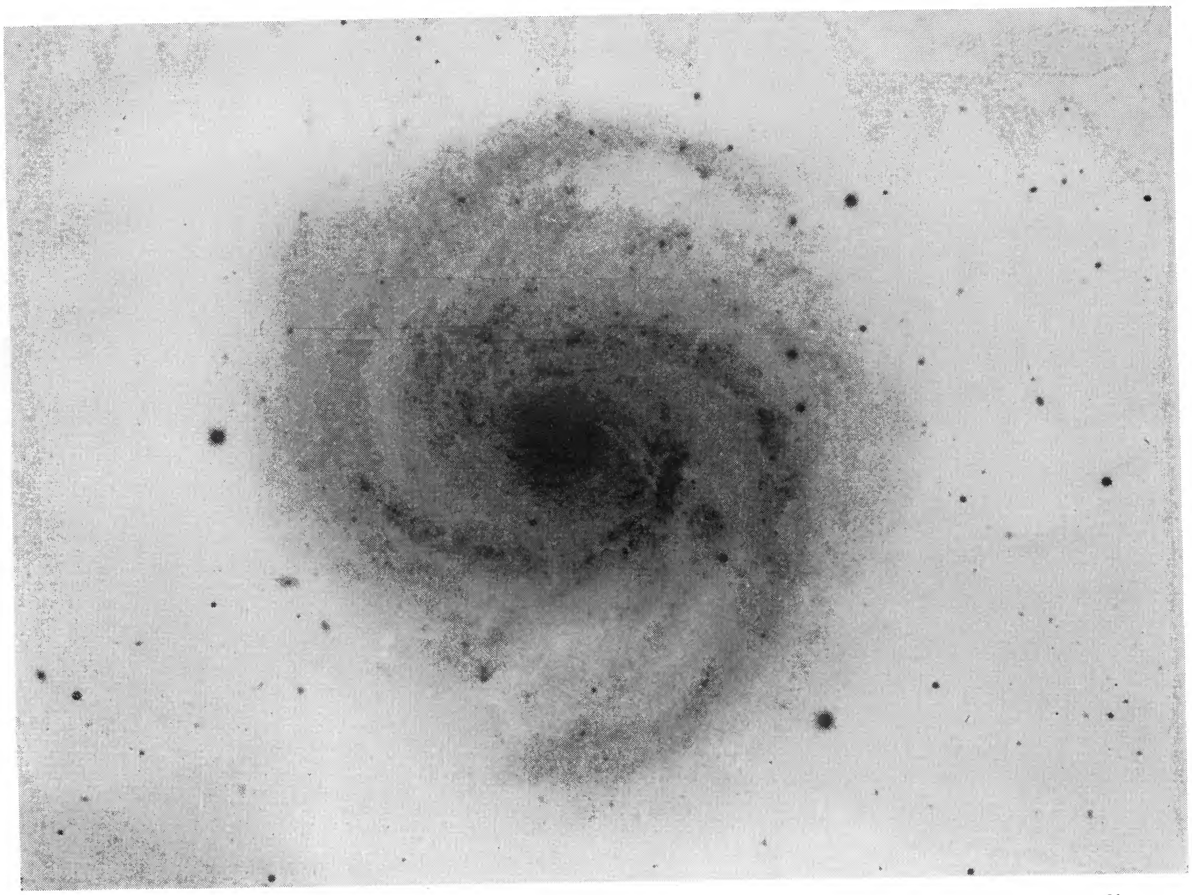

Plate VI. NGC 4321 taken with the 200-inch Hale telescope with a 103a-D plate behind a Schott GG 14 filter. The band pass of this combination is from $\lambda = 5200$ to $\lambda = 6300$.

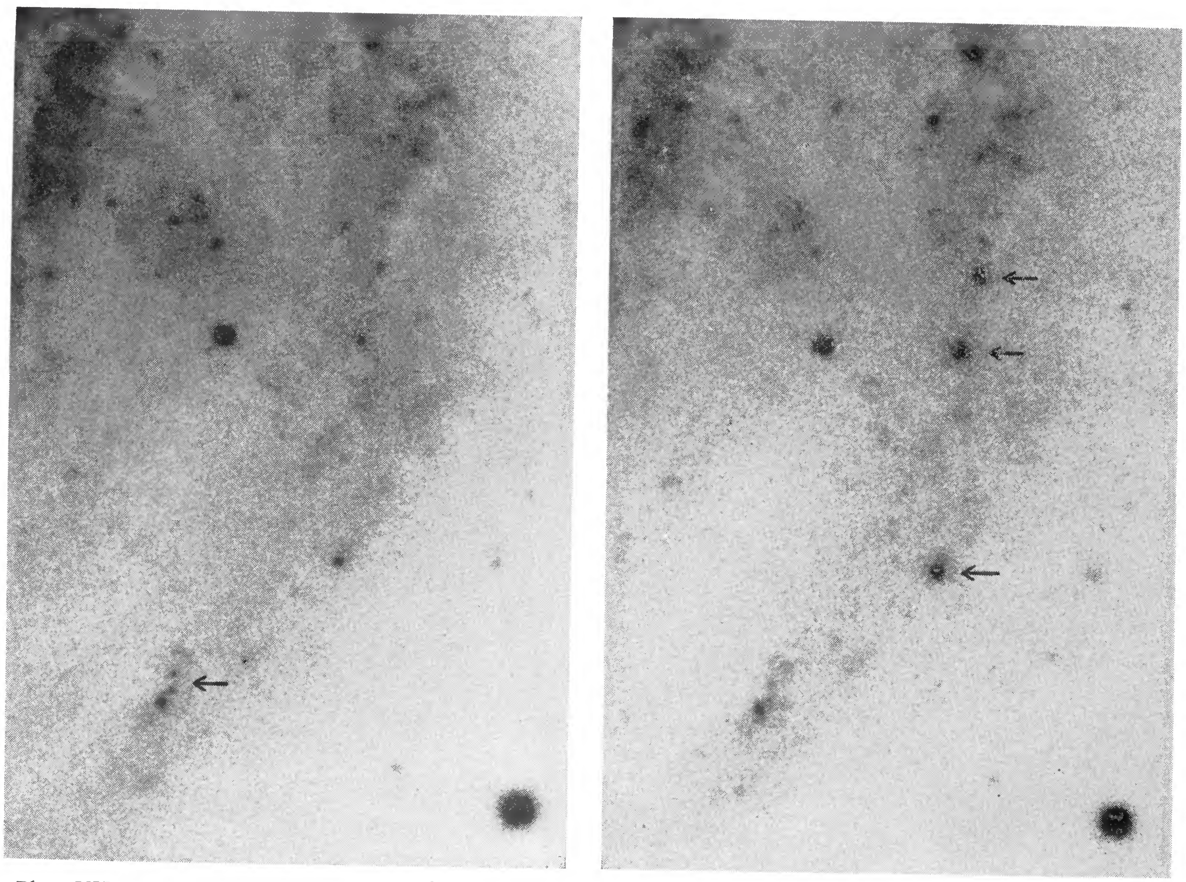

Plate VII. Part of the spiral arm of NGC 4321 which is shown in the lower right of Plate VI. The exposure on the right was made with a 103a-E plate behind a Schott RG 2 filter. This combination isolates $H\alpha$. The exposure on the left is the same as in Plate VI. Some conspicuous *H* II regions are marked on the right. Objects identified as stars are marked on the left.

moduli of 24.25 and 24.15, the stellar absolute magnitudes are −8.25 and −8.50. Furthermore, the mean M_{pg} at maximum light for the 5 blue, irregular variables in M31 and M33 (Hubble and Sandage 1953) is −8.7. The mean of all these values is $M_{pg} = -8.5$, which will be used here. Since these stars have an average color index near zero, the corresponding M_{pv} is −8.5. A more accurate value is not available at present. Again using 0.25 mag. for the photographic half-thickness for our galaxy, the true modulus of NGC 4321 is $m - M = 29.05$. The mean redshift of the Virgo Cluster +1136 km/sec gives $H = 176$ km/sec 10^6 pc. Although it is probably uncertain by 20 per cent, $H = 180$ km/sec 10^6 pc, $1/H = 5.4 \times 10^9$ years appears to be the best obtainable from the present data.

The [log cz, m] relation for the field and cluster nebulae may now be used to give mean absolute magnitudes for the various nebular groups. We

TABLE CI. MEAN ABSOLUTE PHOTOGRAPHIC MAGNITUDES FOR NEBULAR CLASSES WITH $H = 180 \cdot f$ KM SEC^{-1} (10^6 PC)$^{-1}$

Field Nebulae*		Cluster Nebulae	
Class	$\overline{M(m)}_{PC} - 5 \log f$	Class	$\bar{M}_{0PC} - 5 \log f$
Eo	$-18.35 \pm .21$	Brgst Fld Neb	-20.25
So	$-18.04 \pm .25$	Rank 1	-19.78
Sa	$-18.33 \pm .24$	Rank 3	-19.30
Sb	$-18.37 \pm .18$	Rank 5	-18.98
Sc+SBc	$-18.00 \pm .36$	Rank 10	-18.49
SBo+SBa	$-17.92 \pm .26$		
SBb	$-18.54 \pm .23$		
All Types	$-18.21 \pm .13$		

* Tabulated are $\overline{M(m)}$ which is related to $\bar{M}_0$ by $\overline{M(m)} = \bar{M}_0 - 1.382\,\sigma^2$.

shall assume that the true value of H is given by $180f$ km/sec 10^6 pc, where f is a correction factor at present unknown. The absolute magnitudes M_C computed with $H = 180$ km/sec 10^6 pc will be related to the true absolute magnitudes M_T by the equation $M_C = M_T - 5 \log f$.

Solution 2 of Table XIV provides the data necessary to compute M_C for the field nebulae. The solution of Case 2 for the clusters, together with the magnitude differences between the 1st, 3rd, 5th, and 10th cluster members provide the necessary cluster data. Since the field nebulae were chosen according to apparent magnitude, the corresponding mean absolute magnitude $\overline{M(m)}$ differs from the mean per unit volume, $\bar{M}_0$, by the Malmquist (1920) relation $\overline{M(m)} = \bar{M}_0 - 1.382\,\sigma^2$, where σ is the dispersion of the luminosity function. Since σ is not well known, only the directly determined $\overline{M(m)} - 5 \log f$ is tabulated in Table CI containing the total results. It is clear that the values for the brightest field nebulae and for the cluster nebulae are M_0, and not $\overline{M(m)}$, since the statistical selection resulting in the Malmquist relation does not enter these cases.

REFERENCES

Adams, W. S., and Humason, M. L. 1936, *Pub. A. S. P.* **48**, 107.
Baade, W. 1931, *A. N.* **243**, 304.
——. 1940, *Yearb. Carnegie Instn.* **39**, 20.
——. 1945, *ibid.* **44**, 15.
——. 1951, *Mich. Obs. Pub.* X, 7.
——. 1952, *Trans. I. A. U.*, Vol. VIII, 397.
Baade, W., and Minkowski, R. 1954, *Ap. J.* **119**, 215.
Baade, W., and Swope, H. H. 1954, *Yearb. Carnegie Instn.* **53**, 20.
Bigay, J. 1951, *Ann. Astroph.* **14**, 319.
Blaauw, A., and Morgan, H. R. 1954, *B. A. N.* **12**, 95.
Bondi, H. 1952, *Cosmology*, Cambridge University Press.
Bowen, I. S. 1947, *Pub. A. S. P.* **59**, 253.
——. 1953, *Yearb. Carnegie Instn.* **52**, 25.
Curtis, H. D. 1903, *Lick Obs. Bull.* **2**, 67.
Dennison, E. 1954, Thesis University of Michigan, unpublished.
de Vaucouleurs, G. 1948, *Ann. Astroph.* **11**, 247.
——. 1950, *Ann. Astroph.* **13**, 362.
Einstein, A. 1945, *The Meaning of Relativity*, appendix for the second edition, Princeton University Press.
Härm, R., and Schwarzschild, M. 1955, *Ap. J.* **121**, 445.
Hertzsprung, E. 1913, *A. N.* **196**, 201.
Holmberg, E. 1945, *Medd. Lunds Astr. Obs.*, Ser. II, No. 117.
——. 1950, *ibid.*, No. 128.
Hubble, E. 1925, *Ap. J.* **62**, 409.
——. 1929, *Proc. Nat. Acad. Sci.* **15**, 168.
——. 1930, *Ap. J.* **71**, 231.
——. 1936a, *The Realm of the Nebulae*, Yale University Press, New Haven.
——. 1936b, *Ap. J.* **84**, 158.
——. 1936c, *Ap. J.* **84**, 270.
——. 1939, *J. Franklin Inst.* **228**, 131.
——. 1941, *Sci. Mon.* **51**, 391.
——. 1953, *M. N.* **113**, 658.
Hubble, E., and Humason, M. L. 1931, *Ap. J.* **74**, 43.
Hubble, E., and Sandage, A. 1953, *Ap. J.* **118**, 353.
Humason, M. L. 1931, *Ap. J.* **74**, 35.
——. 1936, *Ap. J.* **83**, 10.
——. 1947, *Pub. A. S. P.* **59**, 180.
——. 1954, *Yearb. Carnegie Instn.* **53**, 22.
Humason, M. L., and Wahlquist, H. D. 1955, *A. J.* **60**, 254.
Humason, M. L., and Zwicky, F. 1947, *Ap. J.* **105**, 85.
Malmquist, K. G. 1920, *Medd. Lunds Astr. Obs.*, Ser. II, No. 22.
Mayall, N. U. 1934, *Pub. A. S. P.* **46**, 134.
——. 1935, *Pub. A. S. P.* **47**, 319.
——. 1936, *Pub. A. S. P.* **48**, 14.
——. 1939, *Lick Obs. Bull.* **19**, 33.

——. 1948a, *Sky and Telescope* **8**, 3.
——. 1948b, *Pub. A. S. P.* **60**, 266.
——. 1950, *Pub. Obs. Univ. Michigan* **10**, 19.
Mayall, N. U., and Aller, L. H. 1942, *Ap. J.* **95**, 5.
Mayall, N. U., and Eggen, O. J. 1953, *Pub. A. S. P.* **65**, 24.
Mayall, N. U., and Wyse, A. B. 1941, *Pub. A. S. P.* **53**, 120.
McVittie, G. C. 1956, *General Relativity and Cosmology*, Chapman and Hill, London.
Mineur, H. 1945, *C. R. Acad. Sci. Paris* **220**, 445.
Nassau, J. J., and Seyfert, C. K. 1945, *Ap. J.* **102**, 377.
Neyman, J., and Scott, E. L. 1952, *Ap. J.* **116**, 144.
Ohlsson, J. 1932, *Ann. Obs. Lund*, No. 3.
Oke, J. B., and Schwarzschild, M. 1952, *Ap. J.* **116**, 317.
Pease, F. G. 1918, *Pub. A. S. P.* **30**, 255.
Pettit, E. 1940, *Ap. J.* **91**, 159.
——. 1954, *Ap. J.* **120**, 413.
Robertson, H. P. 1933, *Rev. Mod. Phys.* **5**, 62.
——. 1938, *Zs. Astroph.* **15**, 69.
——. 1955, *Pub. A. S. P.* **67**, 82.
Russell, H. N. 1917, *Ap. J.* **45**, 60.
Sandage, A. R. 1954a, *A. J.* **59**, 180.
——. 1954b, Liege Symposium Volume, *Les Processus nucleaires dans les Astres*, p. 254.
Sandage, A. R., and Schwarzschild, M. 1952, *Ap. J.* **116**, 463.
Seares, F. 1943, *Ap. J.* **98**, 302.
Seyfert, C. K. 1943, *Ap. J.* **97**, 28.
——. 1951, *Pub. A. S. P.* **63**, 72.
Shane, C. D., and Wirtanen, C. A. 1950, *Proc. Amer. Phil. Soc.* **94**, 13.
——. 1954, *A. J.* **59**, 285.
Shapley, H. 1918, *Ap. J.* **48**, 89.
Shapley, H., and Seyfert, C. 1935, *Bull. Astr. Obs. Harv.*, No. 899, 16.
Shapley, H., and Ames, A. 1932, *Ann. Harv. Coll. Obs.* **88**, 43.
Shapley, H., and Boyd, C. 1940. *Proc. Nat. Acad. Sci.* **26**, 41.
Shapley, H., and Mohr, J. 1938, *Bull. Astr. Obs. Harv.*, No. 907, p. 6.
Stebbins, J., and Whitford, A. E. 1937, *Ap. J.* 86, 247.
——. 1945, *ibid.* **102**, 318.
——. 1948, *ibid.* **108**, 413.
——. 1952, *ibid.* **115**, 284.
Stebbins, J., Whitford, A. E., and Johnson, H. L. 1950, *Ap. J.* **112**, 469.
Strömberg, G. 1925, *Ap. J.* **61**, 353.
Struve, O., and Linke, W. 1940, *Pub. A. S. P.* **52**, 139.
Wilson, O. C. 1949, *Pub. A. S. P.* **61**, 132.
Wilson, R. E. 1923, *A. J.* **35**, 35.
——. *Ap. J.* **89**, 218.
Whitford, A. E. 1936, *Ap. J.* **83**, 424.
——. 1953, *A. J.* **58**, 49.
——. 1954, *Ap. J.* **120**, 599.
Zwicky, F. 1938, *Pub. A. S. P.* **50**, 218.
——. 1942, *Phys. Rev.* **61**, 489.

Mount Wilson-Palomar Observatories,
Carnegie Institution of Washington,
California Institute of Technology,
and Lick Observatory, Mount Hamilton,
University of California,
1955 *July.*

MEASURES OF DOUBLE STARS *

By CHARLES E. WORLEY

Abstract. Measures of 130 double stars, made with the 12-inch refractor of Lick Observatory, are presented.

The observations of double stars contained in Table 1 were made with the 12-inch refractor of the Lick Observatory. The list contains 424 measures of 130 double stars, and the arrangement of the material in the table is self-explanatory. Asterisks denote remarks, which may be found at the end of the table. These are mainly comparisons with the latest available orbits, obtained from the catalog of Muller (1953) and its recent supplement (Muller 1954). A few comparisons are from other sources, in which case the reference is given.

The high quality of the 12-inch refractor for double star work is well known; it is attested to by the many double star discoveries and measures made with it by Burnham, Aitken, Hussey, Kuiper, and others. Under good observing conditions, elongations of 0″.25, or less, are detectable for bright, equal pairs. The micrometer used is the 12-inch Clark, with the value 14″.059 for one revolution of the micrometer screw. It, and the telescope, have been described fully elsewhere (Holden 1887). The magnification used was generally 600, with a few measures made with lower powers.

A method of measurement similar to that described by Aitken (1935) was used. However, for the position angles, the line joining the stars was placed alternately on either side of the wire, and the micrometer rotated until parallelism was obtained. For the distances, darkened wires were used when practicable. Ordinarily, four position-angle, and four double-distance settings were made.

The program of observation has been made up principally of pairs having distances less than 2″.0, showing orbital motion. Certain wide pairs have been measured as a part of a continuing

* *Lick Observatory Bulletin*, No. 541.